Migration and structure formation in sheared slurries

Samireh Vahid, BSc

A thesis submitted in partial fulfillment of the requirements

for the degree of Doctor of Philosophy

Kingston University

September 23, 2008

ORIGINAL COPY TIGHTLY BOUND

Abstract

This thesis is concerned with the sheared flow of medium dense slurries, consisting of rigid particles in a Newtonian fluid. The particles are rough. The interaction between rough particles in the lubrication limit is studied and expanded on. In a shear gradient geometry a migration phenomenon occurs, in which the particles congregate in the low shear rate region. The literature on this phenomenon is reviewed and for each model that is available a sample calculation of channel flow is calculated. Two models appear to yield realistic results. They incorporate the fluctuations in particle motion (which is a necessary feature of sheared dense slurries). These two models require further attention. The first is the granular temperature model. This model is studied as an isotropic cell model, which permits first order estimates for its many parameters, thus making the model more suitable for practical calculations. The second is the anisotropy-induced model for which in the literature only a phenomenological version is available. The latter model is studied by setting up an analytical continuum calculation that entails explicit fluctuations. It is shown that in steady-state shear a linear approximation never leads to a stable result, unless a substantial repulsive particle interaction is present. The theory is then modified to include a non-linear term (associated

with a rough particle interaction), elaboration of which yields stability, but at the same time structures formation. The latter problem (in two dimensions) is then further studied by carrying out numerical simulations employing the Discrete Element Method. The analytical results are qualitatively replicated: structures form when the particle interaction does not involve a substantial repulsive element; they disappear when a repulsive elastic interaction is implemented. Thus the understanding of the physics of medium dense slurry flow is improved.

1. Introduction

1.1. General

This thesis is concerned with aspects of the mathematical description of the physics of dense slurry flow. A "dense slurry" needs to be defined. Typically it is a particle fluid mixture, consisting of more or less spherical particles immersed in a Newtonian fluid. The solids volume fraction needs to be sufficiently large so that the particles cannot suffuse through their own pore space. This means that a lower limit of the solodosity ϕ of some 0.25 must be imposed. In order for the slurry to flow the solids must not continually be jammed (ephemeral, localised jamming *is* allowed), which imposes a maximum on the solids volume fraction of approximately 0.6. In this thesis two-dimensional slurries will at times be studied and for this situation the upper and lower limits are somewhat higher and range from 0.4 to 0.65.

The particle properties also need to be considered. These are rigid particles and - this will be a main theme of the thesis - they are not perfectly smooth, but have some roughness on their surfaces, which is characterised by an asperity height parameter. The ratio of the latter to the particle radius is small, much less than unity.

The emphasis will be on the constitutive/physical properties of the slurry. The physical environment in which it operates is chosen to be a slow-flow (low Reynolds number), low temperature (infinite Peclet number) one. Brownian motion is unimportant, compared to the motion of the particles induced by the overall strainrate of the problem. Gravity can be added to the theoretical considerations as a refinement, but it is not essential for the development; sedimentation problems, for example, are not considered.

The above does not mean that there are no practical applications for the work here. A variety of problems in geology (for example, flow in volcano pipes, see Petford and Koenders (1998)), chemical engineering (for example, filtration problems, see Wakeman and Tarleton (1999) and Gundogdu *et al* (2003b)), civil and environmental engineering (for example, erosion problems Tuzson. and Clark (1998)) and medical/biological applications (flow of cell-laden sinovial fluid, for instance, Buschmann *et al* (1995), Jay *et al* (1998)). Note that the length scales of all these problems are very different and the study of slurries leads to a very wide range of applicability.

1.2. Migration

One of the most fascinating phenomena exhibited by slurry flows is migration in a shear rate-gradient field. Typically such fields occur in simple geometries such as pipe or channel flow. Figure 1.1 illustrates this.

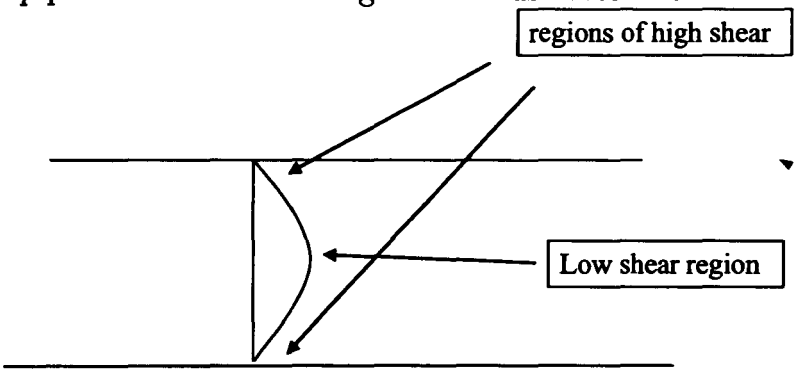

Fig 1.1. Illustration of velocity field in channel flow and indication of high and low shear zones.

The effect was first reported by Bagnold (1954), who also suggested a qualitative model. The particles in dense slurries flowing in such geometries tend to migrate to the low-shear region and congregate in the centre of the channel. The effect has been measured in the literature, notably by Lyon and Leal (1998). At this stage it is necessary to indicate that there is also some theory to describe this

phenomenon. Some of these descriptions require that the solids volume fraction at the centre of the channel is the maximum packing fraction (at which the effective slurry viscosity becomes infinite). Whether such a state actually exists or not is beside the point, as the experiments show very clearly that the solidosity at the centre is *not* anywhere near the maximum density.

Another geometry in which migration is important is in agitated slurries, see Gundogdu *et al* (2003a). In these a septum is vibrated from the bottom of a container (a so-called dead-end filter). In this geometry the particles migrate away from the point of agitation and form a solidosity profile that is depth-dependent. In this problem there is no mean flow and any theories relying solely on mean flow cannot describe this phenomenon and are therefore incomplete.

A key physical property of sheared dense slurries is that particles cannot move in straight lines, but they must have fluctuational motion to be able to overtake one another, see sketch in Figure 1.2. The fluctuational motion must be part of the description of the particle-fluid mixture, otherwise the physics is not adequately represented. The migration phenomenon, which is in some sense similar to thermal diffusion, is then associated with higher and lower intensity of fluctuations in the shear-gradient field. This mechanism will be explored in depth in this thesis.

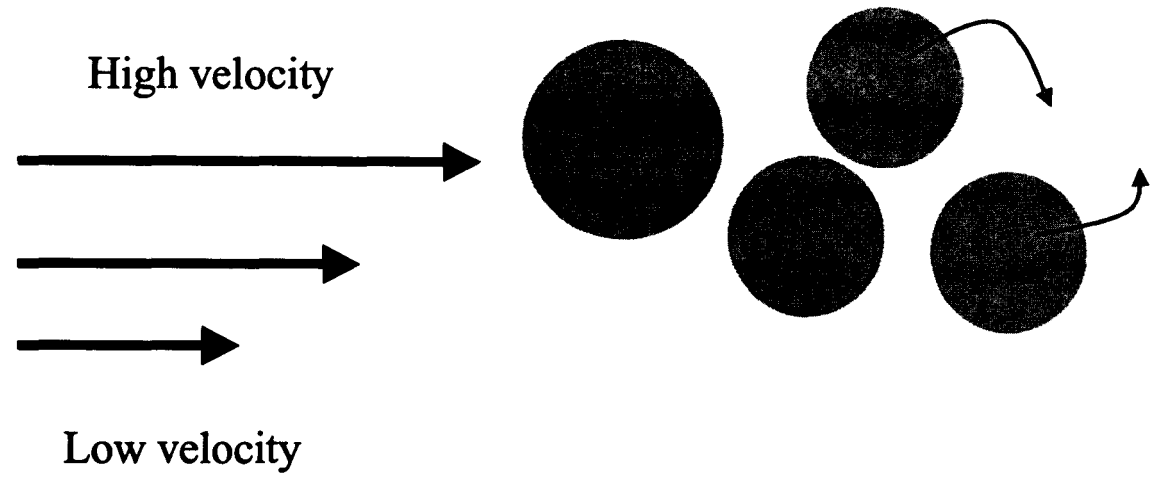

Fig 1.2. Sketch of motion of particles in a shear field.

Another mechanism that is believed to take place is that in a shear field the slurry becomes anisotropic. If such anisotropy is present there is a normal stress associated with the sheared mixture. In a shear-gradient system this normal stress varies and its gradient causes migration. This will also be explored in depth in this work.

It is furthermore well-known that the shear viscosity of a slurry increases dramatically with increasing solids volume fraction. While there are good estimates for this effect in the literature (the work by Thomas (1965) has been very significant), for dense slurries improved modelling is possible. In passing it is noted that for dilute slurries estimates for the increased viscosity are available. The simplest one goes back a long time: Einstein (1911). The next order correction is

by Batchelor and Green (1972), who also highlighted the major problems that the description of dilute slurries present; it is even doubtful whether for semi-dilute systems a unique viscosity actually exists.

1.3. Outline of the contents

Chapter 2 will be devoted to preliminary considerations, particularly regarding the two-particle interaction in the lubrication limit and the elastic interaction, which is frequently used to stabilise numerical simulations of slurry flow.

Chapter 3 is devoted to existing models for migration. We discuss phenomenological models (that are essentially diffusion-type theories), granular temperature models (these take explicit account of the fluctuations in the motion of the particles in the slurry) and some recent anisotropic theories. All the theories are explored in the context of channel flow.

In chapter 4 a cell model is developed to come to an estimate of the parameters in the granular temperature theory. This is a very useful theory and is unique in that the dead-end filtration problem can be solved (this is a problem in which there is no overall strainrate). An improved solution over the ones given in the literature is presented making use of the coefficients that have been obtained from the cell model.

In chapter 5 the fluctuations in a uniformly deforming system are studied. This is done with the aid of continuum theory with fluctuations that arise at the meso-scale (this is the scale of a particle and its next-neighbours). Linear stability theory is invoked and shows that a sheared slurry is never stable, implying that at least some account has to be taken of quadratic terms. The theory employs Fourier space.

Chapter 6 follows on by studying a particular form of the quadratic terms. A form for the pressure that arises from collisions of rough particles is put forward and formulated in Fourier space. The resulting quadratic theory is studied. There are attractors in the system; these are associated with the formation of structures. The structures are aligned with the compressive quadrant of the imposed shear field. A further elastic interaction (such as frequently used in Stokesian Dynamics simulations) would lead to the disappearance of the structures.

In chapter 7 the findings of the theory of chapter 6 are tested by studying the results of a numerical simulation. The simulation is of the Discrete Element Method type. Simulations of a sheared slurry are run with and without an extra repulsive interparticle force. The theoretical predictions are verified. Implications are discussed.

Chapter 8 summarises the thesis and makes suggestions for further research.

Finally appendices are included.

2. Two-particle interaction

2.1. Introduction

The study of assemblies of particles in a suspension is commenced with the investigation of the two-particle interaction. The main contributor to the interaction is the force mediated by the fluid. In slow flow, for dense suspensions, the particles can come very close, in other words, the ratio of the film thickness between particles h is small compared to the diameter D. Under these circumstances the so-called "lubrication limit" is valid. It is well-known - and will be shown again below - that in the lubrication limit for two smooth surfaces the force becomes singular at finite relative velocity. This has serious implications, because while a large force can be handled (especially numerically), a singular force cannot be accommodated in either a numerical simulation or even in analytical analysis. The lubrication limit has other peculiar properties as will be shown below (Section 2.2) in that no momentum transfer can take place between particles. This implies that no particle pressure can develop and particles could never touch. Experimentally this is not true, as has been shown by Smart and Leighton (1989) so, the lubrication interaction needs refinement. The physical basis for a refinement is the consideration that "real" particles are rough. The asperity roughness scale is

much smaller than the mean value of h, but in fluctuational motion particles can come very close together and then touch. When that happens a solid interaction takes place. This interaction occurs at a finite relative velocity and the mechanics of a collision needs to be studied.

In work on the numerical simulation of suspensions authors, such as Nott and Brady (1994) Schowalter (1996) and Morris (1999) have taken a different route to the problem of the singularity as $h \rightarrow 0$; they assume a repulsive *elastic* interaction, which becomes manifest at a very short range (similar to the asperity length scale). In this section that interaction is also looked at and will be briefly discussed.

2.2. The lubrication interaction

In this thesis both two and three dimensional approaches will be considered. Therefore, the lubrication limit interaction needs to be available for two cases: two spheres that approach or depart along their line of centres, which is relevant to the three dimensional problem, and two parallel cylinder surfaces that approach or depart in the radial direction - for the two-dimensional problem. For the three-dimensional problem the force between the spheres is calculated, while for the two-dimensional problem the force per unit length is obtained.

2.2.1. Two spheres

The problem of the interactive force between two spheres has been calculated by Jeffreys and Konishi (1984) for arbitrary separations and for arbitrary relative motion. In the limit $h \to 0$ the force exerted on particle μ between two spheres of equal diameter D, with relative translation velocity $\mathbf{v}^\nu - \mathbf{v}^\mu$ and mean angular velocity $\boldsymbol{\omega}$ is

$$\mathbf{F}^{\mu\nu} = -3\pi D\eta \mathbf{A}\left(\mathbf{v}^\nu - \mathbf{v}^\mu\right) - \pi D^2 \eta \mathbf{B}\boldsymbol{\omega}, \tag{2.1}$$

where η is the viscosity and the two tensors $\mathbf{A}$ and $\mathbf{B}$ depend on the film thickness ratio h/D and unit normal vector $\mathbf{n}^{\mu\nu}$ (pointing from μ to ν) as

$$A_{ij} = -\frac{1}{4}\left[\frac{D}{2h} + \frac{9}{10}\ln\left(\frac{D}{2h}\right)\right] n_i^{\mu\nu} n_j^{\mu\nu} - \frac{1}{6}\ln\left(\frac{D}{2h}\right)\left(\delta_{ij} - n_i^{\mu\nu} n_j^{\mu\nu}\right) + O(1), \tag{2.2}$$

and

$$B_{ij} = -\frac{1}{2}\ln\left(\frac{D}{2h}\right)\epsilon_{ij\ell} n_\ell^{\mu\nu} + O(1). \tag{2.3}$$

The leading term is obviously the one that pertains to normal motion - that is $\left(\mathbf{v}_j^\nu - \mathbf{v}_j^\mu\right) n_j^{\mu\nu}$ (which is $\dot{h}$); the logarithmic terms are unimportant when h/D

becomes very small. The leading term is

$$F_i^{\mu\nu} = -\frac{3\pi D^2 \eta}{8h} \left(v_j^\nu - v_j^\mu\right) n_i^{\mu\nu} n_j^{\mu\nu}. \tag{2.4}$$

The problem has also been calculated for two unequal spheres, see Batchelor (1967, p228)

$$-\frac{3\pi\eta \left(D^\mu D^\nu\right)^2}{2h \left(D^\mu + D^\nu\right)^2} \left(v_j^\nu - v_j^\mu\right) n_i^{\mu\nu} n_j^{\mu\nu}. \tag{2.5}$$

2.2.2. Two cylinders

The problem of two parallel cylinders in the lubrication limit is not reported in the literature, but it is easily calculated. The relevant fluid motion equation is the creeping flow equation of motion for an incompressible fluid. The problem only needs a solution in two dimensions; a sketch is given in Figure 2.1. The fluid velocity is denoted by $\mathbf{u}$; the pressure by p. The creeping flow equation is

$$-\frac{\partial p}{\partial x_i} + \eta \frac{\partial^2 u_i}{\partial x_j^2} = 0. \tag{2.6}$$

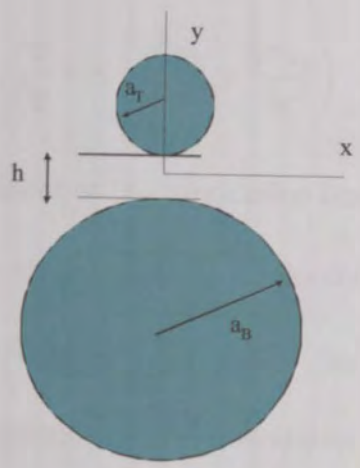

Fig 2.1 Definition sketch of two cylinders.

The equation of continuity reads

$$\frac{\partial u_i}{\partial x_i} = 0. \tag{2.7}$$

The lubrication limit is now applied. The basic assumption is that gradients in the y-direction dominate, because the dimension of the problem in this direction is h and the horizontal dimension is of the order of the particle diameter and h/D is very small. Thus we approximate

$$-\frac{\partial p}{\partial x} + \eta\left(\frac{\partial^2 u_x}{\partial x^2} + \frac{\partial^2 u_x}{\partial y^2}\right) = 0 \;\rightarrow\; -\frac{\partial p}{\partial x} + \eta\frac{\partial^2 u_x}{\partial y^2} = 0; \tag{2.8}$$

and

$$-\frac{\partial p}{\partial y}+\eta\left(\frac{\partial^2 u_y}{\partial x^2}+\frac{\partial^2 u_y}{\partial y^2}\right)=0 \;\rightarrow\; -\frac{\partial p}{\partial y}+\eta\frac{\partial^2 u_y}{\partial y^2}=0. \tag{2.9}$$

The second element of the lubrication limit is to assume that the horizontal speed is much greater than the vertical velocity: $|u_x| >> |u_y|$, so that basically the flow is in the x-direction. It follows that $\partial p/\partial y \simeq 0$ and $\partial p/\partial x$ is independent of y. The top and bottom cylinder boundaries are described by

$$y_T(x)=-\sqrt{a_T^2-x^2}+\frac{h}{2}+a_T;\; y_B(x)=\sqrt{a_B^2-x^2}-\frac{h}{2}-a_B, \tag{2.10}$$

where a_T and a_B are the radii of the top and bottom cylinders. Now equation (2.8) is solved under no-slip boundary conditions. One obtains

$$u_x(y)=\frac{1}{2\eta}\frac{\partial p}{\partial x}\left[y^2-y\left(y_T(x)+y_B(x)\right)+y_T(x)\,y_B(x)\right]. \tag{2.11}$$

The equation of continuity is integrated between the two solid boundaries; the top

one moves at velocity $v_y(T)$ and the bottom one at velocity $v_y(B)$:

$$\frac{\partial u_x}{\partial x}+\frac{\partial u_y}{\partial y} = 0 \rightarrow v_y(T)-v_y(B) = -\int_{y_B(x)}^{y_T(x)} \frac{\partial u_x}{\partial x} dy =$$

$$-\frac{\partial}{\partial x}\int_{y_B(x)}^{y_T(x)} u_x dy = -\frac{1}{12\eta}\frac{\partial}{\partial x}\left[\frac{\partial p}{\partial x}(y_B-y_T)^3\right]. \tag{2.12}$$

The second step is permitted because the velocity u_x vanishes at the boundaries, (see Appendix B). The pressure gradient is now solved in terms of the relative boundary velocity $v_y(T)-v_y(B)$. The problem is symmetric in x and therefore the pressure must be a symmetric function and the horizontal pressure gradient must vanish at $x=0$. Therefore

$$\frac{\partial p}{\partial x} = -\frac{12\eta\left[v_y(T)-v_y(B)\right]x}{(y_B-y_T)^3}. \tag{2.13}$$

The vertical component of the force on a section of length L of the top particle is now easily calculated as

$$F_y = -L\int_{-\pi/2}^{\pi/2} p\cos\varphi r_T d\varphi. \tag{2.14}$$

A little elaboration is convenient; write

$$F_y = -L\int_{-\pi/2}^{\pi/2} p\cos\varphi r_T d\varphi = -L\int_{-1}^{1} p r_T d\sin\varphi \tag{2.15}$$
$$= -L\int_{-r_T}^{r_T} p dx = -L\left[px\right]_{-r_T}^{r_T} + L\int_{-r_T}^{r_T} x\frac{\partial p}{\partial x}dx.$$

The stock term vanishes because the pressure vanishes at large distances, so

$$\frac{F_y}{L} = 12\eta\left[v_y(T) - v_y(B)\right]\int_{-a_T}^{a_T}\frac{x^2}{\left[y_T(x) - y_B(x)\right]^3}dx. \tag{2.16}$$

To do the integral the denominator in the integrand is expanded in a Taylor series in x. The highest order that can be done analytically is six. An algebra program is employed and in the limit $h/a \to 0$ the result for equal radii ($a_T = a_B = a$) is calculated. The intermediate steps are here given. The Taylor expansion is

$$\left[y_T(x) - y_B(x)\right]^3 \to -\frac{x^6\left(3h^2 + 12ha + 8a^2\right)}{8a^5} - \frac{3hx^4\left(h + 4a\right)}{4a^3} - \frac{3h^2x^2}{a} - h^3. \tag{2.17}$$

The approximation $h/a \to 0$ then yields

$$\left[y_T(x) - y_B(x)\right]^3 \to -\frac{x^6}{a^3} - \frac{3hx^4}{a^2} - \frac{3h^2x^2}{a} - h^3. \tag{2.18}$$

The quality of the approximation is very good, as illustrated in Figure 2.2.

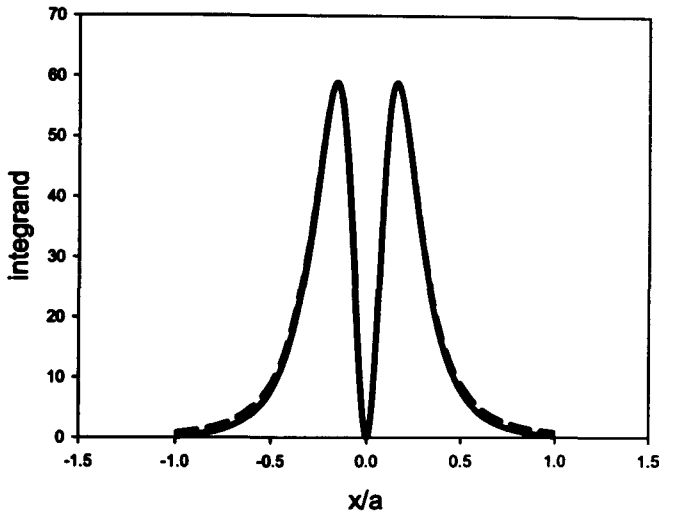

Fig 2.2. The integrand of Equation (2.16) normalise to the particle radius a for $h/a = 0.05$.The integrand is the solid line and the approximation is the dashed line.

$$\int_{-r}^{r} \frac{x^2}{[y_T(x) - y_B(x)]^3} dx \rightarrow \int_{-r}^{r} \frac{x^2}{-\frac{x^6}{a^3} - \frac{3hx^4}{a^2} - \frac{3h^2x^2}{a} - h^3} dx = \tag{2.19}$$

$$\frac{a^{3/2}\left[2(h+a)^2 \tan^{-1}\left(\sqrt{\frac{h}{a}}\right) - \pi h^2 + \sqrt{a}\left(2h^{3/2} - 2\pi h\sqrt{a} - 2a\sqrt{h} - \pi a^{3/2}\right)\right]}{2h^{3/2}(h+a)^2}.$$

Taking again the limit $h/a \to 0$ gives the result

$$\frac{F_y}{L} = 6\pi\eta \left[v_y(T) - v_y(B)\right] \left(\frac{a}{h}\right)^{3/2}. \tag{2.20}$$

For unequal radii the result is somewhat harder to write down in a simple formula, but it is easily presented in graphical form. To that end a factor $Z(a_B/a_T)$ is defined such that the force per unit length is

$$\frac{F_y}{L} = \eta Z\left(\frac{a_B}{a_T}\right) \left[v_y(T) - v_y(B)\right] \left(\frac{a_T}{h}\right)^{3/2}. \tag{2.21}$$

The factor $Z(a_B/a_T)$ is plotted in Figure 2.3.

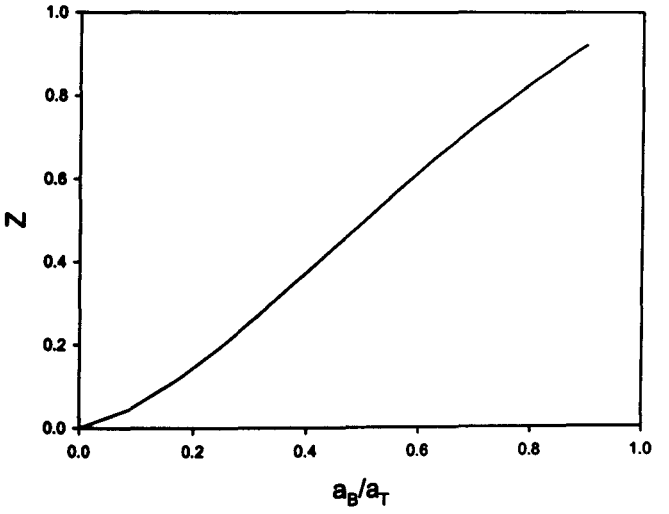

Fig 2.3 The factor Z as a function of the ratio of the cylinders a_B/a_T.

2.3. Rough particles

The result of the fluid-mediated interaction between two particles is essentially that they can never touch at finite relative velocity: if $h \rightarrow 0$ then $\dot{h}$ must vanish. This outcome is the result of the assumption of perfectly smooth surfaces. This analysis is correct when particles are far apart (though still in such a way that $h << D$); when particles come very close together the analysis fails, because real particles are never smooth. This fact has been recognised in the literature and in this section a short review will be presented.

According to Da Cunha and Hinch (1966) the roughness does not affect the interactive force very much while the particles do not touch. The effects of particle roughness are implemented as follows. Instead of considering the gap width h in formulas for the interaction parameter, $h + h_0$ is used, where h_0 is a measure for the size of the asperities. Thus when h approaches zero the force remains finite. Particles can touch and they will do so at finite velocity. This removes the singularity for $h \rightarrow 0$.

Smart and Leighton (1989) consider smooth particles sparsely covered with small hemispherical asperities, see Fig 2.4. They assume, as a first approximation, that the asperities have little or no influence on the behaviour of the fluid flow. The latter is then still treated using the lubrication limit, but the particles can

make solid contact when the asperities touch another solid surface. The asperities have height h_0, so

$$F = -\frac{3\pi\eta r^2 \dot{h}}{2(h+h_0)} \text{ while } h > 0 \text{ and solid contact for } h = 0. \qquad (2.22)$$

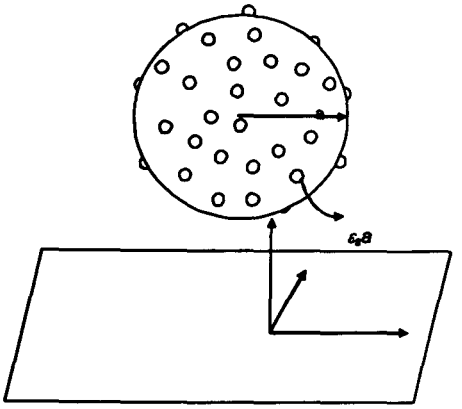

Fig 2.4 Sketch of the particles with roughness as envisaged by Smart and Leighton (1989).

Patir and Cheng (1978) consider a rough surface (densely covered with asperities) and they model the fluid flow numerically using an average flow model. The surface-to-surface distance is characterised by h, but this is the mean distance between the surfaces. It can never become zero, because (see Figure 2.5) asperities will touch when h approaches the standard deviation of the asperity height.

In addition the flow field is modified by the presence of the asperities. Patir and Chang (1978) insert ϕ_r, a factor in the formula for the force. This factor is determined from the numerical simulations and depends on the ratio of the surface-to-surface distance and the standard deviation σ of the surface roughness heights: $\phi_r(h/\sigma) \approx -0.9\exp(-0.56h/\sigma)$. The force is $F_y = -3\pi\phi_r\eta\dot{h}R^4/(2h^3)$.

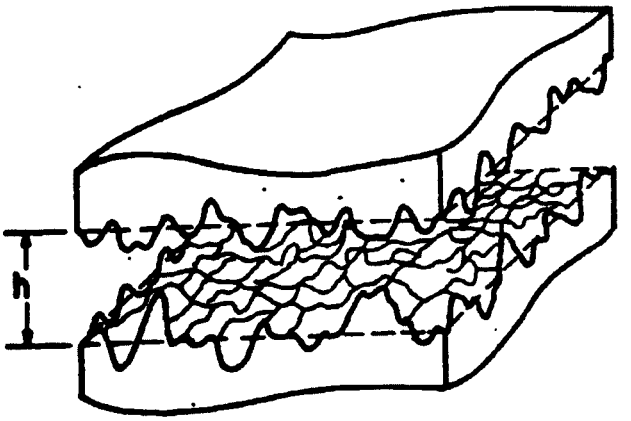

Fig 2.5 Sketch of the particles with roughness as envisaged by Patir and Cheng (1978).

Jenkins and Koenders (2005) propose a model that yields a finite interactive force at zero gap width. In this model the assumption is made that there is a dense covering of asperities, equivalent to a thin layer of porous material at the surface of each sphere. The presence of the layers permits the fluid external to them, the clear fluid, to slip at their outer surfaces. Figure 2.6 is how they envisage it. The

presence of slip at the outer surfaces of the porous layers covering the spheres results in a relation between relative velocity and the force that is not singular.

They compare their theory with both Patir and Chang (1978) and Smart and Leighton (1989). They find that the modelling parameters required for the porous layer are such that they compare well with these two theories for dense and sparse coverings.

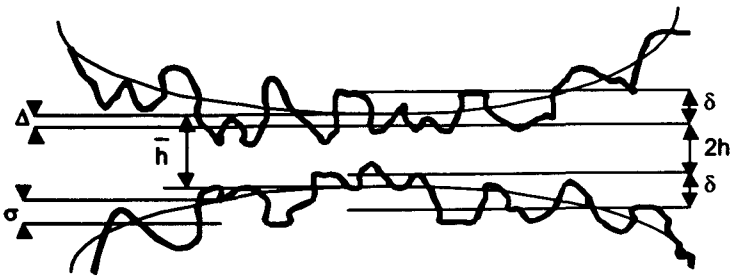

Fig 2.6 Rough particles as envisaged by Jenkins and Koenders (2005).

In what follows a rough interaction is used for the particles. This is implemented by modifying the formulas for the interaction for smooth particles by replacing h with $h + h_0$.

2.4. Collisions

2.4.1. General

When the two particles touch at some stage in the process, then a collision takes place. The dynamics that rules this process is here briefly reviewed, as it will be required later on.

On impact the relative velocity is reversed and the particles will bounce away from one another with a new initial velocity, which is given by the coefficient of restitution e_c. We call the velocities of two particles before the collision $\mathbf{v}_1, \mathbf{v}_2$ and after the collision $\mathbf{v}_1', \mathbf{v}_2'$. Their masses are m_1, m_2. Conservation of momentum dictates that

$$m_1\mathbf{v}_1 + m_2\mathbf{v}_2 = m_1\mathbf{v}_1' + m_2\mathbf{v}_2'. \tag{2.23}$$

The relative velocity before the collision is $\mathbf{v}_{12} = \mathbf{v}_2 - \mathbf{v}_1$ and after the collision $\mathbf{v}_{12}' = \mathbf{v}_2' - \mathbf{v}_1'$. The normal velocity before the collision is

$$\mathbf{g} = \left(\mathbf{v}_{12}.\mathbf{n}^{12}\right)\mathbf{n}^{12}. \tag{2.24}$$

The coefficient of restitution operates such that

$$\mathbf{g}' = -e_c \mathbf{g}. \tag{2.25}$$

The tangential velocity is left unchanged by the collision. Now the resulting velocities can be solved. Call

$$m_{eff} = \frac{m_1 m_2}{m_1 + m_2}. \tag{2.26}$$

then:

$$\mathbf{v}_1' = \mathbf{v}_1 - \frac{m_{eff}}{m_1}(1 + e_c)\left(\mathbf{v}_{12}.\mathbf{n}^{12}\right)\mathbf{n}^{12};\ \mathbf{v}_2' = \mathbf{v}_2 - \frac{m_{eff}}{m_2}(1 + e_c)\left(\mathbf{v}_{12}.\mathbf{n}^{12}\right)\mathbf{n}^{12}. \tag{2.27}$$

The duration of the collision process is here taken to be infinitely short.

These formulas are obviously true for dry contacts, but in this thesis contacts are in a fluid and the question is whether they remain valid. The answer is to compare interaction times. The actual solid contact time is assumed to be very short compared to the the total interaction time of the two particles. So, during solid contact the fluid may be supposed to "stand still". Under these conditions the above formulas are a reasonable approximation of the solid contact physical

process.

2.4.2. Two particles pushed together by a constant force

The above formulae are now employed to study how two spherical particles behave when they are pushed together by a constant force between them. This is a one-dimensional problem. The constant force is called F_0; the particle locations are x_1 and x_2. The lubrication interacitive force for spheres is employed and thus the equations of motion are

$$m\ddot{x_1} = -\frac{3\pi D^2\eta}{8\left(h+h_0\right)}\left(\dot{x}_1-\dot{x}_2\right)+\frac{1}{2}F_0;\; m\ddot{x_2} = \frac{3\pi D^2\eta}{8\left(h+h_0\right)}\left(\dot{x}_1-\dot{x}_2\right)-\frac{1}{2}F_0. \quad (2.28)$$

Subtracting gives

$$m\ddot{h} = -\frac{3\pi D^2\eta}{4\left(h+h_0\right)}\dot{h}+F_0. \quad (2.29)$$

This is integrated once to give

$$m\left[\dot{h}\left(t\right)-\dot{h}\left(0\right)\right] = -\frac{3\pi D^2\eta}{4}\ln\left(\frac{h\left(t\right)+h_0}{h\left(0\right)+h_0}\right)+F_0t. \quad (2.30)$$

No further analytical progress can now be made; a numerical solution must be found using a Runge-Kutta procedure. Scaling of the problem, such that h is

expressed in terms of D and t is expressed in terms of $\tau_c \equiv f_\tau m/(\eta D)$, permits non-dimensional plotting. Fig 2.6 shows an illustration of the solution. The particles bounce back and are repeatedly driven together again.

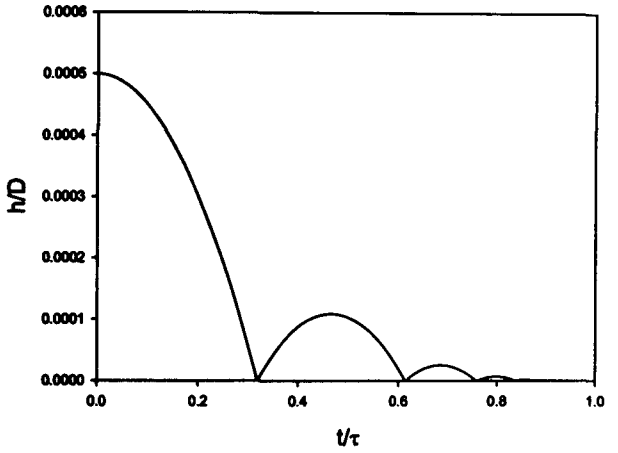

Fig 2.6. Illustration of the bounce properties of collisional/lubrication interaction: h/D as a function of t/τ. In this example the value of the time constant $\tau_c = f_\tau m/(\eta D) = 13s$. The restitution coefficient is 0.5. The force $F_0 = 27N$.

2.5. Repulsive force or definition of overlap

Finally, in this section, we discuss an aspect of the particle interaction that is encountered in the literature, especially the Stokesian Dynamics literature. In practical computing terms a finite time step means that particles will sometimes overlap. To avoid such an unphysical effect, a repulsive short range interaction is introduced, this is fully discussed in Dratler and Schowalter (1996).

A repulsive short-range force is introduced, which has a form, which is similar to the Derjaguin force in physical chemistry, see for example Atkins(1982)

$$\mathbf{F}^{(12)} = \frac{F_0}{h_0} \frac{e^{-\frac{h}{h_0}}}{1 - e^{-\frac{h}{h_0}}} \mathbf{n}^{(12)}. \tag{2.31}$$

Here F_0 is a constant, describing the intensity of the force, and h_0 the range of the interaction. Dratler and Schowalter (1996) find that structures disappear for smooth particles when the range is increased from zero to a small fraction of the mean particle diameter (but this could be of the order of magnitude of the mean surface-to-surface distance). Usually, a short range repulsive force is introduced between the spheres to model qualitatively the effect of this non-hydrodynamic interaction. This is a *numerical convenience*, which has the advantage of preventing any overlapping close encounters between the particles. In our work we already have a roughness length in the lubrication interaction, so there appears to be little need for an extra (elastic) force. However, the introduction of the extra elastic force is so ingrained in the slurry flow simulation community that its effect should be discussed in the simulation results. It has an important effect on structures formation and it will be reviewed in Chapter 7.

3. Existing migration models

3.1. Introduction

In the last 20 years various models have been put forward to describe and explain the migration phenomenon described in Chapter 2. In this chapter the main models are discussed and their features are investigated in a channel flow geometry. Despite being a simple geometry, the advantages and shortcomings of the published models are quite clearly exposed with a minimum of mathematical elaboration. In this geometry, which also permits easy experimentation (see Lyon and Leal (1998)), the particles migrate to the centre of the channel. For simplicity the particles are assumed to be spherical and monodisperse; the latter implies that no segregation has to be accounted for. The particles are not perfectly smooth. The flow regime and particle size are such that the Brownian motion is irrelevant. In practical flow situations this means that the particles are super-micron sized and such particles are never perfectly smooth, though their surface asperity roughness is much smaller than the particle diameter. The flow regime is characterised by the channel Reynolds number and the Peclet number. The former is small (less than unity); the latter infinite. The ratio of the particle diameter to the channel width is very much smaller than unity and the length of the channel is much

greater than its width.

The very fact that there exist various approaches implies that the physics of the subject of dense slurry flow is not entirely settled yet. For historical reasons the Bingham plastic model has been incorporated in the review, though this model was never primarily devised to describe dense slurry flow. Nevertheless, it has some interesting features and produces a cross-streamline profile that could be associated with a solidosity distribution, albeit primitively. The next class of models is due to Leighton and Acrivos (1987) and Phillips *et al* (1992). In these models a phenomenological constitutive diffusion relation (Fick's law) is used. The constitutive features of the diffusion coefficient vary somewhat, but they share properties that are particularly keenly demonstrated in the channel flow problem. A different class of models is the granular temperature set of models due to McTigue and Jenkins (1992) and Nott and Brady (1994). In these models the fluctuational motion is characterised by a temperature field and appropriate equations are developed to characterise this field in conjunction with the other relevant fields. A brief discussion of the boundary conditions is provided below. Finally, a new model that recognises the inherent anisotropy of the field parameters is discussed; this model has been published recently by Morris and Miller (2006), as well as Stickel *et al* (2005), and the channel flow problem exposes its features.

In the sections below the particle radius is denoted by a and the channel width by $2W_w$. The flow velocity in the channel is called u (only one component is needed, as it is a one-dimensional problem). The streamwise and cross-streamwise co-ordinates are x and y, respectively. The pressure is p, the shear stress is denoted by τ and the shear rate $\partial u/\partial y$ is abbreviated to $\dot{\gamma}$.

3.2. Bingham plastic flow model

The Bingham plastic model is one of the oldest models to describe non-uniform flow through a channel, see textbooks, such as Bird *et al* (1982). This model describes plug flow. To make it applicable to particle-laden flow a two-solidosity model must be put forward. There is a critical solidosity ϕ_s. Inside the plug the condition $\phi > \phi_s$ holds and outside the plug $\phi < \phi_s$. Inside the plug the particles are interlocked to such an extent that they cannot shear. Introducing two volume fractions ϕ_p and ϕ_f, such that $\phi_p > \phi_s$ and $\phi_f < \phi_s$, a simple - first order - model can be set up. The flow is assumed to organise itself in such a way that all the particles inside the plug are at a volume fraction ϕ_p and all the particles outside the plug are at ϕ_f. Now, if the plug width is $2P$ then plainly

$$\overline{\phi} = \frac{1}{W_w}\left(P\phi_p + (W_w - P)\,\phi_f\right). \tag{3.1}$$

This defines the plug half-width P for the cases of sufficiently dense flow: $\overline{\phi} > \phi_f$. In a Bingham model in a channel flow situation the shear stress is given by

$$\tau = \frac{\partial p}{\partial x} y; \tag{3.2}$$

therefore the yield stress is $\tau_0 = P\partial p/\partial x$. The other parameter in the Bingham model is the fluid viscosity, which here is $\mu(\phi_f)$. (In the next section a simple viscosity function of the solidosity will be introduced, see also Section 3.3).

So, instead of the traditional two parameters of the Bingham model, the yield stress τ_0 and the fluid viscosity μ, two solidosities are introduced that lead to these parameters: ϕ_p and ϕ_f. In the traditional Bingham model the yield stress is a given material parameter, but in the application here it is a parameter that depends on the pressure gradient. While this is an exceedingly primitive model, it does give a first-order idea of the migration in a channel. The constitutive model then reads

$$\tau = \pm\tau_0 + \frac{\partial u}{\partial y}\mu(\phi_f), \quad |y| > P. \tag{3.3}$$

Thus for $y > P$ the fluid velocity gradient is

$$\begin{aligned} \frac{\partial u}{\partial y} &= \frac{1}{\mu(\phi_f)} \frac{\partial p}{\partial x} (y - P), \quad y > P \\ \frac{\partial u}{\partial y} &= \frac{1}{\mu(\phi_f)} \frac{\partial p}{\partial x} (y + P), \quad y < -P \end{aligned} \tag{3.4}$$

Note that the gradient vanishes at the plug boundary $y = P$. To obtain the fluid velocity a boundary condition needs to be applied. No-slip at the boundary $y = W_w$ gives

$$\begin{aligned} u(y) &= \frac{1}{2\mu(\phi_f)} \frac{\partial p}{\partial x} \left[y^2 - 2Py + W_w (2P - W_w) \right], \quad y > P; \\ u(y) &= \frac{1}{2\mu(\phi_f)} \frac{\partial p}{\partial x} \left[y^2 + 2Py + W_w (2P - W_w) \right], \quad y < -P; \\ u(y) &= -\frac{1}{2\mu(\phi_f)} \frac{\partial p}{\partial x} (W_w - P)^2, \quad |y| \leq P. \end{aligned} \tag{3.5}$$

This relation is plotted in Figure 3.1.

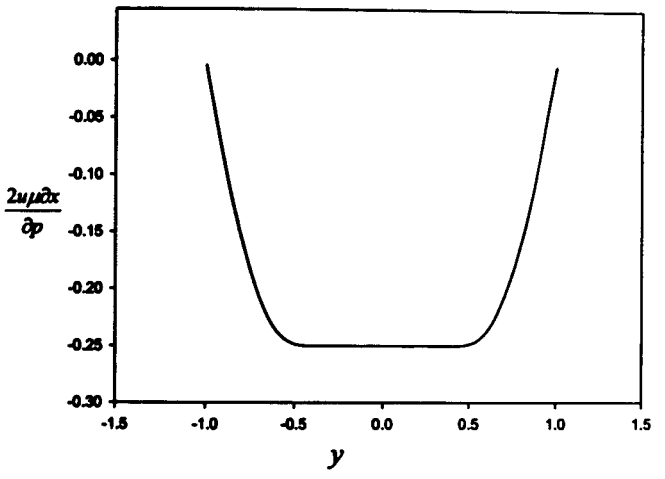

Fig 3.1. Plot of velocity inside and outside the plug for Bingham plastic model, equation (3.5).

3.3. Diffusive models

The Diffusive Flux Model was introduced by Leighton and Acrivos (1987) and Phillips *et al* (1992). The initial intention of these models was to describe Couette flow. While these are phenomenological models, the authors do introduce some physical argumentation by way of support.

As an auxiliary feature a solidosity-dependent viscosity is required. A simple relation is the one put forward by Krieger (1972). The viscosity of the mixture μ

depends on the solidosity ϕ as follows

$$\mu(\phi) = \eta\left(1 - \frac{\phi}{\phi_m}\right)^{-n}, \tag{3.6}$$

where η is the fluid viscosity and ϕ_m and n are two parameters. ϕ_m is the maximum packing volume fraction ($\phi_m = 0.68$ for rigid spheres, though this is the static value and the real value may be somewhat lower in practical flow applications); n is determined from experiments (see Thomas (1965)) and a reasonable value appears to be $n = 1.82$.

A note on the maximum packing density should here be provided. The maximum closest packing for equal spheres is the hexagonal close packing, which yields a volume fraction of $\pi/\sqrt{18} = 0.74048....$ The random closest packing has recently been determined at 'roughly' 0.64, see Anikeenko and Medvedev (2007). When Krieger wrote his paper the random close limit was believed to be slightly higher at 0.68. Krieger determined the value from an experimental curve fit of equation (3.6), but in these experiments the maximum density was of course never quite achieved.

In Section 3.3 more will be explained about viscosity relations, because relation (3.6) assumes that the structure of the suspension is isotropic while essentially the

mixture is regarded as a Newtonian fluid. The latter implies that the shear stress τ is obtained from the shear rate $\dot{\gamma}$ as

$$\tau = \mu(\phi)\,\dot{\gamma}. \tag{3.7}$$

Stress equilibrium now states that

$$-\frac{\partial p}{\partial x} + \frac{\partial \tau}{\partial y} = 0. \tag{3.8}$$

The equation of continuity is satisfied automatically in a one-dimensional problem.

The above equations are, of course, standard expressions for the flow of a fluid in a channel; the new element is introduced by considering some form of Fick's law, which states that the instantaneous materials flux $\mathbf{N}$ is proportional to the concentration gradient $\nabla\phi$. The materials flux, which is the volume of material that crosses a unit area per unit time, satisfies the continuity equation

$$\frac{\partial \phi}{\partial t} + \nabla.\mathbf{N} = 0. \tag{3.9}$$

The materials flux for a single species of particle (as is the case for monodisperse mixtures) equals $\phi\mathbf{v}$, where $\mathbf{v}$ is the material velocity (of which u is the

x-component).

The phenomenology that is introduced in the diffusive flux models is now outlined. The authors of these models recognise various mechanisms by which diffusion may take place. These mechanisms give rise to different fluxes, which are all added up to give the total flux. In steady state $\partial\phi/\partial t = 0$, thus $\nabla.\mathbf{N} = 0$. Four mechanisms for diffusion have been recognised: (1) a collisional mechanism, (2) a viscosity gradient mechanism, (3) a shear stress gradient mechanism and (4) a molecular mechanism. In what follows (4) will be neglected as the particles are deemed to be sufficiently heavy that this mechanism is irrelevant. The collisional mechanism, which is a very important feature in dense slurry flow, leads to peculiar results, which ultimately must lead to a rejection of the diffusive flux class of models, as it gives unphysical results.

Generally, diffusion can only take place when there are irreversible processes at work. So for each of these mechanisms the irreversible element needs to be identified.

3.3.1. Collisional mechanism

In the case of the collisional mechanism the particles can touch one another and in the "collision" that takes place transfer of momentum takes place because

the relative speed of impact between a particle pair is greater than the relative speed of separation after the collision. This is a very clear mechanism. It can only take place when the particle surfaces have a roughness. When particles are perfectly smooth they can never touch, see da Cunha and Hinch (1966), Jenkins and Koenders (2005) and Davis and Koenders (2007a). In Section 7.2 this is further elaborated. Phillips *et al* (1992) develop an expression for the diffusion coefficient, based on a scaling argument for irreversible two-body motion. In the argument a test particle experiences a number of collisions that is proportional to $\dot{\gamma}\phi$. The spatial variation in the collision frequency over a distance of the order of the particle radius a is then $a\nabla(\dot{\gamma}\phi)$. The assumption the authors make is that particle migration velocity is linearly proportional to $a\nabla(\dot{\gamma}\phi)$. The flux $\mathbf{N}$ is therefore proportional to $\phi a\nabla(\dot{\gamma}\phi)$. The missing dimensional factor here is a length and therefore the authors suggest that the proportionality constant is set to a nondimensional coefficient K_c (the subscript refers to "collision") times the particle radius a. This simple argument leads to

$$\mathbf{N} = -K_c a^2 \phi \nabla(\dot{\gamma}\phi). \tag{3.10}$$

A solution for the channel flow problem is now easily obtained. From continuity

it follows that $\nabla.\mathbf{N} = 0$, which leads to

$$\frac{\partial}{\partial y}\left[K_c a^2 \phi \frac{\partial(\dot{\gamma}\phi)}{\partial y}\right] = 0. \tag{3.11}$$

In fact the term inside the square brackets vanishes, as it represents the particle flux and in the steady state the particle flux is zero. From (3.8) and (3.7), furthermore, one obtains

$$-\frac{\partial p}{\partial x} + \frac{\partial(\mu(\phi)\dot{\gamma})}{\partial y} = 0. \tag{3.12}$$

The pressure gradient is a constant, independent of y. Furthermore, at the centre of the channel - $y = 0$ - the shear rate $\dot{\gamma}$ vanishes, so the two equations lead to

$$\phi \frac{\partial(\dot{\gamma}\phi)}{\partial y} = 0. \tag{3.13}$$

$$\mu(\phi)\dot{\gamma} = \frac{\partial p}{\partial x} y. \tag{3.14}$$

Or, combining, and assuming that the solidosity is never zero

$$\frac{\partial}{\partial y}\left(\frac{\partial p}{\partial x}\frac{y\phi}{\mu(\phi)}\right) = 0. \tag{3.15}$$

The pressure gradient is independent of y, therefore the solution of Equation (3.15) is

$$\frac{y}{A_c} = \frac{\mu(\phi)}{\phi}, \tag{3.16}$$

where A_c is an integration constant. It is immediately clear that this does not represent a physical solution, because the function $\mu(\phi)/\phi$ is never zero. Therefore, the collisional mechanism on its own does not describe the migration phenomenon.

3.3.2. Viscosity gradient mechanism

This mechanism is also described by Phillips *et al* (1992) and also by Leighton and Acrivos (1987).

The idea is that if two particles form a doublet in the presence of a viscosity gradient the doublet may be wrenched out of the straight streamline by rotation. This would happen, because the viscosity on the densely packed side of the doublet is greater than that on the more dilute side, thus causing more resistance to flow on the dense side to which the doublet will respond by rotation. This is clearly an irreversible process. It is a possible mechanism if doublets are prevalent; this may be the case, because in the lubrication interaction the force required to separate two nearby particles at gap width h is proportional to h^{-1}. Therefore, if particles have taken positions that are very close together their relative velocity will be

small and the endurance of the doublet is great. Thus they operate as one, very elongated particle, which makes the rotation degree of freedom important.

Leighton and Acrivos (1987) suggest an expression for the materials flux associated with a viscosity gradient. This is essentially a scaling argument. The diffusion coefficient itself contains no ingredients with the dimension of a Pascal and therefore the viscosity gradient must be counteracted by the viscosity itself to arrive at a diffusion coefficient. A time scale is again provided by the local shear rate (the interaction frequency is proportional to $\dot{\gamma}a$) and a length scale by the particle radius a. Thus the authors come up with a flux $\mathbf{N}_\mu$ for this particular process that has the form

$$\mathbf{N}_\mu = -K_\mu \dot{\gamma} \phi^2 \left(\frac{a^2}{\mu(\phi)} \right) \frac{\partial \mu(\phi)}{\partial \phi} \nabla \phi. \tag{3.17}$$

Here K_μ is another constant.

The flux due to the viscosity gradient is added to the collisional flux and employing the equation of continuity,as before, the resulting equations are

$$\frac{\partial}{\partial y} \left[K_c a^2 \phi \frac{\partial (\dot{\gamma}\phi)}{\partial y} + K_\mu \dot{\gamma} \phi^2 \left(\frac{a^2}{\mu(\phi)} \right) \frac{\partial \mu(\phi)}{\partial \phi} \frac{\partial \phi}{\partial y} \right] = 0; \tag{3.18}$$

$$-\frac{\partial p}{\partial x}+\frac{\partial\left(\mu\left(\phi\right)\dot{\gamma}\right)}{\partial y}=0. \tag{3.19}$$

Similar manipulations as in the previous sub-sub-section and setting the total particles flux to zero then lead to

$$K_c a^2 \phi \frac{\partial\left(y\phi/\mu\left(\phi\right)\right)}{\partial y}+K_\mu \frac{y}{\mu\left(\phi\right)}\phi^2\left(\frac{a^2}{\mu\left(\phi\right)}\right)\frac{\partial\mu\left(\phi\right)}{\partial\phi}\frac{\partial\phi}{\partial y}=0. \tag{3.20}$$

Will the viscosity gradient mechanism solve the problems at $y=0$ that the collisional mechanism suffered from? The answer is "yes". Equation (3.20) has an analytical solution; introduce an integration constant B, then

$$\frac{|y|}{B}=\phi^{-1}\mu\left(\phi\right)^{1-K_\mu/K_c} \tag{3.21}$$

The function $\phi^{-1}\mu\left(\phi\right)^{1-K_\mu/K_c}$ approaches zero when $K_\mu/K_c>1$. The zero point occurs for $\phi=\phi_m$, implying that no solution can exist that does not lead to the maximum density in the centre of the channel.

Another problem associated with this solution is that the derivative $\partial\phi/\partial y$ may jump in $y=0$; there can be a so-called "0cusp". The derivative in $y=0$ is evaluated from the solution (3.21): $\left(\partial\phi/\partial y\right)_0=\pm 1/\left[B\partial/\partial\phi\left(\phi^{-1}\mu\left(\phi\right)^{1-K_\mu/K_c}\right)_{\phi_m}\right]$.

Simple arithmetic shows that this derivative is infinite in magnitude when $K_c/K_\mu < n/(n+1)$ and zero when $K_c/K_\mu > n/(n+1)$. For $n = 1.82$, $n/(n+1) = 0.645$. Phillips *et al* (1992) have established that $K_c/K_\mu \simeq 0.66$, thereby avoiding the cusp in channel flow in the second decimal place.

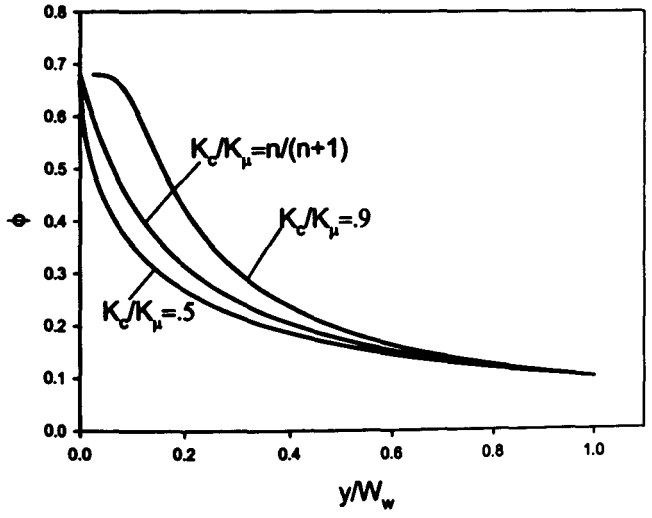

Fig 3.2. Plot of the solidosity as a function of the position in the channel for various values of the ratio K_c/K_μ.

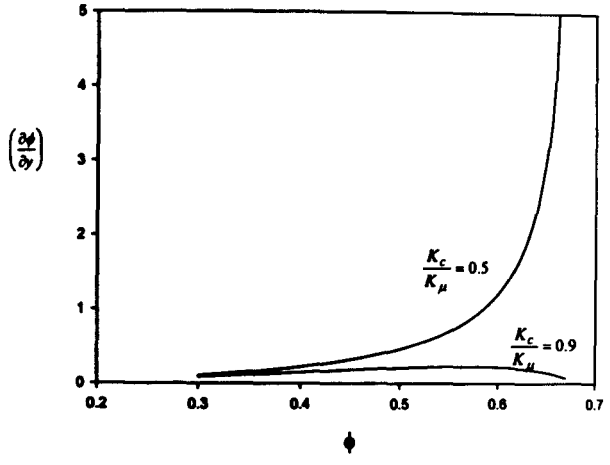

Fig 3.3. Solidosity gradient as a function of the solidosity for various values of K_c/K_μ.

The findings are summarised in the two plots, Figs 3.2 and 3.3. The behaviour of the solidosity profile near the centre of the channel is evident.

3.3.3. The shear stress gradient mechanism

This mechanism is described by Leighton and Acrivos (1987), but not included in the key paper by Phillips *et al* (1992). The mechanism operates not on a solidosity gradient, but occurs in a homogeneous mixture where there is a stress gradient. A scaling argument similar to that for the viscosity gradient mechanism leads to

an expression for the particles flux of the form

$$N_\tau = K_\tau \frac{\phi^2}{\tau} \frac{\partial \tau}{\partial y} \dot{\gamma} a^2 \tag{3.22}$$

Leighton and Acrivos (1987) employ this expression to calculate the onset of migration in start-up flow. Otherwise, it has not been employed by other authors. It has no application to the problem of migration in steady channel flow, as there is no solidosity gradient in Formula (3.22).

3.4. Granular Temperature models

3.4.1. General outline

These models are entirely different from the phenomenological models discussed so far. The main versions of the granular temperature models are due to McTigue and Jenkins (1992) and Nott and Brady (1994), both stemming from the early 1990s. Here the McTigue and Jenkins version will be used, because it is based on a simple scaling, while Nott and Brady's paper (1994) is founded on a numerical simulation. In order to do justice to these theories tensor notation will be employed, (see appendix A).

Granular temperature theory is a continuum theory. The conservation of mass

and linear momentum are of course valid. A particle-fluid mixture as described in the introduction of this chapter possesses a solidosity ϕ and a stress tensor $\boldsymbol{\sigma}$. The equations of continuity of mass and linear momentum for steady state processes read

$$\frac{\partial(\phi v_i)}{\partial x_i} = 0; \tag{3.23}$$

$$f_i + \frac{\partial \sigma_{ij}}{\partial x_j} = 0. \tag{3.24}$$

Here the vector $\mathbf{f}$ represents the body force, for example one associated with the gravity field $\phi(\rho_s - \rho_f)\,\mathbf{g}$ (ρ_s and ρ_f are the mass densities of the solid and fluid, respectively and $\mathbf{g}$ is the acceleration due to gravity). The vector $\mathbf{v}$ is the mixture velocity. In McTigue and Jenkin's (1992) version the spheres are deemed to be neutrally buoyant ($\rho_s = \rho_f$) and the fluid merely mediates the interactive force between the particles. The fluid motion is not solved in any detail and the fluid stress is represented by a pressure term only. The stress tensor $\boldsymbol{\sigma}$ is therefore the intergranular stress minus a fluid pressure. The theory is easily amended to introduce body forces, *etc.* The simplifying assumptions are made to clarify the structure of the theory.

The equations of continuity themselves are not sufficient to solve a problem in a given geometry. If constitutive equations are supplied in the usual way, relating

the components of the stress tensor to those of the velocity gradient, there are five variables in the problem (ϕ, v_x, v_y, v_z and the pressure p) and four equations. So there is no possible solution. McTigue and Jenkins(1992) propose to solve this problem by introducing another field variable, the granular temperature T, an extra equilibrium equation and two further constitutive equations: Fourier's law for the heat flux and a relation between the intergranular pressure and the granular temperature. This is common practice in the description of dry granular flow (see for example Jenkins and Savage (1983)). Purely from a mathematical perspective this leads to a system in which the number of equations equals the number of variables. It is a more complicated theory than the theories discussed above.

The physical background to the theory is as follows. In a dense slurry purely affine motion (that is motion entirely associated with a uniform strain rate) is impossible; particles need to make excursions to avoid one another. The extra motion - in addition to the motion given by the strain rate - needs to be accounted for, as it represents extra work done. The extra fluctuational motion is characterised by a scalar variable, the temperature - just like the molecular motion in a gas. So, when an energy dissipation balance is set up, effects from the fluctuational motion need to be accounted for. Furthermore, in the granular temperature model, the

fluctuations are responsible for an extra pressure term in the intergranular stress; this is the so-called *particle pressure*. The particle pressure describes the transfer of momentum in collisions between particles. The collisions - or solid contacts - will only take place when the particles are rough (this has been explored in much greater detail in Section 2.3). In addition McTigue and Jenkins (1992) hypothesise that the momentum transfer that takes place is proportional to the speed of the fluctuational motion. The theory leads to migration effects. The idea that collisions and fluctuations are somehow linked had already been put forward by Leighton and Acrivos (1987) and Phillips *et al* (1992), see Section 3.3.

3.4.2. Scaling the granular temperature theory and general formulae

The key interaction between particles, as mediated by the fluid, is the lubrication interaction, which is valid when the ratio of the gap width h to the particle diameter D is much smaller than unity. The force with which particles oppose their relative normal motion equals $3\pi\eta D^2\dot{h}/(8h)$. Therefore, the non-dimensional ratio D/h provides a good scaling parameter. Dimensions are completed by supplying factors of η and D. Furthermore, all bulk physical parameters will be proportional to the solidosity ϕ.

The stress σ in a slurry as described in the Introduction will consist of two

parts, a pressure term and a deviatoric part $\mathbf{t}$. The pressure is the sum of the fluid phase pressure p and the particle pressure $\overline{p}$. The viscous part of the intergranular stress is given by an isotropic viscosity-type constitutive equation with two Lamé coefficients $\overline{\lambda}$ and $\overline{\mu}$. So, the tensor $\mathbf{t}$ is related to the strain rate $\mathbf{d}$ ($d_{ij} = \frac{1}{2}\left(\partial v_i/\partial x_j + \partial v_j/\partial x_i\right)$) as

$$t_{ij} = \overline{\lambda} d_{kk}\delta_{ij} + 2\overline{\mu} d_{ij}. \tag{3.25}$$

The granular temperature is defined as the sum of the fluctuation speeds in a physically infinitesimally small element (*i.e.* many particles, but small representative volume; this is similar to the 'material point' in continuum mechanics)

$$T = \frac{1}{2}\overline{\left[\left(v_x'\right)^2 + \left(v_y'\right)^2 + \left(v_z'\right)^2\right]}, \tag{3.26}$$

where the prime denotes a fluctuation (that is $\mathbf{v}' = \mathbf{v} - \overline{\mathbf{v}}$) and the over bar is a volume average.

The rate of working of a control volume (per unit volume) is compensated by two factors. The first is that granular heat can be taken away or supplied to the volume. To describe this a heat flux vector $\mathbf{Q}$ needs to be introduced, the divergence of $\mathbf{Q}$ is the heat source. The second factor is the dissipation - transfer

of granular heat due to the fluctuational motion to "ordinary" thermal heat (the dissipation $\overline{\gamma}$); this term is proportional to the granular temperature. The balance equation for the rate of work of the fluctuational motion then reads

$$-\frac{\partial Q_i}{\partial x_i} + t_{jk}\frac{\partial v_j}{\partial x_k} - \overline{\gamma} = 0. \tag{3.27}$$

The first term is the divergence of the heat flux; the second term the rate of mechanical work and the third term is the dissipation. The heat flux is assumed to satisfy Fourier's law of heat conduction, with heat conduction coefficient $\overline{\kappa}$.

All the coefficients of the theory are now summarised, using the scaling suggested by the lubrication interaction

$$\overline{\lambda} = \alpha_0 \eta\phi\frac{D}{h}; \tag{3.28}$$

$$\overline{\mu} = \alpha_1 \eta\phi\frac{D}{h}; \tag{3.29}$$

$$\overline{\kappa} = \alpha_2 \eta\phi\frac{D}{h}; \tag{3.30}$$

$$\overline{\gamma} = \alpha_3 \frac{\eta\phi}{D^2}\frac{D}{h}T; \tag{3.31}$$

$$\overline{p} = \alpha_4 \frac{\eta\phi}{D}\frac{D}{h}\sqrt{T}. \tag{3.32}$$

The non-dimensional coefficients α_{0-3} are all of order unity; α_4 needs to contain input from the collision rheology, which - in its simplest form - would be a coefficient of restitution. This issue will be addressed more fully in Section 4.4.

3.4.3. Migration in channel flow using granular temperature theory

Practical calculations with the granular temperature model are very rarely done. Part of the difficulty is supplying boundary conditions. Another one is the value of the coefficients α_{0-4}; no measurements of these has been undertaken. For channel flow McTigue and Jenkins (1992) themselves solve the model for smooth boundary conditions. For rough boundaries the same problem was solved by Petford and Koenders (1998). A further "zero motion" problem has been solved. This problem is one of a geometry in which the permeable bottom of a cylindrical vessel is agitated. The slurry inside the vessel is in a fluidized state and because of the particle pressure the bottom septum is cleared of particles and therefore unclogged. It is called the zero-motion problem, because there is no strain rate or transport; the agitation keeps the conformation in a steady state. The solution to the problem is reported by Gundogdu *et al* (2003b) and Davis and Koenders (2007c).

Other than the question as to what exactly the value of the coefficients α_{0-4}

is, the fact that these may be solidosity dependent has never been explored. This is important, as in the channel flow problem the solidosity by the walls drops to a small value ($\phi < 0.2$) and the simple lubrication theory scaling beaks down. The theory can only handle dense systems. Petford and Koenders (1998) solve the dense part and connect a solution for the dilute region by employing simple viscous theory.

In order to demonstrate the capabilities of the theory below the coefficients α_{0-4} will be given an effective value. An estimate of the coefficients will be derived from a cell model in chapter 4.

In the channel configuration the equations in the previous section now take the special form, first derived by McTigue and Jenkins (1992)

$$t_{12} = \overline{\mu}\frac{\partial u}{\partial y};\ -\frac{\partial Q}{\partial y} + \overline{\mu}\left(\frac{\partial u}{\partial y}\right)^2 - \overline{\gamma} = 0;\ Q = -\overline{\kappa}\frac{\partial T}{\partial y}. \tag{3.33}$$

The stress is $\sigma_{ij} = -(p+\overline{p})\,\delta_{ij} + t_{ij}$ (p is the fluid pressure; $\overline{p}$ is the particle pressure); the stress equilibrium equation is expressed as $\partial\sigma_{ij}/\partial x_j$

$$\begin{aligned} -G + \frac{\partial t_{12}}{\partial y} &= 0;\ \frac{\partial \overline{p}}{\partial x} = 0;\ \frac{\partial t_{11}}{\partial x} = 0; \\ \frac{\partial \overline{p}}{\partial y} &= 0, \end{aligned} \tag{3.34}$$

where $G = \partial p/\partial x$. The continuity equation is satisfied automatically, because the velocity does not depend on x.

A scaling is introduced by McTigue and Jenkins (1992), which renders the equations non-dimensional. The particle velocity and granular temperature at the centre of the channel are called u_0 and T_0 respectively. Then

$$\hat{y}W_w = y, \quad \hat{u}u_0 = u, \quad \hat{T}T_0 = T. \tag{3.35}$$

Substituting this into the equations shows that non-dimensionality is achieved when

$$u_0 = \frac{GW_w^2}{\alpha_1 \mu}, \quad T_0 = \frac{\alpha_1}{\alpha_3}\frac{a^2}{W_w^2}u_0^2. \tag{3.36}$$

Now, introducing a parameter $\epsilon = \sqrt{2\alpha_2/\alpha_3}a/W_w$ and again using $s = h/D$, the relevant equations take the form

$$1 + \frac{\partial}{\partial \hat{y}}(\phi s^{-1}\frac{\partial \hat{u}}{\partial \hat{y}}) = 0; \tag{3.37}$$

$$\frac{\partial}{\partial \hat{y}}(\phi s^{-1}\hat{T}^{1/2}) = 0; \tag{3.38}$$

$$\frac{1}{2}\epsilon\frac{\partial}{\partial \hat{y}}(\phi s^{-1}\frac{\partial \hat{T}}{\partial \hat{y}}) + \phi s^{-1}\left(\frac{\partial \hat{u}}{\partial \hat{y}}\right)^2 - \phi s^{-1}\hat{T} = 0. \tag{3.39}$$

Denoting the root-mean-square fluctuation velocity $\hat{T}^{1/2}$ by $\hat{w}$ in equation (3.38) and integrating equation (3.38) once we obtain

$$\phi s^{-1}\hat{w} = \overline{k}^{-1}, \tag{3.40}$$

where $\overline{k}$ is a constant, defined by the boundary condition for the temperature and the solidosity at either the centre or the wall.

The streamwise momentum balance equation (3.37), assuming $\partial\hat{u}/\partial\hat{y}(0) = 0$, integrates to:

$$\frac{\partial\hat{u}}{\partial\hat{y}} = -\phi^{-1}s\hat{y}. \tag{3.41}$$

The equations (3.39), (3.40), and (3.41) combine to give:

$$\epsilon^2\frac{\partial^2\hat{w}}{\partial\hat{y}^2} - (1 - \overline{k}^2\hat{y}^2)\hat{w} = 0. \tag{3.42}$$

Finally, substitution of (3.40) into (3.41) and integration yields

$$\hat{u}(\hat{y}) - \hat{V} = \overline{k}\int_{\hat{y}}^{1}\hat{w}(\xi)\xi d\xi, \tag{3.43}$$

where $\hat{V} = \hat{u}(1)$ is the wall slip velocity.

When the values of $\overline{k}$, ϵ and the slip velocity at the boundaries are supplied these equations can be solved with a Runge-Kutta procedure. The purposes of this section is to demonstrate that solutions are possible and also to see what properties they have - especially for the solidosity field. Now we make use of the work by Torquato *et al* (1990). In this work a connection is given between the mean value of h/D and the solidosity. The connection is given by a constitutive equation for the separation s by Torquato *et al* (1990) for the spherical particles in the regime where the solidosity is not too small ($\phi > 0.2$).

$$s = \frac{(1-\phi)^3}{12\phi(2-\phi)}. \tag{3.44}$$

It was shown by Gundogdu *et al* (2003b) that this expression maybe approximated by the more convenient formula $\phi s^{-1} \approx 0.257e^{9.94\phi}$. Thus from equation (3.40) it follows that $0.257e^{9.94\phi(0)}\hat{w}(0) = \overline{k}^{-1}$.Therefore a solution may be generated by simply specifying $\phi(0)$ and $\overline{k}$, bearing in mind that $\hat{w}'(0) = 0$.

In Fig 3.4, below, two results are shown for $\epsilon = 0.3$ and two values of the constant $\overline{k}$. It is observed that the behaviour at the boundary for the two values is very different and this reflects the physical character of the boundary. To see how, the scaled speed is also plotted: Fig 3.5. It is observed that the temperature

gradient and therefore the granular heat supply is different at the boundary for the two cases. This may reflect the fact that in the case of the smaller temperature gradient the boundary is very bumpy, while for the larger gradient the wall is smoother.

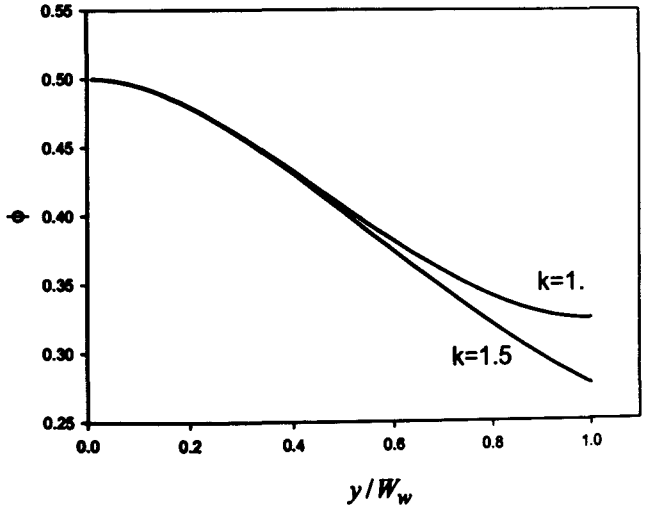

Fig 3.4. The solidosity as a function of position for two values of the integration constant $\overline{k}$. $\phi(0) = 0.5$ and $\epsilon = 0.3$.

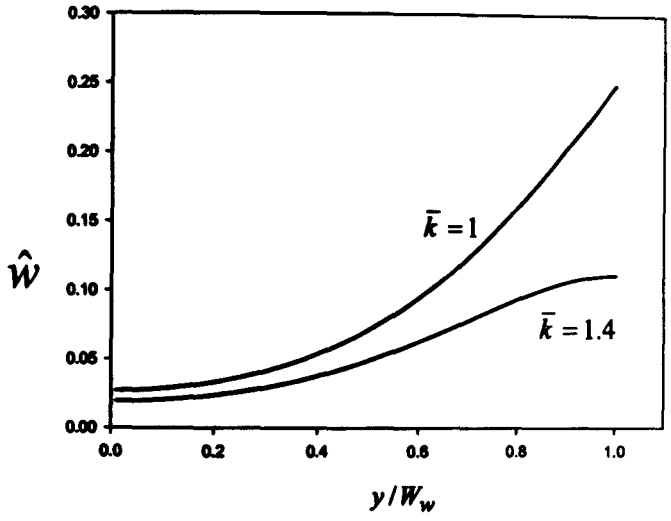

Fig 3.5. The scaled fluctuation speed as a function of position for two values of the integration constant $\bar{k}$. $\phi(0) = 0.5$ and $\epsilon = 0.3$.

This concludes a demonstration of what this model is capable of. It is very important to note that in these examples the solidosity at the centre of the channel does not have the maximum value as was required by the previous models. Solidosities well below the maximum have also been measured: Lyon and Leal (1998).

3.5. Anistropic models

Both Morris and Boulay (1999) and Stickel *et al* (2005) introduce anisotropic models for the suspension stress. In this section these models are briefly reviewed.

The main principle is as follows. The authors put forward that a sheared suspension becomes transverse anisotropic with the direction of the principal axes aligned to the principal axes of the rate of strain **d**. There is then a further extension required to deal with the situation in which there is no rate strain (as at the centre of the channel). Morris and Boulay (1999) introduce a non-local term as they want to avoid having to introduce an extra field as in the granular temperature theory. The non-local term is entirely phenomenological and for the moment this aspect is left to one side, as it is not central to this thesis.

The induced structure in the case of channel flow in which there is a shear field $\dot{\gamma}$, which has the direction of $\pm\pi/4$ with respect to the channel axis. The authors say that the suspension stress is then

$$\sigma_{ij}^{(p)} = -\eta\eta_n\dot{\gamma}Q_{ij} + 2\eta\eta_p d_{ij}, \tag{3.45}$$

where the two coefficients η_n, η_p, as well as the tensor $\mathbf{Q}$, must be determined by inspecting numerical simulations. η_p is well-known and could for example be given by the Krieger (1972) formula: Equation (3.6). The normal form of $\mathbf{Q}$ is

given as

$$\mathbf{Q} = \begin{pmatrix} 1 & 0 & 0 \\ 0 & \lambda_2 & 0 \\ 0 & 0 & \lambda_3 \end{pmatrix}, \tag{3.46}$$

which must be rotated over $\pm\pi/4$ for the case of pure shear to give

$$\mathbf{Q} = \begin{pmatrix} \frac{\sqrt{2}}{2} & -\frac{\sqrt{2}}{2}\lambda_2 & 0 \\ \frac{\sqrt{2}}{2} & \frac{\sqrt{2}}{2}\lambda_2 & 0 \\ 0 & 0 & \lambda_3 \end{pmatrix}. \tag{3.47}$$

From numerical simulations the parameters λ_2 and λ_3 have been determined: $\lambda_2 = 0.8$ and $\lambda_3 = 0.5$. These values are approximate.

The implications of this model are now explored. From equation (3.24) we can get,

$$-\frac{\partial p}{\partial x} + \frac{\partial \sigma_{11}^{(p)}}{\partial x} + \frac{\partial \sigma_{12}^{(p)}}{\partial y} = 0; \tag{3.48}$$

$$\frac{\partial \sigma_{12}^{(p)}}{\partial x} + \frac{\partial \sigma_{22}^{(p)}}{\partial y} = 0; \tag{3.49}$$

as before $\partial\sigma_{11}^{(p)}/\partial x = 0$ and $\partial\sigma_{12}^{(p)}/\partial x$ also vanishes.

$$\frac{\partial \sigma_{12}^{(p)}}{\partial y} = -\eta \frac{\partial \left(\eta_n \dot{\gamma}\right)}{\partial y} Q_{12} + 2\eta \frac{\partial \left(\eta_p d_{12}\right)}{\partial y}. \tag{3.50}$$

So,

$$-\frac{\partial p}{\partial x} - \eta \frac{\partial \left(\eta_n \dot{\gamma}\right)}{\partial y} Q_{12} + 2\eta \frac{\partial \left(\eta_p \dot{\gamma}\right)}{\partial y} = 0; \tag{3.51}$$

and

$$\frac{\partial \sigma_{22}}{\partial y} = -\eta \frac{\partial \left(\eta_n \dot{\gamma}\right)}{\partial y} \frac{\sqrt{2}}{2} \lambda_2 = 0. \tag{3.52}$$

It follows that

$$\eta_n \dot{\gamma} = C. \tag{3.53}$$

Now there is a boundary condition $\dot{\gamma}(0) = 0$ and so the model collapses unless η_n becomes infinite at the centre of the channel. Miller and Morris (2006) introduce the functional relation $\eta_n = K_n \left(\phi/\phi_m\right) \left(1 - \phi/\phi_m\right)^2$, implying that - unless non-local terms are introduced that would add a contribution to the right-hand side of equation (3.52) the solidosity must be maximal at the centre, just like in the models by Phillips (1992) and Acrivos (1987). The anisotropy does nothing but provide an alternative formulation for the transverse contribution to the stress. The model is therefore similar to the Phillips and Acrivos models and gives similar results.

3.5.1. Discussion

In this chapter four types of models have been introduced. All these are phenomenological, though tentatively informed by possible physical processes. The Bingham flow model is of course old. However, the formulation in this chapter in which the yield stress is solidosity-dependent (whereas in the traditional formulation there is a yield stress which is a given constant, which makes the plug width velocity-dependent). It gives a first order clue to the kind of rheology that is required to obtain the migration effect. It is a very crude model, which cannot handle the continuous solidosity profiles that are observed in experiments.

The diffusion models by Phillips (1992) and Acrivos (1987) are now well-established. They cannot inform on the zero-motion problem, but would appear to give reasonable answers in the channel flow (and also Couette flow) problem). As such they offer an improvement over the Bingham flow model. However, they must possess maximum solidosity at the centre of the channel, which is not observed in experiment, see Lyon and Leal (1998). A point to note is that the literature on these models is somewhat misleading. Nott and Brady (1994), for example, note the cusp that is possible in these models. They fail to explore this further and do not see that for larger values of K_c/K_μ the sharp cusp disappears. For some reason the Nott and Brady (1994) paper is widely quoted, see for example

Morris and Boulay (1999). While it is still necessary to have maximum solidosity at the zero-shear-rate point, the analysis shown in this chapter demonstrates that no sharp cusp is necessary.

The granular temperature model is a mature physical model. One of its drawbacks is that it needs so many coefficients. In the next chapter it will be shown how those coefficients can be obtained by theoretical means. However, the model is phrased in isotropic terms and cannot cope with structure formation. For this reason it has been rejected, partly based on experiments by Shapley *et al* (2002). The anisotropic models by Morris *et al* (2006) and Stickel *et al* (2005) rely heavily on input from numerical simulations. The difficulty is that these simulations all employ the elastic particle interaction, described in section 2.5. None use collisional rheology. It is therefore necessary to develop a new theory that predicts structures formation based on collisional rheology. This will be done below in chapter 7. Further numerical simulations, involving collisional rheology will be developed and described in chapter 7.

4. Particle fluid flow in a cell model

4.1. Introduction

For dense slurries it is possible to elaborate cell models. These are small assemblies of particles, for example one central particle surrounded by its nearest neighbours. The idea is that for dense assemblies the contribution to the mechanics of the central particle will be dominated by the interaction of the nearest neighbours and all other particles will exert a far smaller influence. A further concept that is important is the *mean field assumption.* This is a first order approximation which says that the volume average of the cells is manifest in the rheological parameters (for example, a viscosity parameter) only. In this chapter a cell model is developed for the isotropic version of the granular temperature theory. For the predictions of the viscosity a comparison with experiments is available, which turns out to be rather encouraging. For the prediction of the other parameters no experimental data are available at this stage. We calculate a test in which the parameters of the granular heat conduction and dissipation dominate and it is hoped that soon experimental data will be available. A test is currently being run at Edinburgh University.

4.2. Isotropic viscosity estimate

The fluid viscosity is η and the particles have equal diameters D. The lubrication interaction is used; the gap width between particles is h. In addition a notation due to Koenders(1997) will be used: particles are distinguished by a Greek superscript. Parameters that represent properties of two particles will be given two superscripts; for example the branch vector linking the centres of two nearby particles (labelled μ and ν) with positions $\mathbf{x}^\mu$ and $\mathbf{x}^\nu$ is $\mathbf{c}^{\mu\nu} \equiv \mathbf{x}^\nu - \mathbf{x}^\mu$, see Fig 4.1 The unit normal vector aligned with the branch vector is $\mathbf{n}^{\mu\nu} \equiv \mathbf{c}^{\mu\nu}/c^{\mu\nu}$ ($c^{\mu\nu}$ is shorthand for $|\mathbf{c}^{\mu\nu}|$), and is directed along the line centers from $\mathbf{x}^\mu$ to $\mathbf{x}^\nu$.

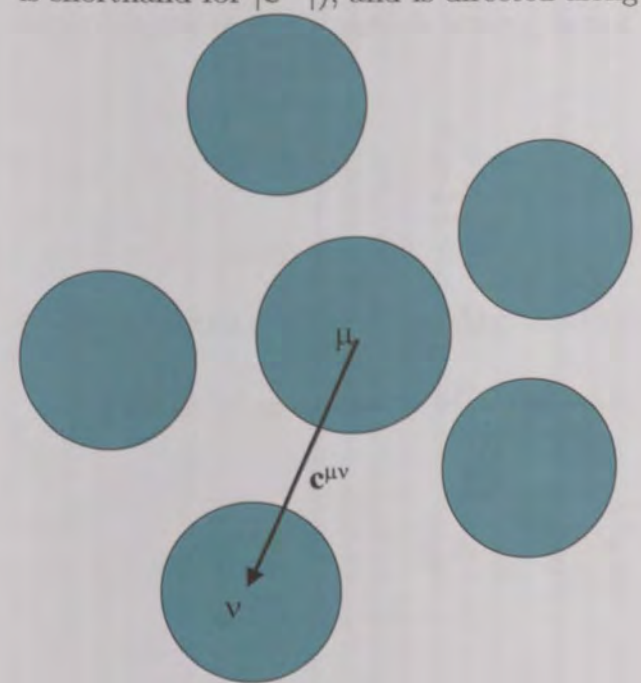

Fig. 4.1. Illustration of the cell model.

For particles in close proximity a cell model considers particles and their immediate neighbours. A paper by Jenkins and Koenders (2005) is relevant. In this paper interacting particles are considered with interaction K••. The lubrication force for two particles in close proximity with velocities $\mathbf{v}^\mu$ and $\mathbf{v}^\nu$ is

$$F_i^{\mu\nu} = \frac{3}{8}\pi\eta D^2 \frac{\left(v_j^\nu - v_j^\mu\right) n_j^{\mu\nu}}{h^{\mu\nu}} n_i^{\mu\nu}. \tag{4.1}$$

The interaction is the particle-pair interaction, defined in such a way that $F_i^{\mu\nu} = K_{ij}^{\mu\nu}\left(v_j^\nu - v_j^\mu\right)$, thus $K_{ij}^{\mu\nu} = 3\pi\eta D^2 n_i^{\mu\nu} n_j^{\mu\nu} / (8h^{\mu\nu})$. In quasi-static equilibrium the sum of forces on each particle is zero, hence

$$\sum_{\nu=1}^{N^\mu} K_{ij}^{\mu\nu}\left(v_j^\nu - v_j^\mu\right) = 0, \tag{4.2}$$

where N^μ is the number of neighbours of particle μ.

The stress of an assembly of N particles, occupying a volume V, is

$$t_{ij} = \frac{1}{2V}\sum_{\mu=1}^{N}\sum_{\nu=1}^{N^\mu} F_i^{\mu\nu} c_j^{\mu\nu}. \tag{4.3}$$

With the lubrication interaction the stress tensor is automatically symmetric.

This is correct as long as the interaction between particles is merely due to

the fluid-mediated force. However, collisions may also take place and the stress contribution given by (4.3) is merely the viscous part of the stress. Furthermore, in order to accommodate collisional momentum transfer an appropriate term should be added to (4.2). However, in the simplest approximation (4.2) is not used. An immediate estimate for the viscosity of the medium can be obtained using a mean-field approximation. The latter implies that the motion of nearby particles is given by the mean strain rate **d**, so that $v_j^\nu - v_j^\mu = d_{jk} c_k^{\mu\nu}$. Substituting in the expression for the viscous stress gives

$$t_{ij} = \frac{3\pi\eta D^2}{16V} \sum_{\mu=1}^{N} \sum_{\nu=1}^{N^\mu} \frac{n_i^{\mu\nu} c_j^{\mu\nu} c_\ell^{\mu\nu} n_k^{\mu\nu}}{h^{\mu\nu}} d_{k\ell}. \tag{4.4}$$

In the approximation each of the terms in the sum over μ gives the same contribution and therefore the double sum may be written as a single sum

$$t_{ij} = \frac{3\pi\eta D^2 N}{16V} \overline{\sum_{\nu=1}^{N^\mu} \frac{n_i^{\mu\nu} c_j^{\mu\nu} c_\ell^{\mu\nu} n_k^{\mu\nu}}{h^{\mu\nu}}} d_{k\ell}, \tag{4.5}$$

where the over bar denotes the average. Now using $N/V = 6\phi/(\pi D^3)$ and replacing $h^{\mu\nu}$ with its average value given by formula (3.44) one is left with

$$t_{ij} = \frac{9\eta\phi}{8D^2}\frac{D}{h}\overline{\sum_{\nu=1}^{N^\mu} n_i^{\mu\nu} c_j^{\mu\nu} c_\ell^{\mu\nu} n_k^{\mu\nu} d_{k\ell}} \tag{4.6}$$

$$= \frac{3\eta(1-\phi)^3}{32D^2(2-\phi)}\overline{\sum_{\nu=1}^{N^\mu} n_i^{\mu\nu} c_j^{\mu\nu} c_\ell^{\mu\nu} n_k^{\mu\nu} d_{k\ell}}.$$

To evaluate the summation an angular particle distribution function $w(\Omega)$ is introduced. For an isotropic distribution $w(\Omega)$ is constant and such that $\int w(\Omega)\, d\Omega = N_c$ - the number of nearest neighbours. So, $w(\Omega) = N_c/(4\pi)$. For the nearest neighbours $h << D$ and therefore $\mathbf{c} = D\mathbf{n}$. Now the sum is replaced by an integral with weighting function $w(\Omega)$

$$\overline{\sum_{\nu=1}^{N^\mu} n_i^{\mu\nu} c_j^{\mu\nu} c_\ell^{\mu\nu} n_k^{\mu\nu}} \rightarrow \frac{N_c D^2}{4\pi}\int_0^{2\pi} d\alpha \int_0^{\pi} d\theta \sin\theta n_i n_j n_\ell n_k = \tag{4.7}$$

$$\frac{N_c D^2}{15}\left(\delta_{ij}\delta_{\ell k} + \delta_{i\ell}\delta_{jk} + \delta_{ik}\delta_{\ell j}\right).$$

The integrals are listed in Batchelor (1976, p 252).

This result is interpreted in terms of the Lamé constants $\overline{\lambda}$ and $\overline{\mu}$

$$t_{ij} = \overline{\lambda} d_{kk}\delta_{ij} + 2\overline{\mu} d_{ij}. \tag{4.8}$$

Substitution gives

$$\overline{\lambda} = \overline{\mu} = \frac{3\eta\phi N_c}{40}\frac{D}{h}. \tag{4.9}$$

Using formula (4.9) the value of $\overline{\mu}/\eta$ is plotted in Figure 4.2 for $N_c = 6$; the same plot shows the Krieger approximation - Equation (3.6)- and the Thomas approximation (1965); the latter is based on a best fit to measured data. For $N_c = 6$ experiments and mean field approximation coincide quite well.

This gives some confidence that the cell model represents a valid approximation of the rheology. Two of the five parameters of the Granular Temperature model are now estimated; they are α_0 and α_1, which take the form

$$\alpha_0 = \alpha_1 = \frac{3N_c}{40}; \tag{4.10}$$

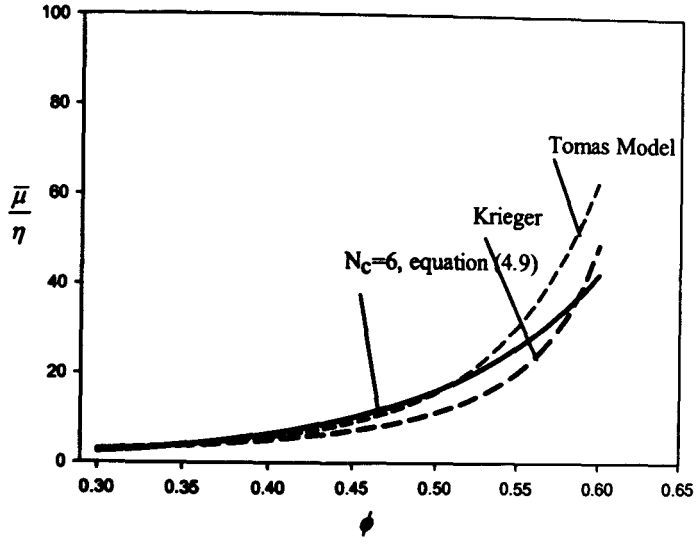

Figure 4.2. Relative viscosity as a function of solidosity for various models

4.3. The rate of working balance

In this section the fluctuation energy balance that is required for the granular temperature model will be discussed. Using the cell model the formulas for the granular temperature theory (McTigue and Jenkins(1992)) can be rediscovered and estimates for the various parameters can be obtained. Two parameters have already been found in the previous section; they are α_0 and α_1. The other parameters (α_2 and α_3) are associated with the rate of working balance. In the cell model the rate of working balance is more complicated than the straightforward

stress calculation and there is a physical background that needs to be addressed.

The total energy of a sample of the slurry with volume V is (see Becker and Bürger (1975), section 4.8)

$$E = \int_V \left(\rho e + \frac{1}{2} \rho v^2 \right) dV, \tag{4.11}$$

where ρ is the mass density of the material and e the internal energy per unit volume. The first law of thermodynamics is invoked to decompose the rate of change of the total energy in a "work" part (W) and a "heat" part (Q_c) (the heat here is the - traditional - caloric heat and the subscript c has been added to distinguish it from the "granular heat" of the granular temperature theory). The rate of change (co-moving with a continuum material point) is denoted by a dot.

$$\dot{E} = \dot{W} + \dot{Q}_c. \tag{4.12}$$

The heat is supplied or extracted from the volume V by means of a (caloric) heat flux $\mathbf{q}_c$ through the boundaries with area A,

$$\dot{Q}_c = \int_A \mathbf{q}_c . \mathbf{n} dA. \tag{4.13}$$

Combining and employing Gauss' theorem leads to

$$\dot{W} = \int_V \left(-div\mathbf{q}_c + \dot{(\rho e)} + \frac{1}{2}\dot{(\rho v^2)} \right) dV. \tag{4.14}$$

In the granular temperature theory the changes in the interior of the material is supposed to be arranged in such a way that the internal energy remains unchanged, in other words, heat is supplied to, or extracted from, any sample of the material so that

$$\int_V \left(-div\mathbf{q}_c + \dot{(\rho e)} \right) dV = 0. \tag{4.15}$$

For a practical realisation of this requirement one may consider that the internal energy depends on the temperature only, which would imply that heat is supplied to, or extracted from, the experiment to keep it at a constant temperature.

The implication of the requirement of constant internal energy is that the rate of working only becomes manifest through a change in the kinetic energy

$$\dot{W} = \int_V \left(\frac{1}{2}\dot{(\rho v^2)} \right) dV. \tag{4.16}$$

For quasi-static experiments this would imply that the rate of working on a volume vanishes. This is the basis for the rate of working balance.

The rate of working balance for the cell model requires an adaptation. The continuum mechanics form of the rate of working is $\dot{W} = \int_A \tau_i v_i dA$, where the vector $\boldsymbol{\tau}$ is the traction. The discrete form would be the sum over the inner product of contact force and velocity, but the contact forces are defined in between the particles, while the velocities are defined at the centres of the particles. In order to arrive at a sensible expression for the rate of working of one cell (a particle μ and its set of neighbours $\{\nu\}$) the form $\sum_{\nu=1}^{N^\mu} \mathbf{F}^{\mu\nu}(\mathbf{x}^\mu) \cdot \mathbf{v}^\mu$ needs to be evaluated. To that end an extrapolation of the contact force is performed: $\mathbf{F}^{\mu\nu}(\mathbf{x}^\nu) = \mathbf{F}^{\mu\nu} - \frac{1}{2}(\nabla\mathbf{F})_{\frac{1}{2}(\mathbf{x}^\mu+\mathbf{x}^\nu)} \cdot \mathbf{c}^{\mu\nu}$. So the rate of working per unit volume in an assembly of N particles is

$$\dot{w} = \frac{1}{V} \sum_{\mu=1}^{N} \sum_{\nu=1}^{N^\mu} \left(\mathbf{F}^{\mu\nu} - \frac{1}{2}(\nabla\mathbf{F})_{\frac{1}{2}(\mathbf{x}^\mu+\mathbf{x}^\nu)} \cdot \mathbf{c}^{\mu\nu} \right) \cdot \mathbf{v}^\mu. \tag{4.17}$$

The flux dot here means 'co-moving with the centre of gravity of the particles in the assembly'. The expression (4.17) is now further elaborated. The velocity of the particles is decomposed into an average motion, $\langle\mathbf{v}\rangle$, the motion due to its first order gradient $\nabla\mathbf{v}$ and fluctuations $\mathbf{v}'$; thus $\mathbf{v}^\mu = \langle\mathbf{v}\rangle + (\nabla\mathbf{v}) \cdot \mathbf{x}^\mu + \mathbf{v}'^\mu$ and $\mathbf{v}^\nu = \langle\mathbf{v}\rangle + (\nabla\mathbf{v}) \cdot \mathbf{x}^\nu + \mathbf{v}'^\nu$. The first term in expression (4.17) then becomes

$$\sum_{\nu=1}^{N^\mu} \mathbf{F}^{\mu\nu} \cdot \mathbf{v}^\mu = \sum_{\nu=1}^{N^\mu} \mathbf{F}^{\mu\nu} \cdot (\langle \mathbf{v} \rangle^\mu + (\nabla \mathbf{v}) \cdot \mathbf{x}^\mu + \mathbf{v}'^\mu) = \tag{4.18}$$
$$\langle \mathbf{v} \rangle^\mu \cdot \sum_{\nu=1}^{N^\mu} \mathbf{F}^{\mu\nu} + [(\nabla \mathbf{v}) \cdot \mathbf{x}^\mu] \cdot \sum_{\nu=1}^{N^\mu} \mathbf{F}^{\mu\nu} + \mathbf{v}'^\mu \cdot \sum_{\nu=1}^{N^\mu} \mathbf{F}^{\mu\nu}.$$

The first two terms in this contain the sum of forces, which in the quasi-static case would vanish and in the dynamic case leaves an acceleration term. The third term is the granular dissipation. Note that the forces here include forces associated with collisions. The latter are proportional to $\sqrt{\mathbf{v}'^\mu \cdot \mathbf{v}'^\mu}$, so while they give a contribution to the stress, the correlation between the vector fluctuation $\mathbf{v}'^\mu$ and the collisional force vanishes. Therefore, in expression (4.18) the force in the third term is merely the contribution of the lubrication force, which is proportional to $\mathbf{v}^\nu - \mathbf{v}^\mu = \nabla \mathbf{v} \cdot \mathbf{c}^{\mu\nu} + \mathbf{v}'^\nu - \mathbf{v}'^\mu$.

The granular temperature is now defined as the product of the fluctuations $v_i'^\mu v_j'^\mu = T^\mu \delta_{ij}/3$. The third term in expression (4.18) becomes

$$\mathbf{v}'^\mu \cdot \sum_{\nu=1}^{N^\mu} \mathbf{F}^{\mu\nu} = \frac{3}{8} \pi \eta D^2 \sum_{\nu=1}^{N^\mu} \frac{n_j^{\mu\nu} n_i^{\mu\nu}}{h^{\mu\nu}} \left(v_i'^\mu v_j'^\nu - v_i'^\mu v_j'^\mu \right). \tag{4.19}$$

In further evaluating this expression it is assumed that the cross-correlation of

velocity fluctuations between neighbouring particles are negligible compared to the auto-correlate. Furthermore, the auto-correlate is approximately isotropic. The contribution of this term to the rate of working per unit volume is obtained in a way similar to the stress calculation in the previous section

$$\begin{aligned} \frac{1}{V}\sum_{\mu=1}^{N}\mathbf{v}'^{\mu}\sum_{\nu=1}^{N^{\mu}}\mathbf{F}^{\mu\nu} &\rightarrow -\frac{3}{8}\frac{\pi\eta D^2}{h}\frac{1}{3}T\frac{N}{V}\frac{N_c}{4\pi}\int_0^{2\pi}d\alpha\int_0^{\pi}d\theta\sin\theta \\ &= -\frac{\pi}{8}\frac{\eta D^2 T}{h}\frac{N}{V}N_c. \end{aligned} \tag{4.20}$$

The second term in expression (4.17) is

$$\begin{aligned} -\frac{1}{2}\sum_{\nu=1}^{N^{\mu}}\left((\nabla\mathbf{F})_{\frac{1}{2}(\mathbf{x}^{\mu}+\mathbf{x}^{\upsilon})}\cdot\mathbf{c}^{\mu\nu}\right)\cdot\mathbf{v}^{\mu} = \\ -\frac{1}{2}\frac{\partial}{\partial x_\ell}\cdot\left(\sum_{\nu=1}^{N^{\mu}}(F_j)_{\frac{1}{2}(\mathbf{x}^{\mu}+\mathbf{x}^{\upsilon})}c_\ell^{\mu\nu}(v_j)_{\frac{1}{2}(\mathbf{x}^{\mu}+\mathbf{x}^{\upsilon})}\right) \\ +\frac{1}{2}\sum_{\nu=1}^{N^{\mu}}(F_j)_{\frac{1}{2}(\mathbf{x}^{\mu}+\mathbf{x}^{\upsilon})}c_\ell^{\mu\nu}\frac{\partial v_j}{\partial x_\ell}. \end{aligned} \tag{4.21}$$

The second term on the right-hand-side contains the definition of the stress (4.3) and will be treated as such. The first term on the right hand side is elaborated further by setting the velocity in the midpoints between particles μ and ν to $\frac{1}{2}(\mathbf{v}^{\mu}+\mathbf{v}^{\nu})$. This is again written in terms of averages and fluctuations:

$\frac{1}{2}(\mathbf{v}^{\mu}+\mathbf{v}^{\nu}) = \langle \mathbf{v} \rangle + \frac{1}{2}(\nabla \mathbf{v})(2\mathbf{x}^{\mu}+\mathbf{c}^{\mu\nu}) + \frac{1}{2}(\mathbf{v}'^{\mu}+\mathbf{v}'^{\nu})$, which leads to

$$\begin{aligned} & \sum_{\nu=1}^{N^{\mu}} (F_j)_{\frac{1}{2}(\mathbf{x}^{\mu}+\mathbf{x}^{\upsilon})} c_{\ell}^{\mu\nu} (v_j)_{\frac{1}{2}(\mathbf{x}^{\mu}+\mathbf{x}^{\upsilon})} \\ = & \sum_{\nu=1}^{N^{\mu}} \left(F_j^{\mu\nu} c_{\ell}^{\mu\nu}\right) \cdot \left[\langle v_j \rangle + \frac{1}{2} \frac{\partial v_j}{\partial x_{\ell}} (2x_{\ell}^{\mu} + c_{\ell}^{\mu\nu}) + \frac{1}{2}\left(v_j'^{\mu} + v_j'^{\nu}\right) \right]. \end{aligned} \tag{4.22}$$

Each term will now be evaluated. The fist term leads to

$$\langle v_j \rangle \, \partial / x_{\ell} \sum_{\nu=1}^{N^{\mu}} \left(F_j^{\mu\nu} c_{\ell}^{\mu\nu}\right), \tag{4.23}$$

which is proportional to the divergence of the macroscopic stress tensor and vanishes in a quasi-static application. The term $(\nabla \mathbf{v}) \cdot \mathbf{x}^{\mu} \sum_{\nu=1}^{N^{\mu}} (\mathbf{F}^{\mu\nu}\mathbf{c}^{\mu\nu})$, similarly, is small and furthermore when evaluated over an assembly contains the definition of the centre of gravity, which makes it vanish. The term $\frac{1}{2}(\nabla \mathbf{v}) \cdot \sum_{\nu=1}^{N^{\mu}} (\mathbf{F}^{\mu\nu}\mathbf{c}^{\mu\nu}) \cdot \mathbf{c}^{\mu\nu}$ requires the input of the force, which is the collisional force and the lubrication force. The latter leads to a sum over an odd string of unit normal vectors, which vanishes in the mean field approximation. The collisional force is proportional to $\sqrt{\mathbf{v}'^{\mu} \cdot \mathbf{v}'^{\mu}}\mathbf{n}^{\mu\nu}$, which also leaves a string of three unit vectors. Finally, the term $\frac{1}{2}\sum_{\nu=1}^{N^{\mu}} (\mathbf{F}^{\mu\nu}\mathbf{c}^{\mu\nu}) \cdot (\mathbf{v}'^{\mu} + \mathbf{v}'^{\nu})$ is considered. For the interparticle force the lubrication term is used again, which leaves

$$\frac{1}{2}\sum_{\nu=1}^{N^\mu} F_j^{\mu\nu} c_\ell^{\mu\nu} \left(v_j'^{\mu} + v_j'^{\nu}\right) = \tag{4.24}$$
$$\frac{1}{2}\left[\frac{3}{8}\pi\eta D^2 \sum_{\nu=1}^{N^\mu} \frac{\left(v_k^\nu - v_k^\mu\right) n_j^{\mu\nu}}{h^{\mu\nu}} n_k^{\mu\nu} c_l^{\mu\nu} \left(v_j'^{\mu} + v_j'^{\nu}\right)\right].$$

Expanding $(v_k^\nu - v_k^\mu)$ as before and retaining even strings of the unit vector only, leaves the following

$$\frac{1}{2}\sum_{\nu=1}^{N^\mu} F_j^{\mu\nu} c_\ell^{\mu\nu} \left(v_j'^{\mu} + v_j'^{\nu}\right) = \tag{4.25}$$
$$\frac{3}{16}\pi\eta D^2 \sum_{\nu=1}^{N^\mu} \frac{n_j^{\mu\nu}}{h^{\mu\nu}} n_k^{\mu\nu} c_l^{\mu\nu} \left(v_k'^{\nu} v_j'^{\mu} - v_k'^{\mu} v_j'^{\mu} + v_k'^{\nu} v_j'^{\nu} - v_k'^{\mu} v_j'^{\nu}\right).$$

Retaining the autocorrelate of the fluctuations only, reduces the term in brackets to $\left(-v_k'^{\mu} v_j'^{\mu} + v_k'^{\nu} v_j'^{\nu}\right)$ and using the definition of the temperature leads to $-\left(T^\mu - T^\nu\right)\delta_{kj}/3$. The difference in the temperatures is written as $\partial T/3\partial x_m c_m^{\mu\nu}$. The summation is now evaluated in the mean field approximation

$$-\frac{3}{16}\pi\eta \frac{D^2}{h}\frac{1}{3}\frac{\partial T}{\partial x_m}\sum_{\nu=1}^{N^\mu} n_j^{\mu\nu} n_k^{\mu\nu} c_l^{\mu\nu} c_m^{\mu\nu}\delta_{kj} \;\rightarrow$$
$$-\frac{1}{8}\pi\eta \frac{D^2}{h}\frac{\partial T}{\partial x_m}\frac{N_c}{4\pi} D^2 2\pi \frac{1}{3}\delta_{\ell m} = -\frac{1}{48}\pi\eta \frac{D^4}{h}\frac{\partial T}{\partial x_\ell} N_c. \tag{4.26}$$

Altogether one obtains

$$-\frac{1}{2}\sum_{\mu=1}^{N}\sum_{\nu=1}^{N\mu}\left(\left(\nabla\mathbf{F}\right)_{\frac{1}{2}\left(\mathbf{x}^{\mu}+\mathbf{x}^{\upsilon}\right)}\mathbf{c}^{\mu\nu}\right)\cdot\mathbf{v}^{\mu} = \frac{\partial v_i}{\partial x_j}t_{ij}+\frac{\pi\eta D^4 N N_c}{96Vh}\frac{\partial^2 T}{\partial x_k \partial x_l}. \tag{4.27}$$

The rate of working per unit volume is obtained from equations (4.20) and (4.27)

$$\dot{w} = \frac{\pi\eta D^4 N N_c}{96Vh}\frac{\partial^2 T}{\partial x_k \partial x_l}+\frac{\partial v_i}{\partial x_j}t_{ij}-\frac{\pi\eta D^2 T}{4hV}NN_c. \tag{4.28}$$

Finally, using $N/V = 6\phi/(\pi D^3)$, the rate of working per unit volume equation may be written in the form

$$\frac{1}{2}\left(\rho v^2\right)^{\cdot} = -\frac{\partial Q_i}{\partial x_i}+t_{ij}\frac{\partial v_i}{\partial x_j}-\overline{\gamma} \tag{4.29}$$

with

$$\overline{\gamma} = \frac{3\eta\phi N_c}{4hD}T \tag{4.30}$$

and

$$Q_i = -\frac{\eta D\phi N_c}{16}\frac{\partial T}{\partial x_i} \tag{4.31}$$

These results are compared with the constitutive parameters of the Granular Temperature model - expressions (3.30), (3.31) - and thus two other coefficients of the Granular Temperature model are estimated; they are α_2 and α_3, which take the form

$$\alpha_2 = \frac{1}{16} N_c, \qquad \alpha_3 = \frac{3}{4} N_c \tag{4.32}$$

4.4. Particle pressure

This foundation for the particle pressure $\overline{p}$, as used in the Granular Mechanics model, is now investigated. In a dense slurry flow two mechanisms for migration were put forward, a collisional one and a viscosity gradient one. McTigue and Jenkins (1992) consider the collisional mechanism only, which they relate strictly to the velocity fluctuations in the flow. The velocity fluctuations are manifest in the interactive force, just as in the previous section, and therefore - if the pressure is derived from formula (4.3) - the following is obtained

$$\begin{aligned} \overline{p} = -\frac{1}{2V} \sum_{\mu=1}^{N} \sum_{\nu=1}^{N^\mu} F_i'^{\mu\nu} c_i^{\mu\nu} = \\ -\frac{3\pi}{16} \frac{\eta D^2}{V} \sum_{\mu=1}^{N} \sum_{\nu=1}^{N^\mu} \frac{\left(v_j'^{\nu} - v_j'^{\mu}\right) n_j^{\mu\nu}}{h^{\mu\nu}} n_i^{\mu\nu} c_i^{\mu\nu} = \\ -\frac{3\pi}{8} \frac{\eta D^3}{V} \sum_{pairs\ \{\mu\nu\}} \frac{\left(v_j'^{\nu} - v_j'^{\mu}\right) n_j^{\mu\nu}}{h^{\mu\nu}}. \end{aligned} \tag{4.33}$$

One would expect the average of the terms under the sum to be zero as there are as many positive as negative contributions. If, however, collisions are taken into account, the normal speed fluctuation $s' = \left|\left(v_j'^{\nu} - v_j'^{\mu}\right) n_j^{\mu\nu}\right|$ before a collision is systematically greater than the outgoing speed fluctuation due to the fact that energy is lost in the collision. Therefore taking a time average that is long compared to the collision time, but short compared to the evolution of the assembly, the terms that 'are about to' and 'just have' in equation (4.33) need to be considered only. The assembly is so large that there are equal numbers of pairs that are about to take place in a collision with a specified speed and pairs that have just been involved in a collision with the same speed before the collision (in this short time interval over which the average is taken). Because of the loss of mechanical energy in the collision the pair interaction between each equivalent for–and-after event may be grouped as $s'(1 - e_c)$, where e_c is the coefficient of restitution (s' is the speed *before* the collision). s' is always positive and proportional to the magnitude of the velocity fluctuations in the assembly $\sqrt{T}$. Taking a mean field approach the average particle pressure is therefore

$$-\frac{3\pi}{8}\frac{\eta D^3}{V}\sum_{\text{pairs }\{\mu\nu\}}\frac{\left(v_j'^{\nu} - v_j'^{\mu}\right) n_j^{\mu\nu}}{h^{\mu\nu}} \rightarrow -\alpha_4\eta\phi\frac{D}{h}(1 - e_c)\sqrt{T}. \tag{4.34}$$

The particle pressure does not come about due to phenomena that occur on the cell scale. Rather the statistics of the whole assembly are important.

4.5. Granular temperature model in a vibrated dead-end filter

In the past the dead-end filtration problem with oscillated septum has been calculated with the Granular Temperature model:Gundogdu and Koenders (2003b), Davis and Koenders (2007c). The geometry of the problem is defined by a one-dimensional co-ordinate - the z-direction - pointing upwards. The model has been augmented with a gravity term and a drag term to accommodate the effects of the mean fluid flow in the dead-end filter. The fluid drag is described by Darcy's law - see Happel (1991)- and relates the fluid pressure gradient to the superficial fluid velocity **U** by means of a coefficient $\overline{R}$. The latter may be expressed as $\overline{R} = \eta\varkappa\phi\left(D/h\right)/D^2$, where $\varkappa$ is a non-dimensional coefficient with a measured value of 2.2. The particle mass density is ρ_p, the fluid mass density is ρ_f, the acceleration due to gravity is g. Here the equations for the dead-end filtration problem are not re-derived, but taken over from Gundogdu *et al* (2003b). The Granular Temperature model can be reduced to two equations of scaled parameters. The scaling is of the distances, which are expressed in the particle diameter - $z = z^*D$ - and the granular temperature is scaled to the value at the position of

the septum at $z = 0$: $T = \overline{T}T^*$. The equations are

$$f\frac{\partial\phi}{\partial z^*}\sqrt{T^*} + \frac{1}{2\sqrt{T^*}}\frac{\partial T^*}{\partial z^*} - \frac{\phi e_c^{-f\phi} Dg\left(\rho_p - \rho_f\right)}{\overline{f}\eta\alpha_4} - S = 0, \tag{4.35}$$

$$\alpha_2 f\frac{\partial\phi}{\partial z^*}\frac{\partial T^*}{\partial z^*} + \alpha_2\frac{\partial^2 T^*}{\partial^2 z^*} + \alpha_0\left(\frac{\partial\sqrt{T^*}}{\partial z^*}\right)^2 - \alpha_3 T^* = 0. \tag{4.36}$$

The coefficient f which is associated with an exponential fit of formula (3.44) and has the value $f = 9.94$. The parameter $S = \chi\mathbf{U}/\alpha_4 D$ represents the ratio of the drag exerted by the mean fluid flow to the strength of the vibration induced agitation. This ratio and the total solids volume leads to a solidosity profile. In the calculations in Gundogdu and koenders (2003b), Davis and Koenders (2007c) the coefficients α_{0-3} have been used and - in the absence of anything better - have been set to unity. As the main purpose of the present thesis is to show the effects of the improved estimates of the the coefficients, gravity is neglected: $g = 0$ (in a recent paper Davis and Koenders (2008) have done calculations to include the effects of gravity).

Using the new values of coefficients α_{0-3} a solution is obtained for a given set of parameters (fluid velocity, amplitude of agitation). A Runge-Kutta procedure is employed. The resulting values of T^* and ϕ are plotted in figures 4.3 and 4.4

for $N_c = 6$. The graph in figure 4.3 shows that the granular temperature as a function of the position for two different set of values of α_{0-3}; it is observed that - mainly as a result of the fact that the coefficient in the dissipation is much greater than previously thought - the penetration of the fluctuations decay over a much shorter distance than with the parameters set to unity. Similarly, the solidosity in figure 4.4, shows the same effect, though the value at the septum - $z = 0$ - is not so different; the prediction of this value is important for engineering applications. These graphs have been plotted for a solids content of $V_s/A_0 = 4.2D$, where V_s is the given total solids volume and A_0 is the area of the cylindrical filter.

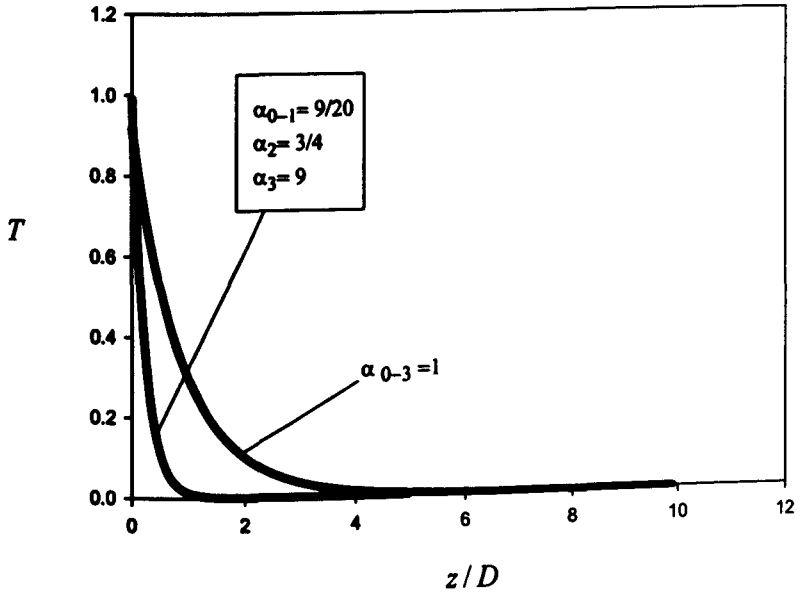

Figure 4.3. Scaled granular temperature as a function of the scaled distance

from the septum for new values of α_{0-3} and $\alpha_{0-3} = 1$. Particles with a size of 100 μm, experiencing an agitation at $250Hz$ with amplitude of two particle diameters against a mean downward flow of $10^{-3}ms^{-1}$. The value of S is approximately equal to 0.04. (using $\chi = 2.2$ and $\alpha_4 = 0.2$).

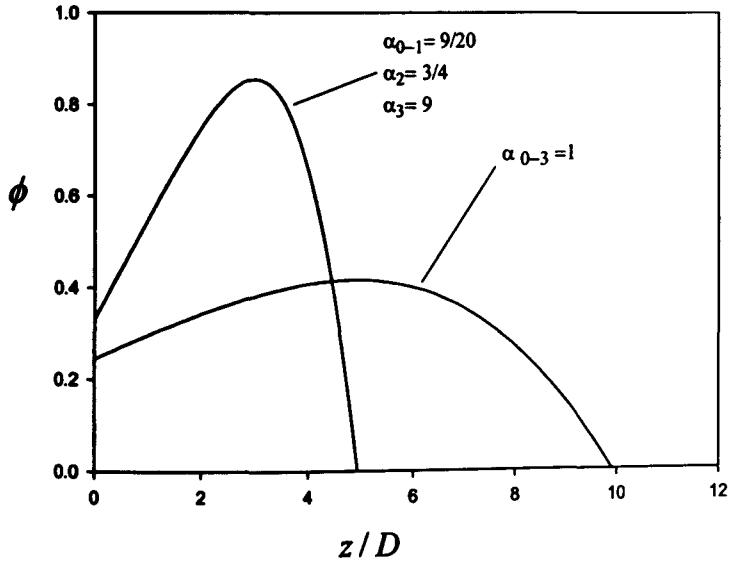

Figure 4.4. Solidosity profiles for new and old values of α_{0-3}. Parameters as in Figure 4.3.

5. Continuum theory with fluctuations

5.1. Introduction

The cell model from the previous chapter gives information in the context of the mean strain theory. In reality fluctuations are present. These occur on the meso-scale, that is a scale of the order of magnitude - or slightly larger - than the cell scale. Later on the problem will be studied further using numerical simulations, however, insight can also be obtained by analytical means. This involves the use of continuum theory.

One of the most startling conclusions of this chapter will be that a flowing sheared slurry is not linearly stable, unless a substantial particle pressure is present. Clearly, that is not a satisfactory situation and the further question of stability needs to be addressed.

5.2. Field equations

The role of the fluctuations can be illuminated by considering a continuum theory in which the field variables may fluctuate. The field variables are the solids velocity $\mathbf{v}$, the fluid superficial velocity $\mathbf{U}$, the fluid pressure p, the solidosity ϕ and the stress tensor $-p\boldsymbol{\delta} + \mathbf{t}$, where $\mathbf{t}$ is the suspension stress tensor. The field equations

are as follows. The two equations of continuity for incompressible phases

$$\frac{\partial \phi}{\partial t} + \frac{\partial (\phi v_i)}{\partial x_i} = 0; \tag{5.1}$$

$$-\frac{\partial \phi}{\partial t} + \frac{\partial [(1-\phi) U_i]}{\partial x_i} = 0. \tag{5.2}$$

The fluid resistance through a packed bed is described by Darcy's law

$$\frac{\partial p}{\partial x_i} = -\overline{R}(\phi)(U_i - v_i), \tag{5.3}$$

where $\overline{R}(\phi)$ is the resistance. The stress equilibrium equation is

$$-\frac{\partial p}{\partial x_i} + \frac{\partial t_{ij}}{\partial x_j} = 0. \tag{5.4}$$

As constitutive equations the isotropic stress-strainrate will be used as before, while the particle pressure $\overline{p}$ is for the moment set to zero. Thus one has as before

$$t_{ij} = \overline{\lambda} d_{kk} \delta_{ij} + 2\overline{\mu} d_{ij}, \tag{5.5}$$

where $d_{ij} = \frac{1}{2}(\partial v_i/\partial x_j + \partial v_j/\partial x_i)$.

These equations are now used to study the fluctuations in the system. In order

to distinguish the continuum fluctuations from the fluctuations in a cell (though at a later stage the two may be identified as being equal) averages and fluctuations are introduced. The former are denoted by $\langle\rangle$ and the latter by a superscript $+$. It is assumed that the slurry is statistically homogeneous, so no spatial derivatives have to be considered. The time differentiations D/Dt are co-moving with the particle phase: $D/Dt = \partial/\partial t + \mathbf{v}.\boldsymbol{\nabla}$. Expanding the equations up to first order in the fluctuations leads to the following set

$$\frac{D\phi^+}{Dt} + \langle\phi\rangle \frac{\partial v_i^+}{\partial x_i} = 0; \tag{5.6}$$

$$-\frac{D\phi^+}{Dt} + \langle 1-\phi\rangle \frac{\partial U_i^+}{\partial x_i} + \langle U_i - v_i\rangle \frac{\partial \phi^+}{\partial x_i} = 0. \tag{5.7}$$

$$\langle\overline{R}\rangle \left(U_i^+ - v_i^+\right) + \frac{\partial \overline{R}}{\partial \phi}\phi^+ \langle U_i - v_i\rangle + \frac{\partial p^+}{\partial x_i} = 0, \tag{5.8}$$

$$-\frac{\partial p^+}{\partial x_i} + \langle\overline{\lambda}\rangle \frac{\partial d_{\ell\ell}^+}{\partial x_i} + 2\langle\overline{\mu}\rangle \frac{\partial d_{ij}^+}{\partial x_j} + \frac{\partial \phi^+}{\partial x_j}\left(\frac{\partial \overline{\lambda}}{\partial \phi}\langle d_{\ell\ell}\rangle \delta_{ij} + 2\frac{\partial \overline{\mu}}{\partial \phi}\langle d_{ij}\rangle\right) = 0. \tag{5.9}$$

The unknowns in this set are ϕ^+, $\mathbf{v}^+$, $\mathbf{U}^+$ and p^+; in three dimensions there are eight unknowns with eight equations. It is a homogeneous system and therefore all the fluctuating fields will be zero! Fluctuations are not possible (It is assumed here that the system is stable). The reasoning leads one to the need to introduce fluctuations that originate on the cell scale.

5.3. Fluctuations on the cell scale

Typically a time and space fluctuating term is needed (average zero) that creates stresses on the small meso scale. These stresses will be called $\mathbf{t}^+$ and the term to be added to equation (5.9) is $\partial t^+_{ij}/\partial x_j$. Even with the simple cell model that has been developed above, it is easy to see where such terms may come from. The local sum in the definition of the stress (4.3) - that is the sum that contains the local, one-cell contribution is

$$\sum_{\nu=1}^{N^\mu} F_i^{\mu\nu} c_j^{\mu\nu}, \tag{5.10}$$

and this will contain a contribution due to local anisotropy that is proportional to $\langle \mathbf{d} \rangle$. In cases where the mean strain rate is zero, a higher order term may be introduced that couples to local asymmetry and is proportional to the strain rate gradient (though this would undermine the assumption that there are no macroscopic gradients in the system). It is emphasised that $\mathbf{t}^+$ does not couple to the velocity fluctuation itself, but to *packing* fluctuations.

5.4. Solution by Fourier transform

A spatial Fourier transform is now carried out; the amplitudes of the fluctuations are denoted by $\hat{\mathbf{a}}$ and the wave vector is called $\mathbf{k}$. The set of algebraic equations

now reads

$$\frac{D\widehat{\phi}}{Dt} + i\langle\phi\rangle k_j \widehat{v}_j = 0; \tag{5.11}$$

$$-\frac{D\widehat{\phi}}{Dt} + i\langle 1-\phi\rangle k_j \widehat{U}_j + i\langle U_j - v_j\rangle k_j \widehat{\phi} = 0. \tag{5.12}$$

$$\langle\overline{R}\rangle\left(\widehat{U}_j - \widehat{v}_j\right) + \frac{\partial R}{\partial\phi}\widehat{\phi}\langle U_j - v_j\rangle + ik_j\widehat{p} = 0, \tag{5.13}$$

$$-ik_\ell\widehat{p} - k_\ell k_j\langle\overline{\lambda}\rangle\widehat{v}_j - \langle\overline{\mu}\rangle\left(k_j^2\widehat{v}_\ell + k_\ell k_j\widehat{v}_j\right) + ik_j\widehat{\phi}\left(\frac{\partial\overline{\lambda}}{\partial\phi}\langle d_{mm}\rangle\delta_{j\ell} + 2\frac{\partial\overline{\mu}}{\partial\phi}\langle d_{j\ell}\rangle\right) + ik_j\widehat{t}_{\ell j} = 0. \tag{5.14}$$

The mean velocity difference between fluid and solids is assumed to be zero: $\langle\mathbf{U}-\mathbf{v}\rangle = \mathbf{0}$. Eliminating $\widehat{p}$, $\widehat{\mathbf{U}}$ and $\widehat{\mathbf{v}}$ leads to the differential equation

$$\frac{D\widehat{\phi}}{Dt} = \frac{\langle\phi\rangle\langle 1-\phi\rangle k_j k_\ell \widehat{t}_{j\ell}}{\langle\overline{R}\rangle + k^2\langle 1-\phi\rangle\left(\langle\overline{\lambda}\rangle + 2\langle\overline{\mu}\rangle\right)} + \frac{\langle\phi\rangle\langle 1-\phi\rangle k_j k_\ell X_{j\ell}}{\langle\overline{R}\rangle + k^2\langle 1-\phi\rangle\left(\langle\overline{\lambda}\rangle + 2\langle\overline{\mu}\rangle\right)}\widehat{\phi}, \tag{5.15}$$

where $X_{j\ell} = \left(\langle d_{mm}\rangle\delta_{j\ell}\partial\overline{\lambda}/\partial\phi + 2\langle d_{j\ell}\rangle\partial\overline{\mu}/\partial\phi\right)$ and $k = |\mathbf{k}|$.

5.5. Linear stability

The first thing that can be read from this differential equation is the stability. The problem is stable while $k_j k_\ell X_{j\ell} \leq 0$ [1]for all vectors $\mathbf{k}$. Purely contracting flows are thus always stable ($\langle d_{mm}\rangle < 0$), while purely expanding flows ($\langle d_{mm}\rangle > 0$) are

[1]Asymptotic stability is obtained when the criterion is expressed without the equal sign.

never stable. For shear the problem is more complicated. Shear in the xy plane leads to $d_{12} = d_{21} = \dot{\gamma}$. Thus $X_{12} = X_{21} = 2\dot{\gamma}k_1k_2$, which can be either positive or negative. Therefore, shear is not stable. In all this the particle pressure has been neglected. Assume that the particle pressure depends on the solidosity only. If a term $-\left(\partial\overline{p}/\partial\phi\right)\left(\partial\phi^{+}/\partial x_i\right)$ is added to the stress equilibrium equation, $\mathbf{X}$ is modified to $X_{j\ell} = \left(\langle d_{mm}\rangle\,\delta_{j\ell}\partial\overline{\lambda}/\partial\phi + 2\,\langle d_{j\ell}\rangle\,\partial\overline{\mu}/\partial\phi\right) - \partial\overline{p}/\partial\phi\delta_{j\ell}$. Therefore, for a shearing mode of flow in which $-\partial\overline{p}/\partial\phi k^2 + 2\dot{\gamma}k_1k_2 < 0$ the flow is stable. This stability aspect under small fluctuations has never been studied before.

In these considerations one must bear in mind that the character of the problem is such that stability under small fluctuations does not necessary mean that there is no global stability. Assume that for some direction $\mathbf{k}/k$ the solidosity grows exponentially, then there comes a point at which the solidosity is so large that the maximum density is reached; at that point all the particles will touch and a collision process must take place, which will lead to a large particle pressure. This effect might be captured by a quadratic approach, but not by linear fluctuations. This is why, in some sense, the quadratic term has to be introduced pre-emptively to make the linear analysis work. A more rigorous quadratic theory will be presented in Section 6.1.

5.6. Linearly stable solutions

Now the analysis is continued for stable problems. Equation (5.15) is readily solved, using a temporal Fourier transform with frequency ω; the amplitude of all Fourier transforms is denoted by a tilde, for example the amplitude of of $\widehat{\phi}$ is denoted by $\widetilde{\phi}$. Note that the amplitude is still a complex variable, because of the spatial Fourier transform. Straightforwardly, one obtains

$$\widetilde{\phi} = \frac{\langle\phi\rangle \langle 1-\phi\rangle k_j k_\ell \widetilde{t}_{j\ell}}{\left(i\omega \left[\langle R\rangle + k^2 \langle 1-\phi\rangle \left(\langle\overline{\lambda}\rangle + 2\langle\overline{\mu}\rangle\right)\right] - \langle\phi\rangle \langle 1-\phi\rangle k_j k_\ell X_{j\ell}\right)}. \tag{5.16}$$

And what has been introduced here into the problem is a time scale through the parameter ω and a length scale through $\mathbf{k}$.

At this point the influence of permeability effects can be discerned. Suppose that there is a fluctuation in the distortion of a cell that leads it to contract or expand. The fluid must then be squeezed in or out into the surrounding medium. If the mean flow resistance is such that $\langle\overline{R}\rangle << k^2 \langle 1-\phi\rangle \left(\langle\overline{\lambda}\rangle + 2\langle\overline{\mu}\rangle\right)$ for all relevant k then this permeability effect may be neglected. In a continuum theory there is no way of telling whether this happens or not, as all values of k are permissible. In reality it is known that only those values of k that correspond to a length scale that is larger than a cell size are important. Call this size

$1/k_0$, then only values of $k < k_0$ need to be considered. The relevant spectrum of values of k is further limited by the consideration that the assembly size imposes a minimum value; let this be N_a/k_0, where N_a represents something like a maximum correlation length (say 10). Thus the relevant range for the magnitude of the wave vector is $k_0/N_a < k < k_0$. If in this range $\langle \overline{R} \rangle << k^2 \langle 1-\phi \rangle \left(\langle \overline{\lambda} \rangle + 2 \langle \overline{\mu} \rangle \right)$ then the effects of seepage may be ignored. In practice that means large particles as $\langle \overline{R} \rangle$ scales as D^{-2}.

5.7. Quantifying the fluctuations

The extra stress caused by the continuum fluctuations is now elaborated. Starting point is the expression for the stress (4.4)

$$t_{ij} = \frac{3\pi\eta D^2}{16V} \sum_{\mu=1}^{N} \sum_{\nu=1}^{N^\mu} \frac{n_i^{\mu\nu} c_j^{\mu\nu} c_\ell^{\mu\nu} n_k^{\mu\nu}}{h^{\mu\nu}} d_{k\ell}. \tag{5.17}$$

The fluctuation is

$$t_{ij}^{+} = \frac{3\pi\eta D^2 N}{16V} \left(\sum_{\nu=1}^{N^\mu} \frac{n_i^{\mu\nu} c_j^{\mu\nu} c_\ell^{\mu\nu} n_k^{\mu\nu}}{h^{\mu\nu}} \right)^{anisotropic} \langle d \rangle_{k\ell}. \tag{5.18}$$

The term in brackets is obviously time dependent. It states how the cell is deformed in the flow process.

Finally the fluctuations in the particle velocities are evaluated in terms of the stress fluctuations; this entails the substitution of the solution for the solidosity fluctuations. The result is rather tedious and reported here for completeness. $\widetilde{\mathbf{v}}$ is

$$\begin{aligned}
\widetilde{v}_\ell = & -\frac{\omega\langle\phi\rangle\langle 1-\phi\rangle\langle R\rangle\left(k_\ell k_i y_i - k^2 y_\ell\right)}{\langle\overline{\mu}\rangle k^2 D_0} k_j k_n \widetilde{t}_{jn} \\
& -\frac{\omega\langle\phi\rangle k^2\langle 1-\phi\rangle^2\langle\overline{\lambda}\rangle\left[\left(k_\ell k_i y_i - k^2 y_\ell\right) + \langle\overline{\mu}\rangle\left(k_\ell k_i y_i - 2k^2 y_\ell\right)\right]}{\langle\overline{\mu}\rangle k^2 D_0} k_j k_n \widetilde{t}_{jn} \\
& -\frac{ik_n\widetilde{t}_{\ell n}}{\langle\overline{\mu}\rangle k^2} + i\frac{\langle R\rangle^2\omega^2 k_\ell + \langle R\rangle\omega^2 k_\ell k^2\langle 1-\phi\rangle\left(2\langle\overline{\lambda}\rangle + 3\langle\overline{\mu}\rangle\right)}{\langle\overline{\mu}\rangle k^2 D_0} k_j k_n \widetilde{t}_{jn} + \\
& -i\frac{k^2\langle 1-\phi\rangle^2\left(\left(\langle\overline{\lambda}\rangle^2 + 3\langle\overline{\lambda}\rangle\langle\overline{\mu}\rangle + 2\langle\overline{\mu}\rangle^2\right)\omega^2 k_\ell k^2 + \langle\overline{\lambda}\rangle^2 k_i y_i\right)}{\langle\overline{\mu}\rangle k^2 D_0} k_j k_n \widetilde{t}_{jn},
\end{aligned} \tag{5.19}$$

where

$$\begin{aligned}
D_0 = & \langle R\rangle^2\omega^2 + 2\langle R\rangle\omega^2 k^2\langle 1-\phi\rangle\left(\langle\overline{\lambda}\rangle + 2\langle\overline{\mu}\rangle\right) + \\
& + \langle 1-\phi\rangle^2\left[\left(\langle\overline{\lambda}\rangle^2 + 4\langle\overline{\lambda}\rangle\langle\overline{\mu}\rangle + 4\langle\overline{\mu}\rangle^2\right)\omega^2 k^2 + \langle\phi\rangle^2 k_i y_i\right],
\end{aligned} \tag{5.20}$$

and $y_j = k_\ell X_{j\ell} = k_\ell\left(\langle d_{ii}\rangle\delta_{j\ell}\partial\overline{\lambda}/\partial\phi + 2\langle d_{j\ell}\rangle\partial\overline{\mu}/\partial\phi - \partial p/\partial\phi\delta_{j\ell}\right)$.

6. Stability and structures formation

6.1. Introduction

The linear perturbation analysis in chapter 5 leads to peculiar stability considerations. Essentially its result is: no sheared slurry flow can be stable unless there is a stabilising particle pressure. The form of the particle pressure used in chapters is one that depends entirely on the solidosity fluctuations. The solution of the solidosity in the Fourier domain is then, see expression (5.16)

$$\widetilde{\phi} = \frac{\langle\phi\rangle\,\langle 1-\phi\rangle\,k_j k_\ell \widetilde{t}_{j\ell}}{\left(i\omega\left[\langle R\rangle + k^2\,\langle 1-\phi\rangle\left(\langle\overline{\lambda}\rangle + 2\,\langle\overline{\mu}\rangle\right)\right] - \langle\phi\rangle\,\langle 1-\phi\rangle\,k_j k_\ell X_{j\ell}\right)}, \tag{6.1}$$

where $X_{j\ell} = \left(\langle d_{\ell\ell}\rangle\,\delta_{j\ell}\partial\overline{\lambda}/\partial\phi + 2\,\langle d_{j\ell}\rangle\,\partial\overline{\mu}/\partial\phi\right) - \partial\overline{p}/\partial\phi\delta_{j\ell}$ and the stress fluctuations originate on the cell-scale with Fourier amplitude $\widetilde{\mathbf{t}}$. The Fourier transforms here are both spatial and temporal. The stability stipulation follows from equation (5.15), and requires that $X_{j\ell}k_j k_\ell \leq 0$. The purpose of this chapter is to accommodate the particle pressure into the stability analysis and to study the implications. At issue is the fact that the particle pressure is not a simple fluctuating term. In the McTigue and Jenkins (1992) version of the theory its form is proportional to $D/h\sqrt{T}$ and this has no first order fluctuation, as is seen when one

tries to expand the expression: $\left(D/h\sqrt{T}\right)^{+} = \partial\left(D/h\right)/\partial\phi\phi^{+}\sqrt{T} + D/h\left(\sqrt{T}\right)^{+}$. As $\sqrt{T}$ is itself already composed of fluctuations there is no first order term. A second order term is therefore imperative.

Now, a problem arises. The analysis as it stands is carried out in the Fourier domain, which is done to avoid the spatial partial differentiations in the problem. If a non-linearity is introduced the Fourier analysis becomes far more complicated. Ultimately numerical tools will have to be introduced and the transparency that comes with an analytical solution is lost. The way forward is to make assumptions that enable one to maintain analytical insight, but which still capture the essence of the problem. Below such an approach is outlined. While all the assumptions that have been made would appear to be reasonable ones, it is always possible to debate the approach, as speculative elements are present.

The key to a successful conclusion of the theory is to introduce a new expression for the particle pressure in the Fourier domain. This expression approximates the McTigue and Jenkins (1992) if a local contribution is taken, but is subtly different. It is also non-linear, which enables a more advanced stability analysis. In general this is of course wrong; a product in the spatial domain should be replaced with a *convolution* in the Fourier domain. The error is corrected by introducing a weighting function. If this can be accepted a non-linear differential

equation replaces equation (5.15). This new differential equation will be shown to possess attractors outside $\widehat{\phi} = 0$. An analytical solution is still possible and the system is stable around the attractors. However, it will be shown that *structures* appear. In this way a link is made with Morris' (2006) work.

6.2. Convolutions

In this sub-section the mathematical properties of the convolution are discussed.

Consider two functions in the space domain $f(\mathbf{x})$ and $g(\mathbf{x})$, each having Fourier transforms $\widehat{f}(\mathbf{k})$ and $\widehat{g}(\mathbf{k})$. The Fourier transform is defined as

$$\widehat{f}(\mathbf{k}) = \int d_3 x f(\mathbf{x}) e^{-i\mathbf{k}.\mathbf{x}}; \tag{6.2}$$

its inverse is

$$f(\mathbf{x}) = \frac{1}{(2\pi)^3} \int d_3 k \widehat{f}(\mathbf{k}) e^{i\mathbf{k}.\mathbf{x}}. \tag{6.3}$$

The delta function is

$$\delta_3(\mathbf{x} - \mathbf{y}) = \frac{1}{(2\pi)^3} \int d_3 k e^{i\mathbf{k}.(\mathbf{x}-\mathbf{y})}. \tag{6.4}$$

The Fourier transform of the product $f(\mathbf{x}) g(\mathbf{x})$ is

$$\widehat{fg}(\mathbf{k}) = \int d_3x f(\mathbf{x}) g(\mathbf{x}) e^{-i\mathbf{k}.\mathbf{x}} = \tag{6.5}$$

$$\frac{1}{(2\pi)^6} \int d_3x \int d_3l \widehat{f}(\mathbf{l}) e^{i\mathbf{l}.\mathbf{x}} \int d_3m \widehat{g}(\mathbf{m}) e^{i\mathbf{m}.\mathbf{x}} e^{-i\mathbf{k}.\mathbf{x}} =$$

$$\frac{1}{(2\pi)^3} \int d_3l \widehat{f}(\mathbf{l}) \int d_3m \widehat{g}(\mathbf{m}) \delta_3(\mathbf{l}+\mathbf{m}-\mathbf{k}) =$$

$$\frac{1}{(2\pi)^3} \int d_3m \widehat{f}(\mathbf{k}-\mathbf{m}) \widehat{g}(\mathbf{m}).$$

Conversely, the inverse transform of a product of two functions is

$$\int d_3k \widehat{f}(\mathbf{k}) \widehat{g}(\mathbf{k}) e^{i\mathbf{k}.\mathbf{x}} = \int d_3k \int d_3y f(\mathbf{y}) e^{-i\mathbf{k}.\mathbf{y}} \int d_3z g(\mathbf{z}) e^{-i\mathbf{k}.\mathbf{z}} e^{i\mathbf{k}.\mathbf{x}} = \tag{6.6}$$

$$(2\pi)^3 \int d_3y \int d_3z f(\mathbf{y}) g(\mathbf{z}) \delta_3(\mathbf{x}-\mathbf{y}-\mathbf{z}) =$$

$$(2\pi)^3 \int d_3y f(\mathbf{y}) g(\mathbf{x}-\mathbf{y}).$$

This is, of course, a well-known result and generally true for a wide class of functions, including all the functions that have physical meaning in continuum mechanics. An important example of a convolution in the context of non-homogeneous media is the 'influence function'. The function $g(\mathbf{x})$ is then a function that multiplies a position-dependent weight to contributions $f(\mathbf{x})$ to give a

weighted sum. Convolutions of this kind occur quite frequently in the calculation of effective ("overall") moduli in a randomly nonhomogeneous medium. As this is the use of the convolution that will be employed below a further elaboration is here given.

By way of example consider the simple isotropic function in two dimensions $\widehat{F}(k) = k^{\ell}e^{-k\overline{a}}$, where ℓ is a number (preferably an integer) and $\overline{a}$ a lengthscale. The inverse Fourier transform of this function in two dimensions is

$$F(|x|,\varphi) = \frac{1}{(2\pi)^2}\int_0^{\infty} dk \int_0^{2\pi} d\vartheta k^{\ell+1}e^{-k\overline{a}}e^{ik|x|\cos(\vartheta-\varphi)} = \tag{6.7}$$

$$\frac{1}{2\pi}\int_0^{\infty} dk k^{\ell+1}e^{-k\overline{a}}J_0(k|x|) =$$

$$(-1)^{\ell+1}\frac{\partial^{\ell+1}}{\partial^{\ell+1}\overline{a}}\int_0^{\infty} dk e^{-k\overline{a}}J_0(k|x|) =$$

$$(-1)^{\ell+1}\frac{\partial^{\ell+1}}{\partial^{\ell+1}\overline{a}}\left(\frac{1}{\sqrt{\overline{a}^2+|x|^2}}\right).$$

Clearly the use of $F(\mathbf{x})$ as an influence function is obvious, as it multiplies any contributions further away from an evaluation point with a decreased weight. The rate at which it does so is controlled by the length scale $\overline{a}$. The greater ℓ is (for higher ℓ the function may be negative) the steeper the decline, see Figure 6.1

where the function is plotted normalised to the value in $|x| = 0$.

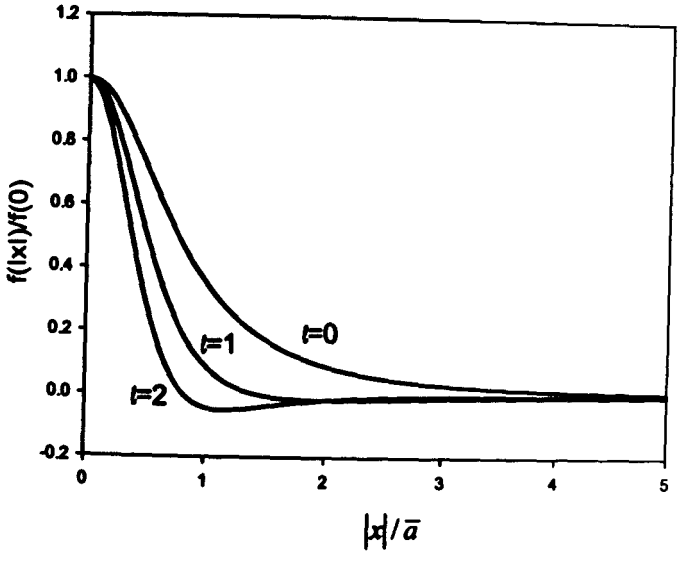

Fig 6.1. The normalised influence function for various values of ℓ.

The example is purely mathematical and for illustration only. However, in studying the physical problem an issue come to the for that was first observed in the previous chapter, the fact that in the continuum theory there is no length scale. For a linear analysis this does not matter, but in a more realistic setting it should be considered that there is no continuum physics on scales less than the cell scale. In the Fourier domain smaller scales correspond to larger wave vectors. To avoid problems for $k \to \infty$ a suppressing factor is introduced. In the above this has been achieved by employing the exponential $e^{-k\bar{a}}$, which 'cuts off' at length scales which are significantly less than $\bar{a}$.

6.3. Cell-scale correction for the equation that governs $\widehat{\phi}$

In this sub-section it is shown that the inclusion of a non-linear term requires an appropriate cells-scale correction. In the previous sub-section it was shown that a multiplicative term, for example of the form $e^{-k\bar{a}}$, needs to be included to avoid problems at the sub-cell-scale. Here that concept is taken further. For simplicity the mean fluid motion is ignored by making $\langle R \rangle = 0$ and the global loading path is one of a pure shear rate with no volume effects: $\langle d_{jj} \rangle = 0$, and therefore $X_{j\ell} = 2 \langle d_{j\ell} \rangle \partial\overline{\mu}/\partial\phi$. Including the particle pressure term in the evolution equation for the solidosity fluctuations gives

$$\frac{D\widehat{\phi}}{Dt} = \frac{\langle\phi\rangle k_j k_\ell \widehat{t}_{j\ell}}{k^2\left(\langle\overline{\lambda}\rangle + 2\langle\overline{\mu}\rangle\right)} + \frac{\langle\phi\rangle k_j k_\ell X_{j\ell}}{k^2\left(\langle\overline{\lambda}\rangle + 2\langle\overline{\mu}\rangle\right)}\widehat{\phi} - \frac{\langle\phi\rangle}{\langle\overline{\lambda}\rangle + 2\langle\overline{\mu}\rangle}\widehat{\overline{p}}. \tag{6.8}$$

The term proportional to $\widehat{\overline{p}}$ is going to be non-linear - say quadratic in $\widehat{\phi}$. If the latter is cut off by a factor $f(k)$ (this was $e^{-k\bar{a}}$ in the previous subsection) then $\widehat{\overline{p}}$ will be cut off as $f^2(k)$. At the same time the second term on the right hand side is cut off according to $f(k)$ and in a stationary model in which the second and third term are balanced a factor $f(k)$ is lost. This is avoided by realising that the equation is flawed in the first place, because it was derived assuming that the partial differentiations that give rise to the factors $k_j k_\ell$ would be valid at sub-cell

scales, which obviously they are not. The problem is circumvented by introducing a cut-off from the outset and replace $k_j k_\ell$ everywhere by $k_j k_\ell f(k)$

$$\frac{D\widehat{\phi}}{Dt} = \frac{f(k)\langle\phi\rangle k_j k_\ell \widehat{t}_{j\ell}}{k^2\left(\langle\overline{\lambda}\rangle + 2\langle\overline{\mu}\rangle\right)} + \frac{f(k)\langle\phi\rangle k_j k_\ell X_{j\ell}\widehat{\phi}}{k^2\left(\langle\overline{\lambda}\rangle + 2\langle\overline{\mu}\rangle\right)} - \frac{\langle\phi\rangle}{\langle\overline{\lambda}\rangle + 2\langle\overline{\mu}\rangle}\widehat{\overline{p}}. \tag{6.9}$$

The question now is: what is an adequate choice for $f(k)$? To find out more $k_j k_\ell f(k)/k^2\widehat{\phi}(\mathbf{k})$ is viewed as a convolution in the spatial domain, that is $k_j k_\ell f(k)/k^2\widehat{\phi}(\mathbf{k}) \to (2\pi)^2 \int [\mathcal{F}^{-1}(k_j k_\ell f(k)/k^2)](\mathbf{x}-\mathbf{y})\phi^+(\mathbf{y})\, d_2 y$ ($\mathcal{F}^{-1}$ is the inverse Fourier transform). It is expected that a local contribution to $\phi^+(\mathbf{y})$ will dominate, though that should not be infinite.

The first possibility is that no weighting function is needed, so set $f(k) = 1$ and evaluate

$$\int_0^\infty dk k \int_0^{2\pi} d\theta \frac{k_j k_\ell}{k^2} e^{i\mathbf{k}.\mathbf{x}} = -\frac{\partial^2}{\partial x_j \partial x_\ell}\int_0^\infty dk \int_0^{2\pi} d\theta \frac{1}{k} e^{i\mathbf{k}\mathbf{x}} = \tag{6.10}$$

$$-2\pi\frac{\partial^2}{\partial x_j \partial x_\ell}\int_0^\infty dk \frac{J_0(k|\mathbf{x}|)}{k} =$$

$$-2\pi n_\ell \frac{\partial}{\partial x_j}\int_0^\infty dk J_1(k|\mathbf{x}|) = 2\pi n_\ell \frac{\partial}{\partial x_j}\frac{1}{|\mathbf{x}|}.$$

This clearly diverges in $|\mathbf{x}| \to 0$ (as $|\mathbf{x}|^{-2}$) and therefore another choice for $f(k)$

is made; as in the previous subsection set $f(k) = e^{-k\bar{a}}$. Now the integrals are

$$\int_0^\infty dk k \int_0^{2\pi} d\theta e^{-k\bar{a}} \frac{k_j k_\ell}{k^2} e^{i\mathbf{k}.\mathbf{x}} = -\frac{\partial^2}{\partial x_j \partial x_\ell} \int_0^\infty dk \int_0^{2\pi} d\theta \frac{e^{-k\bar{a}}}{k} e^{i\mathbf{k}.\mathbf{x}} = \tag{6.11}$$

$$-2\pi \frac{\partial^2}{\partial x_j \partial x_\ell} \int_0^\infty dk \frac{e^{-k\bar{a}} J_0(k|\mathbf{x}|)}{k} =$$

$$-2\pi n_\ell \frac{\partial}{\partial x_j} \int_0^\infty dk e^{-k\bar{a}} J_1(k|\mathbf{x}|) =$$

$$-2\pi n_\ell \frac{\partial}{\partial x_j} \left(\frac{1}{|\mathbf{x}|} \frac{\sqrt{\bar{a}^2 + |\mathbf{x}|^2} - \bar{a}}{\sqrt{\bar{a}^2 + |\mathbf{x}|^2}} \right).$$

This still diverges as $|\mathbf{x}| \to 0$ and $\bar{a} \neq 0$, indicating that a simple exponential is insufficient to suppress the infinity. A sharper cut-off is required and a function

of the form $f(k) = e^{-k^2\bar{a}^2}$ is attempted. The integrals are then

$$\int_0^\infty dk k \int_0^{2\pi} d\theta e^{-k^2\bar{a}^2} \frac{k_j k_\ell}{k^2} e^{i\mathbf{k}.\mathbf{x}} = -\frac{\partial^2}{\partial x_j \partial x_\ell} \int_0^\infty dk \int_0^{2\pi} d\theta \frac{e^{-k^2\bar{a}^2}}{k} e^{i\mathbf{k}.\mathbf{x}} = \tag{6.12}$$

$$-2\pi \frac{\partial^2}{\partial x_j \partial x_\ell} \int_0^\infty dk \frac{e^{-k^2\bar{a}^2} J_0(k|\mathbf{x}|)}{k} =$$

$$-2\pi n_\ell \frac{\partial}{\partial x_j} \int_0^\infty dk e^{-k^2\bar{a}^2} J_1(k|\mathbf{x}|) =$$

$$-\frac{\pi^{3/2}}{2\bar{a}} n_\ell \frac{\partial}{\partial x_j} \left[\frac{1}{|\mathbf{x}|} e^{-|\mathbf{x}|^2/(8\bar{a}^2)} I_{1/2}\left(\frac{|\mathbf{x}|^2}{8\bar{a}^2} \right) \right]. \tag{6.13}$$

This is finite for $|\mathbf{x}| \to 0$ as the modified Bessel function $I_{1/2}(z)$ behaves as $\sqrt{2z/\pi} + O(z^{5/2})$. In passing it is noted that the expression in square brackets declines as $|\mathbf{x}|^{-3/2}$ for $|\mathbf{x}| \to \infty$. Therefore, for a cut-off function the choice $f(k) = e^{-k^2\bar{a}^2}$ is made.

6.4. Stability analysis with non-linear particle pressure

The expression for the particle pressure fluctuations in the Fourier domain are now introduced. Clearly, they must be proportional to $\widehat{\phi}$. However, an influence function is required. For this the choice $\left|\widehat{\phi}\right|$ is made; in other words the magnitude of the fluctuations itself acts as influence function. This choice is the only one possible for positive influence functions, other than that factor of k might be

included. Inspecting the equation of continuity for the particles it is observed that a time scale and a length scale are required to connect between $\left|\widehat{\phi}\right|$ and $|\widehat{\mathrm{v}}|$; the time scale is derived from the overall time scale of the problem, which is $|\langle \mathrm{d} \rangle|^{-1}$ and a length scale follows from k^{-1}. The spatial dimension of the problem is called d. The dimension of $\widehat{\phi}$ is then $length^d$; the other dimensions are standard: $\langle \mathrm{d} \rangle$ has dimension $time^{-1}$, k has dimension $length^{-1}$, $\widehat{\overline{p}}/\eta$ has $time^{-1} length^d$. Dimensional analysis leads then to the following choice of $\widehat{\overline{p}}$

$$\widehat{\overline{p}}\,(\mathbf{k}) = \overline{c}\eta\,|\langle \mathrm{d} \rangle|\,\frac{\left|\widehat{\phi}\right|\widehat{\phi}}{ka^{d+1}}, \tag{6.14}$$

where $\overline{c}$ is a constant; the length scale a is the particle size. The value of $\overline{c}$ is of the order of unity times $(1 - e_c)$ (the solid collisional restitution factor that appears in the particle pressure).

Here the dimension is set to 2. Equation (6.9) becomes for pure shear

$$\frac{D\widehat{\phi}}{Dt} = \frac{\langle \phi \rangle\, k_j k_\ell f\,(k)\,\widehat{t}_{j\ell}}{k^2\left(\langle \overline{\lambda} \rangle + 2\,\langle \overline{\mu} \rangle\right)} + \frac{\langle \phi \rangle\, k_1 k_2 f\,(k)\, X_{12}}{k^2\left(\langle \overline{\lambda} \rangle + 2\,\langle \overline{\mu} \rangle\right)}\widehat{\phi} - \frac{\langle \phi \rangle\, \overline{c}\eta\,|\langle \mathrm{d} \rangle|}{\langle \overline{\lambda} \rangle + 2\,\langle \overline{\mu} \rangle}\frac{\widehat{\phi}\left|\widehat{\phi}\right|}{ka^{d+1}}. \tag{6.15}$$

This equation is multiplied by the complex conjugate of $\widehat{\phi}$ (complex conjugates are denoted by a *); then the complex conjugate of the whole equation is taken

and the result is multiplied by $\widehat{\phi}$. The two equations are then added up; this gives

$$\widehat{\phi}^{*}\frac{D\widehat{\phi}}{Dt}+\widehat{\phi}\frac{D\widehat{\phi}^{*}}{Dt} = \frac{\langle\phi\rangle k_j k_\ell f(k)\left(\widehat{t}^{*}_{j\ell}\widehat{\phi}+\widehat{t}_{j\ell}\widehat{\phi}^{*}\right)}{k^2\left(\langle\overline{\lambda}\rangle+2\langle\overline{\mu}\rangle\right)}+\frac{\langle\phi\rangle f(k) k_1 k_2 X_{12}}{k^2\left(\langle\overline{\lambda}\rangle+2\langle\overline{\mu}\rangle\right)}\widetilde{\phi\phi}^{*} - \frac{\langle\phi\rangle\overline{c}\eta\left|\langle\mathbf{d}\rangle\right|}{\langle\overline{\lambda}\rangle+2\langle\overline{\mu}\rangle}\widetilde{\phi\phi}^{*}\frac{\left|\widehat{\phi}\right|}{ka^{d+1}}. \tag{6.16}$$

Rearranging and using the fact that $\widetilde{\phi\phi}^{*}=\left|\widehat{\phi}\right|^2$ leads to

$$\frac{D\left|\widehat{\phi}\right|^2}{Dt} = \frac{\langle\phi\rangle k_j k_\ell f(k)\left(\widehat{t}^{*}_{j\ell}\widehat{\phi}+\widehat{t}_{j\ell}\widehat{\phi}^{*}\right)}{k^2\left(\langle\overline{\lambda}\rangle+2\langle\overline{\mu}\rangle\right)}+\frac{\langle\phi\rangle f(k) k_1 k_2 X_{12}}{k^2\left(\langle\overline{\lambda}\rangle+2\langle\overline{\mu}\rangle\right)}\left|\widehat{\phi}\right|^2 - \frac{\langle\phi\rangle\overline{c}\eta\left|\langle\mathbf{d}\rangle\right|}{\langle\overline{\lambda}\rangle+2\langle\overline{\mu}\rangle}\frac{\left|\widehat{\phi}\right|^3}{ka^{d+1}}. \tag{6.17}$$

The homogeneous part of this equation contains attractors. The part proportional to $\left(\widehat{t}^{*}_{j\ell}\widehat{\phi}+\widehat{t}_{j\ell}\widehat{\phi}^{*}\right)$ fluctuates in time, so the physical interpretation of equation (6.17) is that $\left|\widehat{\phi}\right|^2$ fluctuates around the attractors, the fluctuations being driven by the anisotropic cell fluctuations. The attractors are found by setting

$$\frac{\langle\phi\rangle k_1 k_2 f(k) X_{12}}{k^2\left(\langle\overline{\lambda}\rangle+2\langle\overline{\mu}\rangle\right)}\left|\widehat{\phi}\right|^2-\frac{\langle\phi\rangle\overline{c}\eta\left|\langle\mathbf{d}\rangle\right|a^{-d-1}}{\langle\overline{\lambda}\rangle+2\langle\overline{\mu}\rangle}\frac{\left|\widehat{\phi}\right|^3}{k}=0, \tag{6.18}$$

which leads to

$$\frac{k_1 k_2 f(k) X_{12}}{k^2} \left|\widehat{\phi}\right|^2 - \bar{c}\eta \left|\langle \mathbf{d} \rangle\right| \frac{\left|\widehat{\phi}\right|^3}{k a^{d+1}} = 0, \tag{6.19}$$

or

$$\left|\widehat{\phi}\right|_1 = 0; \ \left|\widehat{\phi}\right|_2 = \frac{k_1 k_2 f(k) X_{12} a^{d+1}}{k\bar{c}\eta \left|\langle \mathbf{d} \rangle\right|}. \tag{6.20}$$

The location of the attractors is illustrated by making a phase diagram. Choosing the sign of the shear rate such that $X_{12} > 0$, then the phase diagram looks like Figure 6.2.

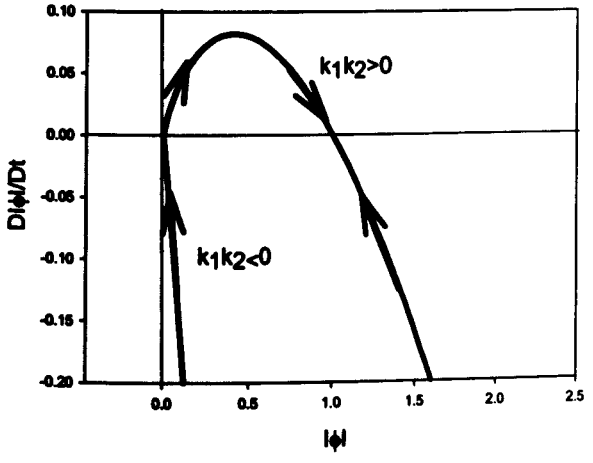

Figure 6.2. Illustration of the phase diagram of equation (6.17). In this picture k has been set to unity.

It is observed that for $k_1 k_2 < 0$ $\left|\widehat{\phi}\right| = 0$ is the attractor, while for $k_1 k_2 > 0$ $\left|\widehat{\phi}\right| = \left[k_1 k_2 f(k) X_{12} / \left(k\bar{c}\eta \left|\langle \mathbf{d} \rangle\right| a^{-d-1}\right)\right]$ is the attractor and $\left|\widehat{\phi}\right| = 0$ is the repeller.

Using this finding the harmonic intensity is as illustrated in fig 6.3.

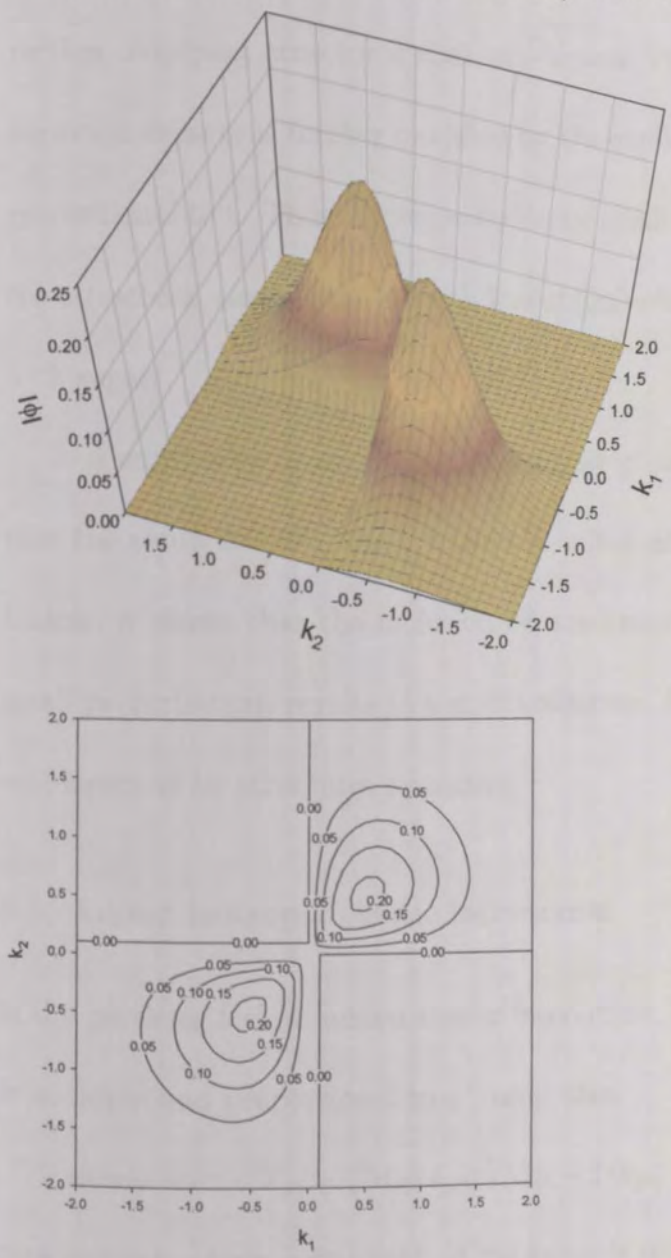

Figure 6.3. The harmonic density as it follows from the homogeneous part of Equation 6.17; the loading here is pure shear.

The result shows that there are peaks in the spectrum in the expansive direction, implying structures that are layered in the contractive direction. The harmonic density is further modified by the explicit time-dependence of the terms proportional to $\widehat{\mathbf{t}}$. These are expected to be small and will cause excursions around the attractors, causing the smooth line of figure 6.3 to be clouded, as if it is topped with sugar.

It is emphasised again that the analysis given in this sub-section is wrong in that the result is directional, while the initial assumption was isotropic. Nevertheless, it shows that the inclusion of non-linearity into the equations that rule small perturbations results in a stable outcome. It also shows that the stability is accompanied by structures formation.

6.5. Added isotropic elastic interaction

If the particles feel an added elastic interaction, that is a term arises in $\overline{p}$ which is isotropic and proportional to ϕ^+ only, then

- as was seen - $X_{j\ell} = \left(\langle d_{\ell\ell}\rangle\, \delta_{j\ell}\partial\overline{\lambda}/\partial\phi + 2\,\langle d_{j\ell}\rangle\, \partial\overline{\mu}/\partial\phi\right) - \partial\overline{p}/\partial\phi\delta_{j\ell}$ and $X_{j\ell}k_jk_\ell$ gets and extra term $-\partial\overline{p}/\partial\phi k^2$. If the latter is sufficiently large then $X_{12}k_1k_2 \leq 0$ and the system is linearly stable. The stability equation from the previous sub-section becomes

$$\frac{-k^2 \partial \overline{p}/\partial \phi + k_1 k_2 f(k) X_{12}}{k^2} \left|\widehat{\phi}\right|^2 - \bar{c}\eta \left|\langle \mathrm{d} \rangle\right| a^{-d-1} \frac{\left|\widehat{\phi}\right|^3}{k} = 0, \qquad (6.21)$$

with the front factor to the first term negative. This implies that there is no solution for the attractor other than $\left|\widehat{\phi}\right| = 0$, which means that there are no structures. If the term $\partial \overline{p}/\partial \phi$ is slowly increased from zero then the attractor outside $\left|\widehat{\phi}\right| = 0$ will move to the left (the structure amplitude becomes less) until it is zero.

So, this theory predicts that when an elastic interaction of increasing strength is introduced the structures will gradually disappear. This prediction will be verified in the next section.

6.6. Other higher order terms

The particle pressure introduced here represents a second order term of the form $\widehat{\phi}\left|\widehat{\phi}\right|$. It is added to a system of equations that is linear in $\widehat{\phi}$ and this system was obtained by doing a linear expansion. Naturally there must be terms that can be obtained by expanding further to a quadratic form. In the Fourier domain these terms will take the form of convolutions. These can again be viewed as integrals over weighting functions. The difference between these terms and the term of the

form $\widehat{\phi}\left|\widehat{\phi}\right|$ is that the weighting functions obtained from the quadratic expansion fluctuate with an average of zero, while the weighting function for the term of the form $\widehat{\phi}\left|\widehat{\phi}\right|$ is $\left|\widehat{\phi}\right|$. The latter is always positive and truly adds the contributions of $\widehat{\phi}$ from its surroundings, while a fluctuating weighting function will more or less cancel out. This is the reason that the quadratic fluctuations are dominated by the $\widehat{\phi}\left|\widehat{\phi}\right|$ term.

7. Simulation

7.1. Introduction

Numerical simulations, which take account of the hydrodynamic force between suspended particles have been developed in recent years; they are swift becoming useful tools for studying the dynamics and rheological properties of suspensions. In order to understand and interpret the results of the simulations theory is required that provides a framework for the interrogation of the numerical experiment. In this thesis the theory has been developed first – previous chapters – and now the simulation is developed.

In the last fifteen years a number of papers have been published describing simulations of particle fluid mixtures. These will now be briefly reviewed. The simulist's ideal would be to simulate the fluid particles and solid particles in the suspension simultaneously. For the systems envisaged in this thesis, where the particles are macroscopic, non-Brownian objects, computers are not powerful enough yet to accomplish such a calculation (though for smaller, colloidal particle-fluid systems – at given temperature - good progress is being made, see Heyes (1995)). The fluid must therefore be modelled as a continuum. There are two groups of these simulations: those that employ a Stokesian Dynamics (SD) method: Bossis

and Brady (1984) Dratler and Schowalter (1996), Sighh and Nott (2002), Marchior and Acrivos (2001) and those that use a Lattice Bolzmann (LB) approach, Ladd (1994). In the former the Stokes equations (that is the very low-Reynolds number Navier Stokes equations) are solved by means of a 'multipole expansion' that is broken off after a finite number of terms. In LB, the evolution of a discretized velocity distribution of the fluid particles is calculated on a grid (lattice); this method is ideal for the very complicated boundary conditions that are encountered in particle fluid systems.

Both methods break down when the distance between the particles becomes small. In LB, for example, the distance between the particle surfaces may become smaller than the lattice dimension and then special measures have to be taken to keep the method going. In both LB and SD the problems associated with close proximity between particles may be resolved by noting that an analytical solution of the fluid flow for narrow gaps between smooth surfaces is available: this is of course the lubrication limit, see Section 2.2. The motion of the particles is determined by the force they exert on one another and the lubrication limit provides an approximation for the force between two smooth particles that move relative to one another. This force is singular (normal relative motion between two spheres is resisted by the force proportional to h^{-1}) when h vanishes and

in practical computing terms where time steps are finite the implication is that particles will sometimes overlap. This is highly unphysical and must be avoided at all cost. Therefore, in the literature on both SD and LB, a strongly repulsive short-range interaction is introduced, which keeps the particles away from one another. The short-range interaction is also described in this thesis, see Section 2.5.

In the simulation that is proposed here neither Lattice Bolzmann, nor Stokesian Dynamics will be used and the role of the repulsive short-range force is re-examined. The approach taken here is to take the view that – as a result of the singularity of lubrication interaction – the actual fluid motion in the pores of the slurry is relatively unimportant, and the whole simulation is done with the lubrication interaction only. Furthermore, the particles are rough and the velocity-distance-dependence of the interactive force is given by equation (2.11) . At the same time a collision rheology for particle pairs is implemented, just like in Section 2.4.

The fluid is now merely a medium for the transferral of the interactive force, which applies at "contact points" – these are the points of closest proximity – and the simulation is done using the Discrete Element Method (DEM). What this implies is a very quick and very transparent simulation.

The purpose of our simulation (which is really a solution of a many-particle problem) is to use the theory developed in Section 2.2 to investigate the outcome. In brief the theory states that structures form when there is a collisional rheology for the particle pressure and that these structures disappear when a strong interaction is introduced that repels the particles. The latter is of course exactly what the authors of the LB and SD methods do and the question is whether their simulations are in any way trustworthy for the understanding of slurry flow behaviour. Put another way: is a slurry in which a short-range interaction operates a different system than one in which there is merely a collisional contact rheology? Bear in mind that the current mainstream papers on slurry simulation do not employ the rough particle interaction and rely entirely on the "Derjaguin" (double layer type) interaction to make the simulation work.

Yet another way of phrasing this is in terms of length scales. The asperity height is one length scale, the range of repulsive force is another one. For "classical" particles (in real, civil engineering or geological slurries) the roughness length scale is much greater than the double layer interaction length scale. So it makes sense to investigate what the implications are that result from a choice of interaction.

The simulation can be done in two, or three dimensions; below a two-dimensional

implementation is featured. This has the advantage of easy visualisation and also makes a comparison with theoretical derivation in chapter 2 more relevant. The simulation is the solution to the shear problem for many particles. This is exactly what the theory also attempts. The shear rate is $\dot{\gamma}$. The fluid viscosity is $\eta = 0.001$Pas, a time step proportional to inverse of shear rate, $(1/\dot{\gamma})$ and particles are restricted to the (x, y)-plane, the plane of shear.

7.2. Discrete Element Method

The Discrete Element Method (DEM) is a family of the numerical methods for computing the motion of a large numbers of particles. The method is for granular materials as individual elements which can make and break contacts with their neighbours and are capable of analyzing interacting bodies undergoing large absolute or relative motions. In the DEM, elements can represent either discrete objects, such as individual grains of sand, or bulk materials. In the experiments presented in this study the former is obviously used. To avoid the assembly falling into a regular packing, the particles are hetero-disperse, drawn from a narrow grainsize distribution. Generally, contact forces are determined between nearest neighbours and the interactive force is in the direction of the vector that connects the line of centres. The collision of two discs produces non-zero forces only when

particles overlap (slightly).

The (DEM) simulation is started by putting all particles in a random position and giving them initial zero velocity. The interactive forces on each particle are summed at each time step and then Newton's law is used to obtain the acceleration.

$$\mathbf{a} = \frac{\mathbf{F}}{m}, \tag{7.1}$$

where m is mass of particle, $\mathbf{F}$ is the sum of forces. There are various possible integration schedules. The simplest one is the Euler system. Integration over a small time Δt will give the velocity and position of the particles at time $t + \Delta t$ as follows

$$\mathbf{v}(t + \Delta t) = \mathbf{v}(t) + \mathbf{a}(t)\Delta t; \tag{7.2}$$

$$\mathbf{x}(t + \Delta t) = \mathbf{x}(t) + \mathbf{v}(t)\,\Delta\, t + \frac{1}{2}\mathbf{a}\,(\Delta t)^2\,. \tag{7.3}$$

A somewhat more efficient scheme is Verlet's schedule, which is designed to suppress the term proportional to $(\Delta t)^3$ by considering the kinetic variables at times

$t \pm \Delta t$. The 'basic' Verlet schedule takes the form

$$\mathbf{x}(t + \Delta t) = 2\mathbf{x}(t) - \mathbf{x}(t - \Delta t) + \mathbf{a}\,(\Delta t)^2\,. \tag{7.4}$$

The incorporation of the velocity in the scheme leads to the so-called 'velocity' Verlet integration

$$\mathbf{x}(t + \Delta t) = \mathbf{x}(t) + \mathbf{v}(t)\,\Delta\, t + \frac{1}{2}\mathbf{a}\,(\Delta t)^2\,; \tag{7.5}$$

$$\mathbf{v}(t + \Delta t) = \mathbf{v}(t) + \frac{1}{2}\,[\mathbf{a}(t) + \mathbf{a}(t + \Delta t)]\,\Delta t. \tag{7.6}$$

All three schedules are commonly used. Cundall and Strack (1979), who invented the DEM method, use the Euler schedule. Where there are collisions in the system, which operate in one time step, the Euler method is probably preferable.

After each integration step the new positions are used to compute the forces during the next step and this loop is repeated for a long series of time steps.

The force that we have considered in our simulation is the lubrication interaction for rough particles, which has been calculated analytically, in chapter 2 for small Reynolds numbers. Because of the roughness, there is no singularity for $h \to 0$. So the particles can touch each other at finite velocity. On touching the

collision rheology described in chapter 2 is invoked.

7.3. Details of the simulation

Particles in this simulation can contact at non-zero velocities so a collision mechanism has to be supplied. There are N particles in a two dimensional rectangular box, which leads to a two-dimensional 'volume' fraction $\phi = \pi N a^2/A$, where A is the area of the rectangle. For hetero-disperse aggregates in which there are n_i particles with radius a_i ($\sum n_i = N$) the solidosity is $\phi = \pi \sum (n_i a_i^2)/A$. The particles are positioned in the box by drawing from a grainsize distribution until a preset solidosity is reached. From the latter the mean distance between particles is estimated using formula (3.44); this formula is obviously valid in three dimensions and not in two, but only a rough estimate of h/a is required. The mean velocity between particles is of the order $\dot{\gamma}a$. The time step is then such that $\Delta t << h/(\dot{\gamma}a)$. In the program $\Delta t = 0.1h/(\dot{\gamma}a)$ is chosen.

Boundary conditions are applied by making the top and bottom walls of fixed particles with average radius. These walls are given equal sized velocities in opposite directions. The boundary conditions in the horizontal direction are periodic. The initial conditions is that all particles have zero velocity. It then takes about 10,000 steps before the motion at the boundary is communicated to all the parti-

cles and the study of the result can commence. The initial particle positions are randomly generated.

The program uses a scaled unit system. All lengths are scaled to a factor a_s; all masses to m_s and all times to t_s. In a three dimensional setting the mass density scaling is now $m_s/(a_s)^3$; the viscosity scale is $m_s/(a_s t_s)$; the velocity scale is a_s/t_s. The lubrication interaction is also used in its three dimensional version in which a front factor $D^2\eta$ appears, which has to be declared in the program. Typical values for the particle diameters are order of magnitude of millimeters, for the particle mass density order $10^3 kg/m^3$ and for the viscosity the water value $10^{-3} Pas$. Typical velocities are of the order of $10^{-2} m/s$.

The simulation is performed using different particle sizes; the initial configuration for $N = 80$ is presented in figure 7.1. The restitution coefficient for the collisional rheology is $e_c = 0.26$. The asperity height is $0.01\,\langle a \rangle$.

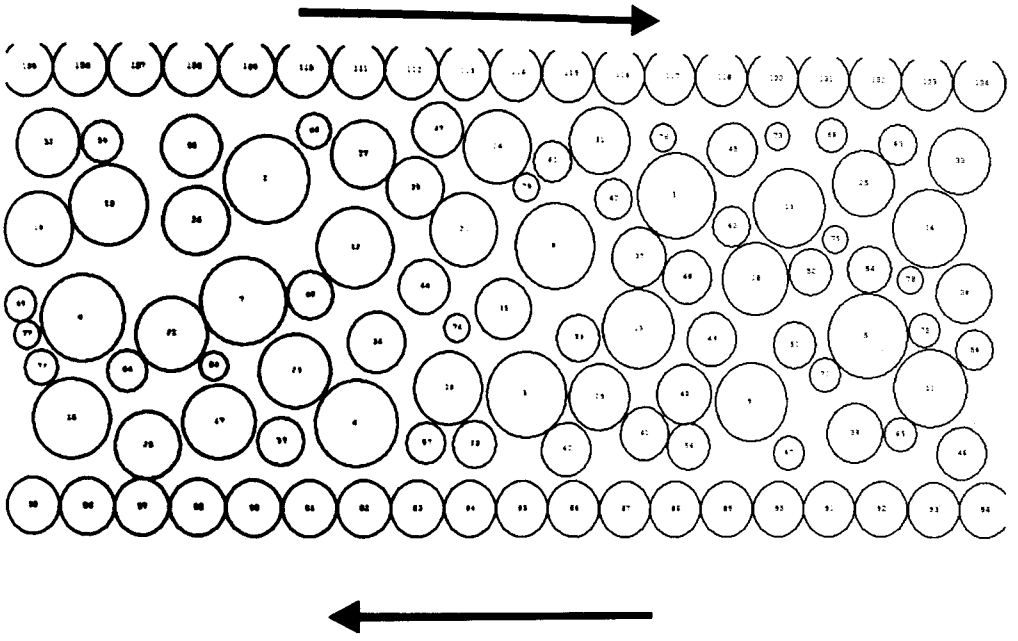

Fig 7.1. Initial configuration of particles in a shear box.

7.4. Structures formation

The first simulation that is shown here is the one with parameters as in the previous sub-section. The interparticle interaction is here *the lubrication interaction with collisions only.* In figures 7.2, 7.3 and 7.4 the resulting particle positions are displayed at progressive times for an average solidosity of 0.55.

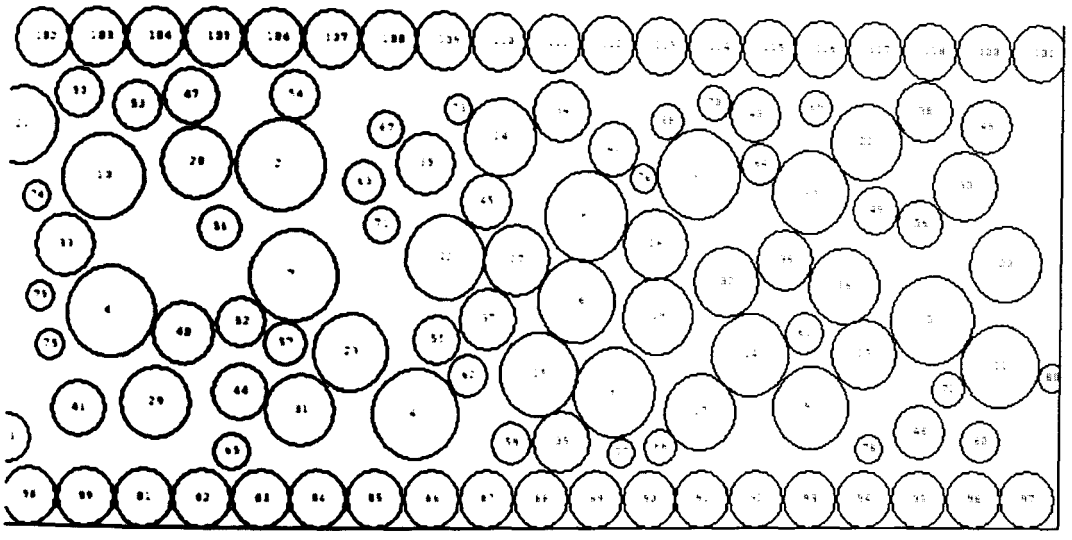

Fig 7.2. The shear box simulation with rough lubrication interaction only after **600 time steps.**

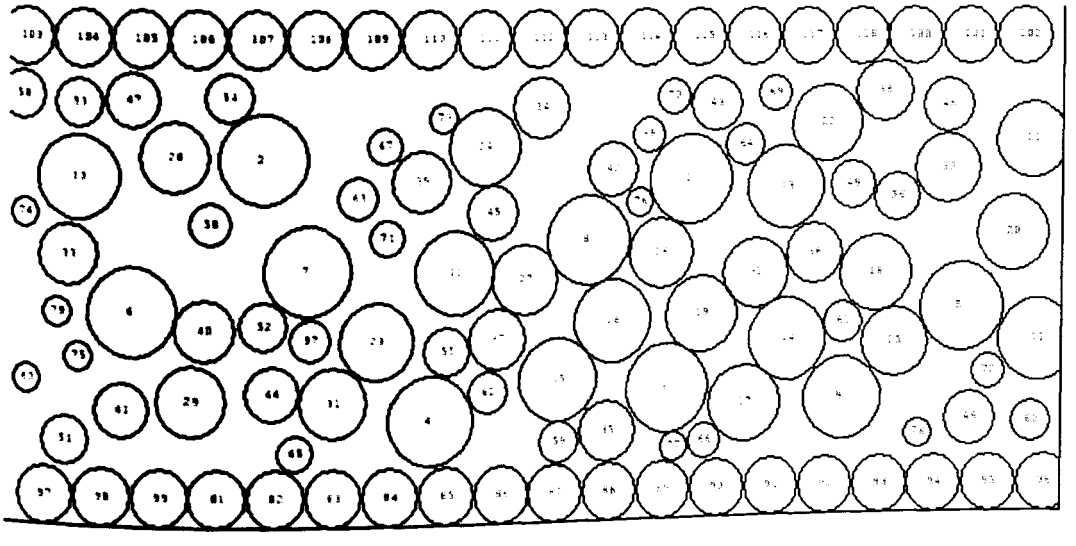

Fig 7.3. The shear box simulation with rough lubrication interaction only after **1000 time steps.**

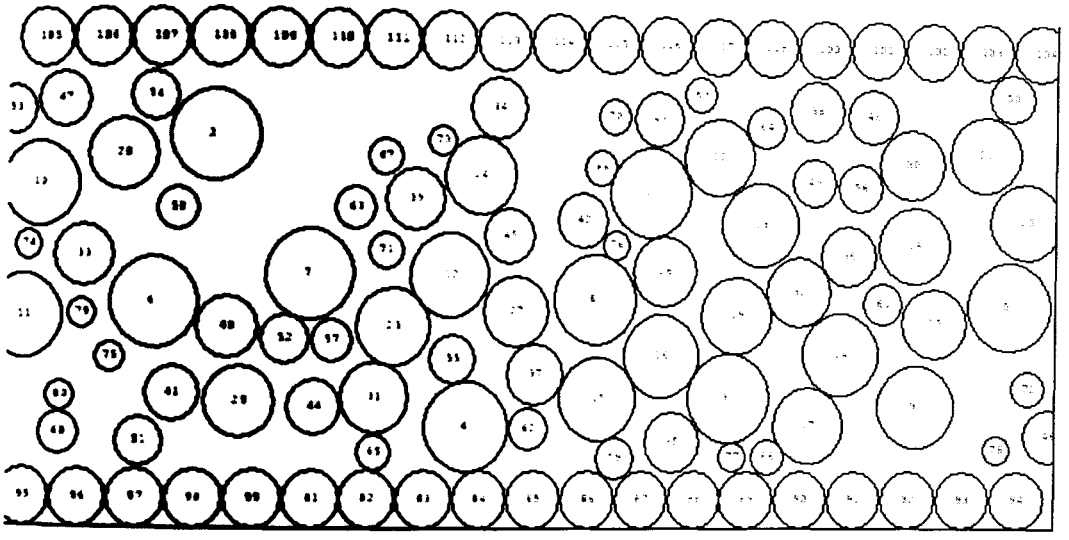

Fig 7.4. The shear box simulation with rough lubrication interaction only after **1500 time steps.**

It is clearly seen that 'streets' develop. The simulation organises itself in **structures. The wavelength of the** structures is some three particles.

The effect is to a large extent, independent of the solidosity. However, for high **solidosites ($\phi > 0.65$) an effect called** "jamming" occurs. When the assembly gets **in to the jammed state particles** make enduring contact and no smooth flow takes **place. This regime is not the** subject of this thesis.

7.5. Effect of repulsive force

To prevent particle overlap, the Stokesian Dynamics community introduce an inter-particle repulsive interaction of the form discussed in Section 2.5.

$$\mathbf{F} = \frac{F_0}{h_0} \frac{e^{-\frac{h}{h_0}}}{1 - e^{-\frac{h}{h_0}}} \mathbf{n}. \tag{7.7}$$

A useful reference here is Dratler and Schowalter (1996). They experiment with the repulsive force and find that when it is very small or very short range structures form, just as the ones found in the previous sub-section. They then increase the strength of the interaction and the structures disappear. Their conclusion is extraordinary: structures are undesirable and therefore the repulsive force is imperative.

Here the repulsive force will also be used in the simulation. Figures 7.6, 7.7 and 7.8 show the result at different time steps for average solidosity of 0.58, $h_0 = 0.03 \langle a \rangle$ and F_0 a 'large' value of 10.

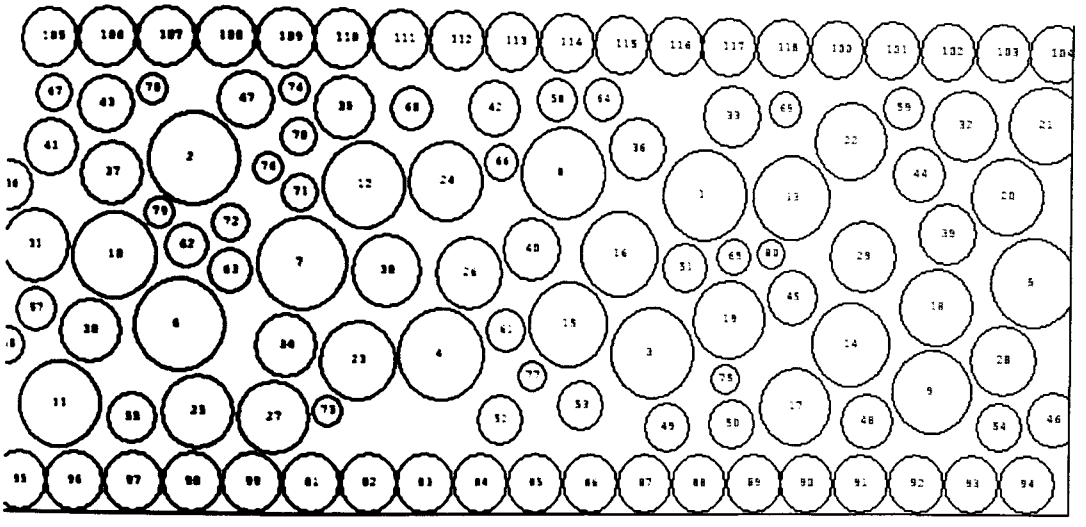

Fig 7.7. Simulation with repulsive interaction after 2000 time steps.

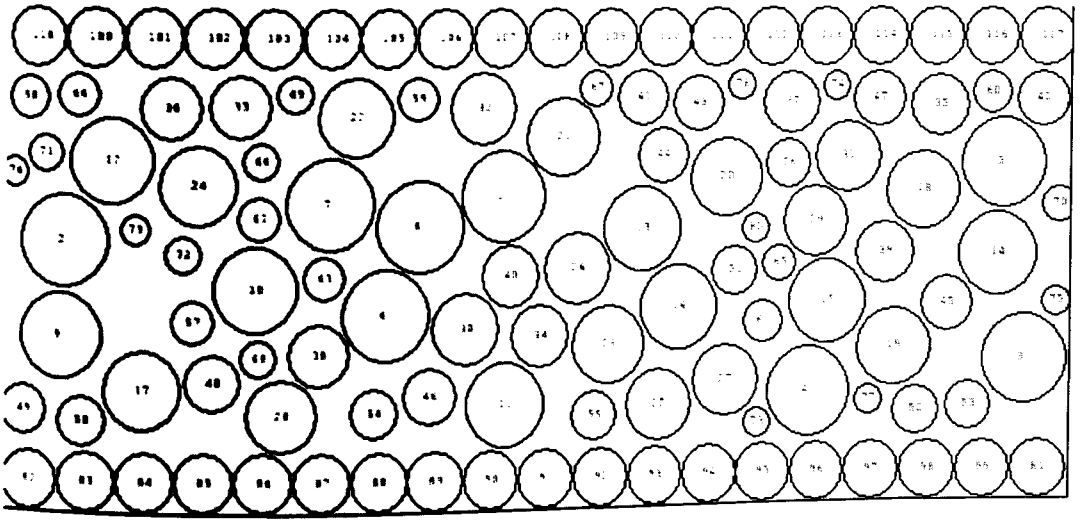

Fig 7.8. Simulation with repulsive interaction after 7500 time steps.

The results are consonant with Dratler and Schowalter (1996). No 'streets' appear, as in the previous sub-section. There may be a mild general anisotropy in the compressive quadrant direction, but no structures formation.

The interpretation is different than Dratler and Schowalter's (1996) conclusions, however. The theory in the previous chapter shows that when there is an elastic interaction structures will become less prominent and for a strong enough interaction they will even disappear altogther. Thus the system with a repulsive interaction is a different physical system than the one without. When there is no repulsive interaction (and only a collisional contact rheology for rough particles) structures must form; they are a natural part of the system.

7.6. Discussion

The first thing to note is that the loading sequence used in these two-dimensional simulations is in fact not pure shear, but also involves a rotation. The rotation will have the effect of destroying the structures somewhat, but apparently the creation of structures is a very strong effect, so they are still prominent. The fact that there is theory in the context of which the simulation can be interrogated is very useful. This is what Dratler and Schowalter (1996) did not have.

Once structures form the aggregate obviously becomes very anisotropic, which would strengthen the argumentation put forward by Morris and Miller (2006) as to the origin of the driving force for migration in shear gradient geometries. The fact that a collisional rheology is required strengthens the McTigue and Jenkins

(1992) case. It is now clear that for slurries of non-interacting rough particles both particle pressure and anisotropy are required ingredients. There is apparently no such thing as a 'simple slurry'.

The correspondence between theory and simulation suggests that the form for the particle pressure used in section 6.4 is probably correct. There is a non-local element, which in the space domain is represented as a convolution with a weighting function. The strength of the weighting function is the fluctuation intensity itself. The non-locality also assists in extrapolating the theory to zero shear regions.

8. Conclusions

8.1. Main conclusions

The main conclusions of this thesis are as follows.

1. In Chapter 2 it is found that a rough particle interaction with additional collision rheology added to a lubrication limit analysis can be devised. This is used as the interaction between two particles.

2. In reviewing the existing models in Chapter 3 it was found that the Phillips *et al* (1992) model leads to the maximum solidosity for the slurry at the centre of a channel. In the literature it is widely reported to be a cusp, but it was shown that if the ratio of diffusive to collisional coefficients is chosen to be in a certain range then the derivative of the solidosity profile at the centre of the pipe vanishes. The maximum solidosity is still required, however. This is does not agree with experiments by Lyons and Leal (1998).

3. The diffusive models are not able to describe slurry flow in a channel accurately (though they capture the effect of migration). The granular temperature model by McTigue and Jenkins (1992) *is* able to describe the flow in such a way that the solidsosity at the centre of the channel is not necessarily the maximum solidosity. However, this model requires a large number of constants as well as

boundary conditions for the fluctuation intensity.

4. The Morris and Miller (2006) model derives a normal stress from presumed anisotropy. The coefficients of the anisotropy have been derived from numerical simulations, but no insight is given in how these coefficients follow from the physics of the flow. The experiments by Shapley *et al* (2002) support the idea of anisotropy.

5. The coefficients of the Granular Temperature theory can be obtained from a cell model using mean field assumptions and Torquato *et al*'s (1990) estimate of the gap width between particles in an isotropic packing. The prediction for the shear viscosity is surprisingly correct when compared with an experimental review by Thomas (1965). Improved estimates for the other coefficients can also be found. One of these - the coefficient that describes the dissipation due to fluctuations in the particle motion - is significantly different from the value usually employed in the literature. The oscillated dead-end filtration problem (which is particularly sensitive to this coefficient) has been recalculated with the improved estimate, leading to a sharper gradient of the solidosity profile near the septum compared to previous estimates.

6. Fluctuations are analysed using continuum theory (Chapter 5). A mesoscopic stress fluctuation needs to be introduced into a system in which an average

strain rate operates. Conditions for the necessity to include continuum fluid pressure and fluid flow are derived. A linear stability analysis shows that without a linear particle pressure the problem is never stable in shear. The granular temperature model does not give a linear (elastic) particle pressure - it is quadratic in the fluctuations - but the elastic repulsion force generally used in Stokesian Dynamics simulations is linear. The analysis shows why the SD community is so keen to employ this interaction. It also shows that a sheared slurry requires at least some quadratic input to be stable.

7. The ground is laid for a quadratic term in the stability analysis. The analysis takes place in the Fourier domain; a quadratic term is therefore a convolution in the spatial domain. This is defensible if the term can be interpreted as a convolution with a short-range influence function. For the latter the absolute value of the density fluctuations is chosen.

8. To link the stability analysis on the continuum level with the fluctuations that arise from the meso-cell scale a cut-off is introduced. Analysis shows that a Gaussian form of cut-off (exponential does not decline fast enough) satisfies the requirements of being locally finite.

9. A quadratic stability analysis is carried out and it shown that there are two attractors in the problem. These two are explored. The attractor outside

'fluctuation=zero' denotes structure formation. These structures are manifest through two peaks in the density fluctuation spectral intensity.

10. A simulation is carried out using a Discrete Element Method with particles interacting via the fluid lubrication limit with added roughness and collision rheology. The simulation clearly displays the formation of structures in shear. The direction of the structures is aligned with the compressive quadrant of the shear field.

11. Structures disappear when an additional repulsive interparticle force is introduced. These findings are consonant with the theoretical predictions.

8.2. Suggestions for further research

The anisotropy obtained from the non-linear analysis should incorporated in a granular temperature model to arrive at a complete description of dense slurry flow. The anisotropy can be introduced at cell level. A concomitant experimental programme of work should determine the components of the viscosity tensor and make verifications of the theoretical predictions. Other numerical simulations - the ones reported here are somewhat primitive - should also be carried out, especially in three dimensions.

Further theoretical work should extend to three dimensions. A more thorough

study of other quadratic effects is the subject of another PhD thesis. A link between cell models and continuum models should be explored more to gain better insight in the role of the fluctuations. The current cell model, which is based on the mean field assumption is somewhat primitive, though a good start.

9. Appendices

9.1. Appendix A: Cartesian tensors and summation convention

Vectors and tensors are denoted by bold-face characters. Their Cartesian components are indicated by subscripts. Throughout this thesis we use Einstein's summation convention: whenever the same Latin subscript appears twice in a term, it means a sum over the value of that index. Here are two examples. The scalar product of two vectors **v** and **w** is

$$v_i w_i = v_1 w_1 + v_2 w_2 + v_3 w_3.$$

The divergence of a vector field **v** is

$$\frac{\partial v_i}{\partial x_i} = \frac{\partial v_1}{\partial x_1} + \frac{\partial v_2}{\partial x_2} + \frac{\partial v_3}{\partial x_3},$$

where **x** is the position vector.

9.1.1. Invariance properties

The components of Cartesian vectors and tensors are given in a coordinate frame. On rotation of the frame the components change. The components of the tensor

in the rotated frame is denoted by $\overset{*}{T}_{ij}$. The rotation transformation is called $\mathbf{Q}$, which has the property $\det(\mathbf{Q}) = 1$ and the inverse $\mathbf{Q}^{-1} = \mathbf{Q}^T$ (the transposed). Here is a list of transformation properties and invariants.

9.1.2. Scalars (tensors of order zero)

Scalars do not change value under rotation. Examples of physical quantities that are scalar are energy, pressure, *etc.*.

9.1.3. Vectors (tensors of order 1)

Vectors $\mathbf{v}$ transform as $\overset{*}{v}_i = Q_{ij}v_j$. There are no invariant vectors. The scalar $v_\ell v_\ell$ (the quadratic length of the vector) is invariant. Physical examples of vectors are the velocity or the position vector.

9.1.4. Tensors of order 2

A second order tensor $\mathbf{T}$ transforms as $\overset{*}{T}_{ij} = Q_{i\ell}Q_{jk}T_{\ell k}$. Physical examples are the stress, the strain, *etc.*; these are all symmetric tensors: $T_{\ell k} = T_{k\ell}$. The inverse of $\mathbf{T}$ is $\mathbf{T}^{-1}$, which is defined by means of the introduction of the Kronecker delta δ_{ij}, which equals 1 when $i = j$ and zero otherwise: $T_{ij}T^{-1}_{j\ell} = \delta_{i\ell}$. The tensor $\boldsymbol{\delta}$ is the identity. Invariant 2-tensors are a multiple of $\boldsymbol{\delta}$.

On rotation the eigen values of $\mathbf{T}$ do not change. Hence the equation that generates the eigenvalues remains unchanged and the coefficients of this equation are invariant under rotation. In two dimensions there are two invariants: the trace T_{ii} and $\det(\mathbf{T})$.

9.1.5. Tensors of order 3

These are used very rarely in physics, except for the Levi-Cevita tensor ϵ, defined as zero when any two subscripts are the same, $\varepsilon_{123} = 1$ and any even permutation of subscripts multiplies the result by -1. There are no invariant third order tensors.

9.1.6. Tensors of order 4

A fourth order tensor $\mathbf{A}$ transforms as $\overset{*}{A}_{ijk\ell} = Q_{ip}Q_{jq}Q_{kr}Q_{\ell s}A_{pqrs}$. The product of two tensors is $\mathbf{AB}$, with components $A_{ijk\ell}B_{k\ell mn}$. In physical applications one mostly has symmetries $A_{ijk\ell} = A_{jik\ell} = A_{ij\ell k}$. Sometimes the symmetry $A_{ijk\ell} = A_{k\ell ij}$ is encountered. Physical examples are the stiffness tensor, the compliance tensor and the viscosity tensor. The inverse of a fourth order tensor with symmetries in the first and last two subscripts is $\mathbf{A}^{-1}$, defined such that $A^{-1}_{ijk\ell}A_{k\ell mn} = I_{ijmn}$; the identity for symmetric fourth order tensors is $\mathbf{I}$, defined

as $I_{ijmn} = \frac{1}{2}(\delta_{im}\delta_{jn} + \delta_{jm}\delta_{in})$. Invariant fourth order, symmetric tensors have the form $A_{ijk\ell} = \overline{\lambda}\delta_{ij}\delta_{k\ell} + \overline{\mu}(\delta_{ik}\delta_{j\ell} + \delta_{i\ell}\delta_{jk})$; $\overline{\lambda}$ and $\overline{\mu}$ are called the Lamé coefficients (elasticity theory) or the bulk and shear viscosity (fluid dynamics).

9.1.7. Tensor notation

The contraction of a vector v_i with the second index of a tensor t_{ij} would be

$$t_{ij}v_j = t_{i1}v_1 + t_{i2}v_2 + t_{i3}v_3.$$

Note that the result is now a vector.

Here, the two-index tensor t_{ij} is, in a given coordinate system, a collection of nine scalars

$$\begin{pmatrix} t_{11} & t_{12} & t_{13} \\ t_{21} & t_{22} & t_{23} \\ t_{31} & t_{32} & t_{33} \end{pmatrix}$$

which must transform in a particular way under a change of coordinates: let the old coordinates be x_i and the new coordinates ξ_i, and let the components of the

same tensor be denoted τ_i in the new coordinates. Then

$$\tau_{ij} = \frac{\partial x_k}{\partial \xi_i} \frac{\partial x_l}{\partial \xi_j} t_{kl}.$$

This is just a generalization of the transformation for vectors.

9.2. Appendix B: Lemma

In this part we will prove that if $f(\alpha(z), \eta) = f(\beta(z), \eta) = 0$ then

$$\frac{\partial}{\partial z} \int_{\beta(z)}^{\alpha(z)} f(z, \eta)\, \partial\eta = \int_{\beta(z)}^{\alpha(z)} \frac{\partial}{\partial z} f(z, \eta)\, \partial\eta.$$

For small values of Δz the left hand side is:

$$\begin{aligned} & \frac{1}{\Delta z} \left[\int_{\beta(z+\Delta z)}^{\alpha(z+\Delta z)} f(z+\Delta z, \eta)\, \partial\eta - \int_{\beta(z)}^{\alpha(z)} f(z, \eta)\, \partial\eta \right] \qquad (9.1) \\ = & \frac{1}{\Delta z} \int_{\beta(z+\Delta z)}^{\beta(z)} f(z+\Delta z, \eta)\, \partial\eta + \int_{\beta(z)}^{\alpha(z)} f(z+\Delta z, \eta)\, \partial\eta \\ & + \int_{\alpha(z)}^{\alpha(z+\Delta z)} f(z+\Delta z, \eta)\, \partial\eta - \int_{\beta(z)}^{\alpha(z)} f(z, \eta)\, \partial\eta \end{aligned}$$

But

$$\frac{1}{\Delta z}\int_{\beta(z+\Delta z)}^{\beta(z)} f(z+\Delta z,\eta)\,\partial\eta = f(\beta(z)+\Delta z,\eta)$$

and

$$\frac{1}{\Delta z}\int_{\alpha(z)}^{\alpha(z+\Delta z)} f(z+\Delta z,\eta)\,\partial\eta = f(\alpha(z)+\Delta z,\eta),$$

and the no-slip condition gives

$$f(\beta(z)+\Delta z,\eta)+f(\alpha(z)+\Delta z,\eta)=0.$$

Hence (9.1) becomes

$$\begin{aligned}&\frac{1}{\Delta z}\left[\int_{\beta(z)}^{\alpha(z)} f(z+\Delta z,\eta)\,\partial\eta - \int_{\beta(z)}^{\alpha(z)} f(z,\eta)\,\partial\eta\right]\\ =\ &\int_{\beta(z)}^{\alpha(z)} \frac{f(z+\Delta z,\eta)\,\partial\eta - f(z,\eta)\,\partial\eta}{\Delta z}.\end{aligned}$$

Taking the limit as Δz approaches zero, we obtain the required result.

9.3. Program description

This is the basic program used in chapter 7. Modifications include the insertion of the elastic force and different initial conditions.

real:x(2000),y(2000),R(2000),vx(2000),vy(2000),rho(2000),m(2000)

In this program x,y are arrays holding position coordinate.

R containing radii.

vx,vy containing velocity in x and y .

rho and m is density and mass of particles.

wall particle centres xtwc:top wall, xbwc: bottom wall

real: xtwc(2000),ytwc(2000),xbwc(2000),ybwc(2000)

xtwc, ytwc,xbwc,ybwc contain position coordinate for **the** *center of the wall particles.*

integer: ip(2000),N,p(2000)

p is to distinguish particles,it is 1 for particles.

N is number of particles excluding wall particles.

ip

real: xp(2000),yp(2000),vxp(2000),vyp(2000)

xp,yp,vxp,vyp are temporary storage for calculating new velocities and positions.

integer:w,h,grhnd,bhnd,dhnd,mytime

w, h are width,height,grhnd,bhnd,dhnd animation handles.

parameter(grhnd=11,bhnd=12,dhnd=13)

external copy2clpbrd *For copying to clipboard*

real: xmax,ymax,xmin,ymin,rmax,rmin,crp

xmax, ymax, they are bound area that the particle can be in side.

common/maxmin/xmax,ymax,xmin,ymin,rmax,rmin,ipmin,ipmax

rmax and rmin are maximum and minimum radii.

rwal is radius of wall that is average particle radii in side the box.

common/params/crp,pi

crp is multi pliers to display the animation on screen.

common/params1/visef,avr,rwall,boxl,boxw

visef is coefficient in the force, in terms of viscosity, ... etc.

boxl and box w are length and width od box.

avr is anarage

rwall is radius of wall

open (4,file='simo_c.out')

pi=ACOS(-1.0)

write (4,105) pi

105 format (E12.3)

visef=0.001 *coefficient in the force, in terms of viscosity, ... etc.*

np=7 *Number of imaginary rectangular*

N=80 *N is number of particles excluding wall particles.*

phi=0.55 *phi is solidosity*

rmin=0.002

rmax=0.008

mytime=1

boxl=20*(rmin+rmax) *boxl is length of box.*

np=7 *number of imaginary rectangular in side box.*

produce partcle radii.

call radius(N,rmin,rmax,r,avr)

rwall=avr

vol=0.0 *vol is volume of box that is summation of each disc or particles.*

do i=1,N

vol=vol+pi*r(i)2**

rho(i)=1.0

p(i)=1 *p identify particle type, p=-1 is for particle in walls and p=1 is for particle in middle.*

enddo

boxw=vol/(phi*boxl) *boxw is width of box*

nwall=nint(boxl/(2*avr))

write(*,10)boxl,boxw,rwall,nwall

format('boxl=',f8.2,2x,'boxw=',f8.2,2x,'Rwall=',f8.2,2x,'Nwall=',i5)

For calculating the position of particles in the top and bottom of the wall , particle are added to the array contain the particle inside the box.

Npart=N

do i=1,Nwall

xbwc(i)=2*(i-1)*rwall+rwall

ybwc(i)=rwall

xtwc(i)=2*(i-1)*rwall+rwall

ytwc(i)=boxw+ybwc(i)+2*rwall

end do

call positions(N,r,boxl,boxw,rwall,x,y)

Add wall particles to the list

N=Npart

DO i1=1,Nwall *Nwall is the number of particles in wall.*

N=N+1

```
x(N)=xbwc(i1)
y(N)=ybwc(i1)
R(N)=rwall*0.99
rho(N)=10**4
p(N)=-2          For bottom wall particle identification
enddo
do i1=1,Nwall
N=N+1
x(N)=xtwc(i1)
y(N)=ytwc(i1)
rho(N)=10**4
R(N)=rwall*0.99
p(N)=2           For top wall particle identification
end do
give wall particles a velocity
DO i1=Npart+1,N-Nwall
vx(i1)=10.0
vy(i1)=0.0
vx(i1+Nwall)=-10.0
```

```
      vy(i1+Nwall)=0.0
      end do
      vwall=1.0
      phicoeff=((1-phi)**3)/(6*phi*(2-phi))   A constitutive equation for the
separation given by Torquato.
      h1=rwall*phicoeff   mean gap between particles
      t=0.00001*(h1*boxw)/(vwall*rwall)   time step
      write(4,15)phicoeff,h1,t
   15 format('phicoeff=',f6.4,2x,'h1=',f8.2,2x,'t=',f8.2)
   find max. and min of particle locations.
      call find_max_min(N,x,y,r)
   Find particle masses.
      call find_mass(N,r,rho,m)
   copy arrays into prime arrays
      do i=1,N
      xp(i)=x(i)
      yp(i)=y(i)
      vxp(i)=vx(i)
      vyp(i)=vy(i)
```

```
 enddo
 boxl=nwall*(2*rwall)
  crp=1000/boxl          A factor for display purposes
  xlength=(boxl)*crp
  ylength=(ymax+rwall)*crp
  w=nint(xlength)!width
  h=nint(ylength)!height
 iw=winio@('%sp%es%ca[Roughsimo_c Particles]&',0,0)
  iw=winio@('%lw&',lwhnd)
  iw=winio@('%mn[&File[E&xit]]&','EXIT')
  iw=winio@('%mn[&Edit[&Copy to Clipboard]]&',copy2clpbrd)
  iw=winio@('%'gr[rgb_colours,white]',w,h,grhnd)
  tsleep=0.05          waiting time for the animation update
   do istep=2,100          Number of step
callanimate_particles(N,grhnd,lwhnd,dhnd,w,h,ylength,x,y,r,ip)
call sleep@(tsleep)
callindividual_particle_motion(N,t,p,r,m,x,y,vx,vy,xp,yp,vxp,vyp)
do i=1,N
 x(i)=xp(i)
```

y(i)=yp(i)

vx(i)=vxp(i)

vy(i)=vyp(i)

enddo

call densfunc(np,N,x,y,boxl,boxw,mytime)

mytime=mytime+1

this periodic boundary has been reorganised in the final version;

call periodic_boundary(N,x)

call clear_screen@

enddo

stop

end.

subroutineindividual_particle_motion

This subroutine calculate hydrodynamic force and also new position, new velocity and utilizing momentum law.

real:x(2000),y(2000),vx(2000),vy(2000),xp(2000),yp(2000)

real:vxp(2000),vyp(2000),r(2000),m(2000)

integer: N,p(2000)

real: rmin ,rmax

common/params1/visef,avr,rwall,boxl,boxw,rmin ,rmax

write(4,33)

33 format(' —- Individual particles —-')

dc=avr *distance criterion*

e=0.26 *coefficiant restituation*

do i=1,N

flubx and fluby are the x and y component of the forces exerted on the particle by another particles .

flubx=0.0

fluby=0.0

if(p(i)2.ne.4) then**

do j=1,N

dists=SQRT((x(j)-x(i))2+(y(j)-y(i))**2)-R(j)-R(i)** *Distance between surface to surface of particles*

if(dists.lt.dc.and.i.ne.j)then *look into the criterion again*

h0=0.0001*avr *h0 is roughness parameter of the particles*

distc=SQRT((x(j)-x(i))2+(y(j)-y(i))**2)** *Distance between centre to centre of particles*

rnx=(x(j)-x(i))/distc *Normal vector*

rny=(y(j)-y(i))/distc flubx=flubx+visef*((vx(j)-vx(i))*rnx+(vy(j)-vy(i))*rny)*rnx/(dists+h0) *hydrodynamic force*

fluby=fluby+visef*((vx(j)-vx(i))*rnx+(vy(j)-vy(i))*rny)*rny/(dists+h0)

endif

enddo

78 format ('dist',E12.3)

endif

For new position I have calculated the amount of displacement due to the above forces from the velocities of individual particles, and then utilizing conservation lows(momentum) calculating the velocity after collision ,sending the particle a way from each other.

ax=flubx/m(i) *accelaration*

ay=fluby/m(i)

Temporary storage for calculating new velocities and position.

xp(i)=x(i)+0.5*ax*t2+vx(i)*t**

yp(i)=y(i)+0.5*ay*t2+vy(i)*t**

vxp(i)=vx(i)+ax*t

vyp(i)=vy(i)+ay*t

enddo

```
 39 format (I3,4E15.3)
 do i=1,N
 do j=1,N
 dists= SQRT((x(j)-x(i))**2+(y(j)-y(i))**2)-R(j)-R(i)
 if(dists.lt.dc.and.i.ne.j) then
 distc=SQRT((x(j)-x(i))**2+(y(j)-y(i))**2)
 rnx=(x(j)-x(i))/distc
 rny=(y(j)-y(i))/distc
```

Check for collision for particles inside the box.

```
 if (dists.lt.0.0) then
 if ((p(j)**2.ne.4).and.(p(i)**2.ne.4)) then
```

collision for particles in slurry

```
 vxi=vxp(i)
 vyi=vyp(i)
 vxj=vxp(j)
 vyj=vyp(j)
 vxp(i)=vxi-m(i)*m(j)*(1+e)*((vxi-vxj)*rnx)*rnx/(m(i)*(m(i)+m(j)))
 vyp(i)=vyi-m(i)*m(j)*(1+e)*((vyi-vyj)*rny)*rny/(m(i)*(m(i)+m(j)))
 vxp(j)=vxj+m(i)*m(j)*(1+e)*((vxi-vxj)*rnx)*rnx/(m(j)*(m(i)+m(j)))
```

```
vyp(j)=vyj+m(i)*m(j)*(1+e)*((vyi-vyj)*rny)*rny/(m(j)*(m(i)+m(j)))
xp(i)=xp(i)-(0.5+0.0002)*(R(i)+R(j)-distc)*rnx
xp(j)=xp(j)+(0.5+0.0002)*(R(i)+R(j)-distc)*rnx
yp(i)=yp(i)-(0.5+0.0002)*(R(i)+R(j)-distc)*rny
yp(j)=yp(j)+(0.5+0.0002)*(R(i)+R(j)-distc)*rny
else

if (p(j)**2.eq.4)then
```

when j is the wall particle

```
vxi=vxp(i)
vyi=vyp(i)
vxj=vxp(j)
vyj=vyp(j)
vxp(i)=vxj-e*(vxi-vxj)
vyp(i)=vyj-e*(vyi-vyj)
xp(i)=xp(i)-(1.+0.0002)*(R(i)+R(j)-distc)*rnx
yp(i)=yp(i)-(1.+0.0002)*(R(i)+R(j)-distc)*rny
else
```

when i is the wall particle

```
vxi=vxp(i)
vyi=vyp(i)
vxj=vxp(j)
vyj=vyp(j)
vxp(j)=vxi+e*(vxi+vxj)
vyp(j)=vyi+e*(vyi+vyj)
xp(j)=xp(j)+(1.+0.0002)*(R(i)+R(j)-distc)*rnx
yp(j)=yp(j)+(1.+0.0002)*(R(i)+R(j)-distc)*rny
endif
end if
end if
end if
enddo
enddo
36format('==>','i=',i3,2x,'parmass=',f10.2,1x,'flubx=',f10.2,1x,&
& 'fluby=',f10.2,1x,'x=',f8.2,1x,'y=',f8.2,1x,'vx=',f8.2,1x,'vy=',f8.2)

return
end.
```

Subroutine densfunc(np,N,x,y,boxl,boxw,mytime)

This suborning calculates, the densities with in imaginary vertical strips within simulation, this done to follow the migration of particles.

```
dimension x(2000),y(2000)

dimension a1(20),a2(20),b1(20),b2(20)

generate box boundaries

open file to see a result

OPEN(5,FILE='h.dat')

do m=1,np

a1, a2, b1, b2, defined the rectangular strip suborning position.

a1(m)=float(m-1)*boxl/float(np)

a2(m)=.5*boxw+.5*boxl/float(np)

b1(m)=float(m)*boxl/float(np)

b2(m)=.5*boxw-.5*boxl/float(np)

end do

do m=1,np

icount=0

do i=1,N

itest=0
```

Investigate particle are inside the imaginary rectangular.

```
if ((x(i).gt.a1(m)).and.(x(i).lt.b1(m))) itest=itest+1

if ((y(i).lt.a2(m)).and.(y(i).gt.b2(m))) itest=itest+1

if (itest.eq.2) icount=icount+1


enddo

print *,m,icount,mytime

write (5,131)m,icount,mytime

end do

131 format (3I9)

return

end .
```

Subroutine positions(N,r,boxl,boxw,rwall,x,y)

Initializes position within the box and tests that no particles are overlapping with walls or other particles.

```
real r(2000),x(2000),y(2000)

integer rej,try

seed=1.324

penfact=1.0    a measure of the penetration of the particles
```

```
do 50 i=1,N
rej=1
try=0
do while (rej.eq.1)
try=try+1
if(try.gt.10) then
try=0
seed=2.1*seed
endif
rej=0
seed=rastgele(seed)
posx=seed*boxl
seed=rastgele(seed)
posy=seed*(boxw+2*rwall)
!seedy=seed
```

check overlap with the walls

```
if(posx.lt.r(i)) rej=1
if(posx.gt.(boxl-r(i))) rej=1
if(posy.lt.(r(i)+2*rwall)) rej=1
```

```
if(posy.gt.((boxw+2*rwall)-r(i))) rej=1
```

check overlap with other particles

```
if(i.ne.1)then
j=1
99 if(j.le.i-1)then
if(rej.eq.1) j=i-1
dist=(posx-x(j))**2+(posy-y(j))**2
if(sqrt(dist).lt.penfact*(r(i)+r(j))) rej=1
j=j+1
goto 99
endif
endif
end do
x(i)=posx
y(i)=posy
50 continue
return
end.
```

function rastgele(seed)

```
real: help
help=(3.141593+seed)**4
rastgele=help-int(help)
return
end
```

subroutine radius(N,rmin,rmax,r,avr)

```
real r(2000),rmin,rmax,avr
integer bins,cnt,N
```

We splits the total number of particles in to 10 bins containing the particle in the same size.

```
bins=10
```

lots is the number of particle in each bin.

```
lots=N/bins
cnt=1
radmin=99999.
radmax=-99999.
rtot=0.0
do 15 j=1,bins
```

rad is radiuse of particle in each bin.

```
rad=rmax-(j-1)*(rmax-rmin)/bins
do i=1,lots
r(cnt)=rad
cnt=cnt+1
end do
if((N-cnt).lt.lots)then
do i=cnt,N
r(i)=rmin
end do
endif
15 continue
```

To find maximum and minimum of particle by comparison, and then fine the average size of the particles.

```
do i=1,N
radmin=min(radmin,r(i))
radmax=max(radmax,r(i))
rtot=rtot+r(i)
end do
```

```
      avr=rtot/N
      print*,avr
      write(4,10)radmin,radmax,avr
   10 format('radmin=',f8.2,2x,'radmax=',f8.2,2x,'average r=',f8.2)
      return
      end.
```

Subroutine periodic_boundary(N,x)

```
      real x(2000),xr(2000),xl(2000)!r(2000)
```
xl left padded and xr: right padded array

```
      integer ipl(2000),ipr(2000)
      real xmax,ymax,xmin,ymin,rmax,rmin
      common/maxmin/xmax,ymax,xmin,ymin,rmax,rmin,ipmin,ipmax
      common/params1/visef,avr,rwall,boxl,box
```

il, ir, are counter to keep track of the number of the discs replace in the top and bottom of the wall.

ipl,ipr is an arry of the indices for xr and xl arrays.

xl, xr are arrays holding the coordinates of the wall particles.

```
      il=0
      ir=0
```

do i=1,N

It cheek if it is out of the visible wall, if so a new particle add it to the wall.

if(x(i).gt.boxl)then ! *r(ipmax) idi rwall yerine***

ir=ir+1

ipr(ir)=i

xr(ipr(ir))=x(i)

endif

if(x(i).lt.0.0)then *r(ipmin) idi rwall yerine*

il=il+1

ipl(il)=i

xl(ipl(il))=x(i)

endif

enddo

If one of the particles moves out side the wall the boxl either added or subtracted to placed it at the beginning of the wall.

do k=1,ir

x(ipr(k))=xr(ipr(k))-boxl *r(ipmax) idi rwall yerine*

enddo

do k=1,il

```
x(ipl(k))=xl(ipl(k))+boxl !r(ipmax) idi rwall yerine
enddo
return
end
```

Subroutine find_max_min(m,d1,d2,d3)

It set some preliminary value for reduce x and y, min and max and compares with each of the stores values to test new min and max

```
real d1(2000),d2(2000),d3(2000)
integer m
real xmax,ymax,xmin,ymin,rmax,rmin,crp
common/maxmin/xmax,ymax,xmin,ymin,rmax,rmin,ipmin,ipmax
common/params/crp,pi
ipmin=0
ipmax=0
xmax=-999999.
xmin=999999.
ymax=-999999.
ymin=999999.
rmax=-999999.
```

```
rmin=999999.
do i=1,m
if(d1(i).gt.xmax)then
ipmax=i
xmax=d1(i)
endif
if(d1(i).lt.xmin)then
ipmin=i
xmin=d1(i)
endif
ymax=max(ymax,d2(i))
ymin=min(ymin,d2(i))
rmax=max(rmax,d3(i))
rmin=min(rmin,d3(i))
enddo
return
end
```

10. List of symbols

Latin Symboles

$\mathbf{A}$ interaction tensor for relative translation velocity

A area of rectangle

A_c integration constant

A_0 area of the cylindrical filter

a particle radius

a_T, a_B radii of top and bottom cylinders

a_s length scale

$\overline{a}$ length scale

$\mathbf{a}$ acceleration

$\mathbf{B}$ interaction tensor for relative angular velocity

B integration coefficient

C integration constant

c coefficient

$\overline{c}$ constant

$\mathbf{c}$ branch vector

D particle diameter

d dimension

$\mathbf{d}$ strain rate tensor

E total energy

e_c coefficient of restitution

e internal energy per unit volume

$\mathbf{e}$ unit vector along the co-ordinate axes

f coefficient

f_τ time constant coefficient for the collisional problem

$\mathbf{F}$ force

$\widehat{F}$ example of simple of isotropic function in two dimensions $\widehat{F}(k) = k^\ell e^{-k\bar{a}}$

$\mathbf{f}$ body force

G fluid pressure gradient

$\mathbf{g}$ normal velocity between particles in a collision problem and also gravitational acceleration

h gap width between two particles

h_0 roughness length scale (or range of elastic interaction)

$\mathbf{I}$ unit tensor

K_c, K_μ, K_τ proportionality coefficients for collisional (c), viscous (μ) and shear stress gradient (τ) transport mechanisms

$\mathbf{k}$ wave vector

k magnitude of $\mathbf{k}$

k_0 cell size inverse

$\overline{k}$ integration constant in the granular temperature theory

L section length of a cylinder

ℓ number

m particle mass

m_s mass scale

$\mathbf{N}$ materials flux (subscripts denote which mechanism)

N number of particles

N_a maximum correlation length

N_c Number of nearest neighbors

$\mathbf{n}$ unit normal vector

n parameter in the Krieger (1972) viscosity model

n_i number of density

P half plug width in the Bingham model

p fluid pressure or viscous suspension pressure

$\overline{p}$ particle pressure

$\mathbf{Q}$ granular heat flux

Q tensor rotation

Q_c Caloric heat

R radius of curvature

$\overline{R}$ flow resistance factor in Darcy's law

$\mathbf{S}$ any second order tensor

S parameter, $S = \chi \mathbf{U}/\alpha_4 D$

s separation

s' normal speed fluctuation

T granular temperature

$\mathbf{t}$ viscous stress

t_s time scale

$\mathbf{U}$ superficial velocity

$\mathbf{u}$ fluid velocity

u x-component of the particle velocity $\mathbf{v}$

V volume of assembly

V_s solid volume

$\mathbf{v}$ particle velocity

W_w half channel width

W work

w work per unit volume

$\mathbf{x}$ position vector

x x-component of $\mathbf{x}$

y y-component of $\mathbf{x}$

$y_{T,B}$ functions describing the top and bottom cylinder surfaces

Greek symbols

α_{0-4} non-dimensional coefficients in the granular temperature theory

γ, $\dot{\gamma}$ shear strain, shear rate

$\overline{\gamma}$ granular dissipation

δ asperity height in Jenkins and Koenders(2005)

δ_{jk} Kronecker delta.

η fluid viscosity

ϑ angle between pole and wave vector $\mathbf{k}$

ϕ solidosity

ϕ_f solidosity in the flowing region in the Bingham model

ϕ_m maximum suspension solidosity

ϕ_p plug solidosity in the Bingham model

ϕ_r factor introduced by Patir and Cheng (1978)

ϕ_s critical solidosity in the Bingham model

$\overline{\phi}$ average solidosity in the Bingham model

$\overline{\kappa}$ granular heat conduction coefficient

λ number

$\overline{\lambda}$, $\overline{\mu}$ viscosity Lamé coefficients

μ suspension viscosity

ρ_f fluid mass density

ρ_s solid mass density

$\boldsymbol{\sigma}$ stress tensor

σ standard deviation of the surface rouhgness in Patir and Cheng (1978) and Jenkins and Koenders (2005)

τ shear stress

$\boldsymbol{\tau}$ traction

τ_0 yield stress in the Bingham model

τ_c time scale for the collisional problem

$\boldsymbol{\omega}$ angular velocity

φ angle between vector $\mathbf{x}$ and pole

χ Coefficient for the fluid drag

11. References

Anikeenko, A.V and Medvedev, N.N. (2007) Polytetrahedral Nature of the Dense Disordered Packings of Hard Spheres. *Phys. Rev. Lett.* **98**, 235504.

Atkins, P.W. (1982) Physical Chemistry. *Oxford University Press.*

B

Bagnold, R.A. (1954) Experiments on a gravity-free dispersion of large solid spheres in a Newtonian fluid under shear. *Proc. Royal Soc. London* **A223**, 49-63.

Batchelor, G.K. (1967) An introduction to fluid dynamics. *Cambridge University Press.*

Batchelor, G.K. and Green, J.T. (1972) The determination of the bulk stress in a suspension of spherical particles to order c^2, *J. Fluid Mechanics* **56** (3), 401 - 427

Becker, E. and Bürger, W. (1975) Kontinuumsmechanik. *Teubner, Stuttgart.*

Bird, R.B., Stewart, W.E. and Lightfoot, E.N. (1960) Transport phenomena. *Wiley New York.*

Bossis, G. and Brady, J.F. (1984) Dynamic simulation of sheared suspensions. I. General method. *J. Chem. Phys.* **80** 5141-5154.

Brady J.F., Bossis G. (1985) The rheology of concentrated suspensions of

spheres in simple shear-flow by numerical simulation. *J Fluid Mechanics* **155,** 105-129.

Buschmann, M.D., Gluzband, Y.A., Grodzinsky, A.J. and Hunziker, E.B. (1995) Mechanical compression modulates matrix biosynthesis in chondrocyte/agarose culture. *J. of Cell Science* **108**, 1497-1508.

C

Cundall, P. and Strack, O.D.L. (1979) A discrete numerical method for granular assembiles. *Geotechnique* **29**(1), 47-65.

daCunha, F.R. and Hinch, E.J. (1966) Shear-induced dispersion in a dilute suspension of rough spheres. *J. Fluid Mechanics*, **309,** 211-223.

D

Davis, M. and Koenders, M.A. (2007a) Particle-pressure induced transient changes in oscillated particle-fluid systems. *Trans Filtration Soc.* **7** (4), 326-336.

Davis, M. and Koenders, M.A. (2007b) Oscillated densley packed granular media immersed in a fluid. *J. Sound and Vibration*, **308,** 526-540.

Davis, M. and Koenders, M.A. (2007c) Combined gravity and mean flow effects on agitated slurries in a dead-end filtration set-up, *J. Powder Technology* **182** (2), 307-312.

Davis, M and Koenders, M.A. (2008) Combined gravity and mean flow effects

on agitated slurries in a dead-end filtration set-up. *Powder Technology* **182** (2), 307-312.

Dratler, D.I. and Schowalter, W.R. (1996) Dynamic simulation of suspensions of non-Brownian hard spheres. *J. Fluid Mechanics* **325,** 53-77.

Drew, D.A. (1986) A flow structure in the Poiseuille flow of a particle-fluid mixture. In Papanicolau, G. Advances in Multiphase Flow and Related Problems. *Los Angeles*, **SIAM**, 55-66.

E

Einstein, A. (1911) Eine neue Bestimmiung der Molekuldimensionen. *Ann. Physics*, **17,** 459.

G

Gundogdu, O., Koenders, M.A., Wakeman, R.J. and Wu, P. (2003a) Permeation through a b ed on a vibrating medium: theory and experimental results. *Chem Eng Science* **58** (9), 1703-1713.

Gundogdu, O., Koenders, M.A., Wakeman, R.J. and Wu, P. (2003b) Vibration-assisted dead-end filtration: experiments and theoretical concepts. *Chem. Engineering Research and Design*, **81** (8), 916-923.

H

Happel, J. and Brenner, H. (1991) Low Reynolds Number Hydrodynamics.

Kluwer Academic Publishers, Dordrecht.

Heyes. D. and Mitchell. J. (1995) Brownian -dynamics simulation of Model Stabilised Colloidal Dispersion under shear. *J. Chem.Soc. Faraday Trans* **91** (13), 1975-1989.

J

Jay, G.D., Haberstroh, K. and Cha, C.J. (1998) Comparison of the boundary-lubricating ability of bovine synovial fluid, lubricin, and Healon. *J. of Biomedical Materials Research* **40**, 414-418.

Jenkins, J.T. and Koenders, M. A. (2005) Hydrodynamic interaction of rough spheres. *Granular Matter*, **7** (1), 13-18.

Jeffrey, D. J. and Konishi,Y. (1984) Calculation of the resistance and mobility functions for two unequal rigid spheres in low-Reynolds-number flow. *J. Fluid Mechanics* **139,** 261-290.

Jenkins J.T. and Savage S.B. (1983) A theory for the rapid flow of identical flow of indentical, smooth, nearly elastic, spherical -particles. *J. Fluid Mec*hanics **130,** 187-202.

K

Kim, S. and Karrila, S.J. (1991) Microhydrodynamics: principles and selected applications., *New York: Dover publications.*

Koenders, M. (1997) A first order constitutive model for a particulate suspension of spherical particles. *Acta Mechanica* **122,** 1-19.

Koh, C.J., Hookham, P. and Leal, L.G. (1994) An experimental investigation of concentrated suspension flows in a rectangular channel. *J. Fluid Mechanics* **266,** 1-32.

Krieger, I.M. (1972) Rheology of monodisperse latices. *Adv. Colloid Interface Sci.* **3,** 111-136.

L

Ladd A.J.C. (1994) Numerical simulations of particulate suspensions via a discretized Boltzmann equation. Part 1. Theoretical foundation, *J. Fluid Mechanics* **271**, 285 - 309

Ladd A.J.C. (1997) Sedimentation of homogeneous suspensions of non-Brownian spheres. *Phys. Fluids* **9** (3), 491-499.

Leighton, D. and Acrivos, A. (1987) The shear-induced migration of particles in concentrated suspensions.*J. Fluid Mechanics*, **181,** 415-439.

Lyon, M.K. and Leal, G. *J., (1998)* An experimental study of the motion of concentrated suspensions in two-dimensional channel flow. Part 1. monodisperse systems. *J. Fluid Mechaics* **363,** 25-56.

M

Marchioro, M and Acrivos, A. (2001) Shear-induced particle diffiusivites from numerical simulation. *J. Fluid Mechanics* **443,** 101-28.

McTigue, D.F. and Jenkins, J. T. (1992) Channel Flow of a concentrated suspension. In Shen, H.H., Advances in Micromechanics of Granular Materials, *New York: Elsevier* 381-390.

Morris J.F. and Miller, R.M. (2006) Normal stress-driven migration and axial development in pressure-driven flow of concentrated suspensions. *J. Non-Newtonian Fluid Mechanics* **135,** 149-165.

Morris, J.F. and Boulay, F. (1999) Curvilinear flows of non-colloidal suspension: the role of normal stresses, *J.Rheology* **43,** 1213-1238.

N

Nott, P.R. and Brady, J.F. (1994) Pressure-driven flow of suspensions: simulation and theory, *J. Fluid Mechanics* **275,** 157-199.

P

Patir, N. and Cheng, H.S. (1978) An avrage flow model for determining effects of three- dimensional roughness on partial hydrodynamic lubrication. *J. Lubrication Technology Trans ASME* **100,** 12-17.

Petford, N. and Koenders, M.A. (1998) Granular flow and viscous fluctuations in low Bagnold number granitic magmas. *J. Geological Soc. London* **155,** 873-881.

Phillips, R.J., Armstrong, R.C., Brown ,R.A., Graham, A.L. and Abbott, J.R. (1992) A constititive model for concentrated suspensions that accounts for shear-induced particle migration. *Phys. Fluids A* **4**, 30-40.

R

Rutherford, M.J. and Gardner, J. (1999) Rates of magma ascent. In Sigurdsson, H. (ed) Encyclopedia of Volcanoes. *Academic Press, San Diego*, 207-217.

S

Santra, S.B., Schwarzer, S.and Herrmann, H. (1996) Fluid-induced particle-size segregation in sheared granular assemblies. *Phys Rev E* **54** (5), 5066-5072.

Shapley, N.C., Armstrong, R.C. and Brown, R.A. (2002) Laser Doppler velocimetry measurments of particle velocity fluctuations in a concentrated suspension. *J. Rheology* **46**(1), 241-272.

Singh, A. and Nott, P.R. (2000) Normal stresses and microstructure in bounded sheared suspensions via Stokesian Dynamics simulations. *J. Fluid Mechanics* **412**, 279-30l.

Smart J.R. and Leighton D.T. (1989) Measurement of the hydrodynamic surface roughness of non-colloidal spheres, *Physics of Fluids* A **1** (1); 52-60.

Sparks, R.S.J. (1976) Grain size variations in ignimbrites and implications for the transport of pyroclastic flows. *Sedimentology*, **23**, 147-188.

Stickel J.J. and Powell R.L. (2005) Fluid mechanics and rheology of dense suspensions. *Ann. Rev. Fluid Mechanics* , **37**, 129-149.

T

Thomas, D.G. (1965) Transport characterstics of suspension: VII. A note on the viscosity of Newtonian suspensions of uniform spherical particles. *J. Colloid Science*, **20**, 267-277.

Torquato, S., Lu, B. and Rubinstein, K. (1990) Nearest-neighbor distribution functions in many-body systems. *Phys Rev A* **41** (4), 2059-2074.

Tuzson, J.J. and Clark, H.Mcl. (1998) The slurry erosion process in the Coriolis wear tester. *Proc. FEDSM '98, ASME.* Fluids Engg., Division Summer Meeting, June 21-25, 1998, Washington, D.C., paper no. FEDSM98-5144.

W

Wakeman, R.J. and Tarleton, E.S. (1999) Filtration: equipment selection, modelling and process simulation. *Elsevier Advanced Technology, Oxford.*

Wakeman, R.J. and Smythe, M.C. (2000) Clarifying filtration of fine particle suspensions aided by electrical and acoustic fields. *Trans. I Chem.* E, **78** (A), 125-135.

Williams, J.R., Hocking, G. and Mustoe, G.G.W. (1985) The Theoretical Basis of the Discrete Element Method. NUMETA 1985, Numerical Methods of Engi-

neering, Theory and Applications, *A.A. Balkema, Rotterdam*, 897-906.

Wilson, C.N.J. (1984) The role of fluidization in the emplacement of pyroclastic flows. 2: Experimental results and their interpretation. *J.of Volcanology and Geothermal Research*, **20,** 55-84.

Wilson, H.J. and Davis, R.H., (2000) The viscosity of a dilute suspension of rough spheres, *J. Fluid Mechanics* **421,** 339-367.

Acknowledgment

Firstly, I would like to record my gratitude to Professor Curt Koenders for his supervision, advice and guidance from the very first stage of this research, as well as lending me his extraordinary experience throughout the work. He has encouraged and supported me in many ways. I really thank him for his patience, brilliant ideas which have inspired and enriched my growth as a student, a researcher and as the scientist I would like to become. I am indebted to him more than he knows.

I acknowledge Dr Mastaneh Davis for valuable advice in research, discussion in science, support, using her precious time to read my research and her critical comments.

I gratefully thank my friend Stephen for his advice and guidance, who always grants me his time. Many thanks for his support and helping me to gain a better understanding of mathematics.

My thanks to Nick for his time, support, advice and helping me especially in programming. I would also like thank Simon and Gill, for such a good atmosphere in the office, my friend Amir, for his help and support in many ways, and Andrea for her welcoming me for the week that I was in Salisbury during writing up, by providing pleasant surroundings in which to conduct my research and spend my

leisure time.

Many thanks to Dr. Peter Soan, my second supervisor, for his advice and help.

I gratefully thank my brother Majid for his support in many ways and for providing this opportunity for me to continue with my studies. My thanks to him for sharing his house, food and life with me and his patience during this period. I could never started all this without his support.

Many thanks to my sister Farah for all her kindness, support and encouraging me to be more patient in all the challenges in my life.

Collective and individual acknowledgements to my family, especially my parents who deserve special mention for their tireless support and prayer. My father 'God bless him' who put the fundamental desire to learn into my character, showing me the joy of intellectual pursuit, encouraging and supporting me in each and every endeavour. To my Mum, for supporting and encouraging me and raising me with caring and gentle love. Nazi, Ehsan, Hamid thank for being supportive and caring siblings.

I would like to thank everybody who was important to the successful realisation of this thesis, as well as expressing my apologies that I could not mention personally each and every one.

Many thanks to Kingston University, for the good working environment from

which I benefited throughout my studies.

Finally I would like to thank ORSAS and the Materials Research Group at Kingston University for financial support.